The Notebook Grid: Exact Addresses, Three Reflections, Pell Branches, and Rational Carriers

with Odd-Square Factorizations, Stack Shadows, and Divisor-Shell Arithmetic

Jeffery Huckstead

Cerebral Graphix (cerebralgraphix.com) · ORCID 0009-0007-0234-2177

Version 4.1 · November 2, 2026

Abstract

Writing the positive integers in successive triangular chambers gives an exact address $N(r,c) = T_{r+c-2} + r$ for every cell of the positive integer quadrant. We derive its two inverse formulas, characterize the admissible chamber-offset wedge (m, V), and prove the quadratic address families traced by affine cell paths. Holding a chamber $m = r+c-1$ fixed, three natural phases—the native row fraction $\kappa_{\text{row}} = r/m$, the cell-midpoint fraction $\kappa_{\text{mid}} = (r - \frac{1}{2})/m$, and the nonlinear square-root phase $\kappa_{\text{root}} = \sqrt{2N} - m + \frac{1}{2}$—induce three distinct reflection maps under $\kappa \mapsto 1 - \kappa$. Only the midpoint reflection $R_{\text{mid}}(N) = m^2 + 1 - N$ permutes a whole chamber; the native reflection $R_{\text{row}}(N) = m^2 - N$ preserves the proper subset $1 \le r \le m-1$; and the square-root reflection $R_{\text{root}}(N) = (2m - \sqrt{2N})^2/2$ has an integer image if and only if the cell lies on the superdiagonal $N = 2a^2$ $(m = 2a)$, which it fixes. For scaled-square paths $N_k = A(Qk)^2$, a floor correction ℓ_k partitions the path into exact polynomial branches, separates the first branch departure from sparse power samples, and identifies norm-one triangular seams, algebraic returns at $k = 2P$, and complete negative-Pell diagonal squares. Applying the midpoint fold $\mathfrak{f}(\kappa_{\text{mid}}) = \widetilde{r}\widetilde{c}/(4m^2)$ defines an upper-semicircle carrier map $\mathcal{C}(r,c)$ whose rational points are parameterized uniquely by odd squares $(\widetilde{r}, \widetilde{c}) = \lambda(U^2, W^2)$ with primitive first chamber $m_0 = (U^2+W^2)/2 \equiv 1 \pmod 4$. Its least nontrivial chamber is $m_0 = 5$, and its $45°$ Pell record sequence $m_{0,j} \in \{1, 5, 29, 169, 985, \dots\}$ maps bijectively to diagonal chambers $m = G_j \in \{1, 7, 41, 239, 1393, \dots\}$ carrying square addresses $N = m_{0,j}^2$. On the address sheet $\mathbf{p}_N = (-r/(m+1), 1/(m+1))$, the identity $(2n+1)^2 = 8T_n + 1 = 4n(n+1) + 1$ unites the eight-sector odd-square partition, the balanced split $\{n, n+1\}$ and its finite reciprocal product, Euler's cosine generating function, a fixed-gap Gamma ratio, and depth-weighted isometric stack projection, while the same addresses carry divisor-band progressions, k-dimensional Jordan-totient shells, the factorial-residual dichotomy $Q(N) = N/\gcd(N, m!) \in \{1\} \cup \mathbb{P}$ of asymptotic density $\log 2$, and an entire-function realization of the triangular Taylor coefficients. Two self-contained appendices establish the complete rational-carrier chamber-budget theorems and the all-direction union-shadow theory of the three-dimensional odd-square stack Ω_n.

Route Through the Paper. The exposition follows a single chain of maps, domains, and declared measures:

1. **Triangular Address & Chamber Coordinates (§1–§2):** Positive quadrant cells (r,c) map bijectively to addresses $N(r,c) = T_{m-1} + r$ in chamber $m = r + c - 1$ with offset $V = r - c$ and odd legs $(\widetilde{r}, \widetilde{c}) = (2r-1, 2c-1)$, turning affine lattice rays into degree-2 polynomial address sequences with period-4 offset parity.
2. **Chamber Phases, Three Reflections & Scaled-Square Pell Branches (§3–§4):** Fixing m distinguishes κ_{row}, κ_{mid}, and κ_{root} (with the anti-diagonal pair correspondence $(k, p-k)$), whose reflections and floor-branch drift $\ell_k = \lfloor \frac{1}{2} + k\varepsilon \rfloor$ govern scaled-square Pell branches, norm-one triangular seams, and diagonal square returns.
3. **Rational Carriers, Address Sheet & Odd-Square Factorization (§5–§6, Apps. A–B):** Folding κ_{mid} lifts odd-square cells onto rational points of the upper semicircle $\mathcal{C}(r,c)$, while row normalization embeds the Grid into $Q = [-1, 0] \times [0, 1]$, separating primitive ratio from scale height, active-span rescaling $(1/m)$ from staircase fixed points $(1/k)$, flat screen sampling (2ω) from depth-weighted stack sampling $(6\omega(1-\omega))$, and uniting five routes on $(2n+1)^2 = 8T_n + 1$.
4. **Open Questions, Divisor Shells, Jordan Totients & Factorial Residuals (§7–§8):** Separating finite and open prime-pair and elliptic-curve questions (§7) from proved arithmetic on the addresses (§8) yields divisor-shell progressions, three separate Jordan-totient zeta limits, the complete factorial-residual classification $Q(N) \in \{1\} \cup \mathbb{P}$ with Dickman density $\log 2$, and an entire-function differential lift of $T_n/n!$.

Scope, Proofs, and Verification. Every address, reflection, floor-branch, rational-carrier, address-sheet, odd-square factorization, Brouncker continuant, Euler-transform, divisor-shell, Jordan-totient, factorial-residual, entire-function coefficient-lift, chamber-budget, and three-dimensional stack-shadow theorem in §§1–6, §8, and Appendices A–B is proved algebraically, analytically, or by positive-integer descent in this paper. Classical completeness classifications

on the rails (§4.6) and smooth-number asymptotics (§8.4) cite Nagell [1], Leu and Li [2], Cohn [3], and de Bruijn [13] with explicit hypotheses (with a self-contained 5-adic valuation proof for base 5 on the diagonal). Finite-range numerical and statistical statements carry explicit bounds: the shell-numerator diagnostic table (§8.2, Remark 8.1a) is a deterministic finite calculation at $M \in \{250, 500, 1000, 2000\}$; the odd-chamber mirror-prime verification (§7.1) covers the finite interval $1403 \le m \le 20001$; and all-index mirror-prime existence ($m \ge 1403$), all-index non-intersection of the $a = 2$ and 45° record-chamber families beyond $m_0 \in \{1, 5, 29\}$ (§7.2), two-point prime occupancy (§8.5), and the analytic questions of §8.6 remain open. Throughout, the finite odd-side ($j = 2n + 1$) atomic screen-maximum laws $\Pr_{\text{flat}}(M = i) = (2i - 1)/j^2$ and $\Pr_{\text{stack}}(M = i) = (2i - 1)[1 + \lfloor (j - i)/2 \rfloor]/\binom{j+2}{3}$ are kept distinct from the $j \to \infty$ weak-limit densities 2ω and $6\omega(1 - \omega)$ of M/j; free congruence of the eight half-open max-norm sectors $\Sigma_0, \dots, \Sigma_7$ in the lattice-preserving Euclidean group $\mathrm{E}(2, \mathbb{Z}) = \mathbb{Z}^2 \rtimes \mathrm{O}(2, \mathbb{Z}) \subset \mathrm{E}(2) = \mathbb{R}^2 \rtimes \mathrm{O}(2)$ via $F(a, b) = (b + 1, a)$ is kept distinct from origin-fixing O(2) non-equivalence; and the orthochronous boost conjugacy $C_D L_D C_D^{-1} = \Lambda_{\beta_D} \in \mathrm{SO}^+(1, 1)$ is restricted to the positive Lorentz sheet $P_1 > 0$ (the Cayley images $\mu(1/\sqrt{D})$ are fundamental integer Pell units exactly for $D \in \{2, 3\}$). An optional standard-library Python script (`check_notebook_grid_v4_1.py`) accompanies the supplementary archive for finite-range computational corroboration; no proof step in the paper depends on executing code.

Summary of Main Results

Section	Core Object & Local Coordinates	Principal Theorem / Identity	Proof Method & Scope
§1. Addresses & Chambers	Cell $(r, c) \in \mathbb{Z}^2_{\ge 1}$, chamber $m = r + c - 1$, offset $V = r - c$, odd legs $\widetilde{r} = 2r - 1, \widetilde{c} = 2c - 1$	$N(r, c) = T_{m-1} + r$, $2N = m^2 + V + 1$; admissible iff $m \ge 1, \lvert V\rvert \le m - 1, m + V \equiv 1 \pmod 2$; $m = \lceil (\sqrt{8N + 1} - 1)/2 \rceil = \lfloor \sqrt{2N} + \frac{1}{2} \rfloor$	**Props. 1.1–1.2**, **Fig. 1** (Algebraic proof)
§2. Affine Paths & Rails	Baseline (r_0, c_0), increments (Δ_r, Δ_c), $L = r_0 + c_0 - 2$, $D = \Delta_r + \Delta_c$	Quadratic address polynomial of degree ≤ 2; five rails; fixed-V rail parity $N(r, r - V) \equiv T_{V+1} \pmod 2$ with period 4 $(1, 1, 0, 0)$	**Props. 2.1–2.2**, **Fig. 2** (Algebraic proof)
§3. Three Reflections	Phases $\kappa_{\text{row}} = \frac{r}{m}$, $\kappa_{\text{mid}} = \frac{r - 1/2}{m}$, $\kappa_{\text{root}} = \sqrt{2N} - m + \frac{1}{2}$ $(\varepsilon = \kappa_{\text{root}} - \frac{1}{2})$; pair $(k, p - k)$	$R_{\text{row}}(N) = m^2 - N$, $R_{\text{mid}}(N) = m^2 + 1 - N$, $R_{\text{root}}(N) = (2m - \sqrt{2N})^2/2$; $R_{\text{root}}(N) \in \mathbb{Z} \iff N = 2a^2$; $\frac{3}{8m} < \kappa_{\text{root}} - \kappa_{\text{mid}} \le \frac{1}{2m}$; $(k, p - k) \leftrightarrow R_{\text{mid}}$	**Thm. 3.1, Props. 3.2–3.3, Rem. 3.4**, **Fig. 3** (Algebraic proof)
§4. Floor Branches & Pell	$N_k = A(Qk)^2$, $P = \text{round}(Q\sqrt{2A})$, $\varepsilon = Q\sqrt{2A} - P$, $\delta = P^2 - 2AQ^2$, $\ell_k = \lfloor \frac{1}{2} + k\varepsilon \rfloor$	$m_k = Pk + \ell_k$, $V_k = -\delta k^2 - 2Pk\ell_k - \ell_k^2 - 1$; $\ell_k = 0 \iff -P \le \delta k < P$; seams $k = P$, returns $k = 2P$; diagonal descent $m^2 - 2Q^2 = -1$; rail powers	**Props. 4.1–4.8**, **Fig. 3b** (Algebraic & descent proofs; [1–3] + 5-adic proof in §4.6)
§5. Rational Carriers	Midpoint circle $\mathcal{C}_{(r,c)} = \left(\frac{V}{m}, \frac{\sqrt{\widetilde{r}\widetilde{c}}}{m}\right) = \left(\mathcal{J}(\kappa_{\text{mid}}), 2\sqrt{\mathfrak{f}(\kappa_{\text{mid}})}\right)$	Rational iff $(\widetilde{r}, \widetilde{c}) = \lambda(U^2, W^2)$ $(U, W, \lambda$ odd, $\gcd(U, W) = 1)$, $m_0 = \frac{U^2 + W^2}{2} \equiv 1 \pmod 4$; least nontrivial $m_0 = 5$; bridge $N_{\text{diag}}(G_j) = m^2_{0,j}$	**Thms. 5.1–5.2**, **Fig. 4** (Algebraic & descent proofs)
§6. Address Sheet & Odd-Square Factorization	Site $\mathbf{p}_N = \left(-\frac{r}{m+1}, \frac{1}{m+1}\right)$, odd square $(2n + 1)^2 = 8T_n + 1$, balanced split $\{n, n + 1\}$, stack S_n	Closure, hull & $1/\sqrt{k + 1}$ lift; 8-sector $\mathrm{E}(2, \mathbb{Z})$ split; finite $\mathcal{S}_L \Pi_{\triangle, L}(-1/8) = 1$; PGF $G(\tau)$; Gamma $P_L^{(D)}$; atomic PMFs $\to 2\omega, 6\mathfrak{f}(\omega)$; Brouncker & S_+	**Props. 6.1–6.5, Lem. 6.5a, Thm. 6.5**, **Figs. 5–7, 9, 12** (Algebraic & analytic proofs)
§7. Open Questions	Odd chamber $m = 2M + 1$, center $N_c = (m^2 + 1)/2$; curve $E : C^2 = (A - 2)(A^2 - 200)$	Mirror-prime pairs $(N_c - k, N_c + k)$ verified on $1403 \le m \le 20001$; shared $a = 2$ & 45° records $\{1, 5, 29\}$ pulled back to $E_0, E_1, E_2 \in E(\mathbb{Z})$	**§7.1–§7.3**, **Fig. 8** (Finite verification; all-index questions open)
§8. Shells, Jordan & $Q(N)$	Shells $R_d(k, h) = d^2k - d + h$, Jordan $J_k(d)$, residual $Q(N) = N/\gcd(N, m!)$, entire $E_{\text{Ei}}(z)$	Within-shell uniqueness & $\varphi(d^2) = d\varphi(d)$; three separate Jordan zeta limits; $Q(N) \in \{1\} \cup \mathbb{P}$, exceptional prime powers $\{p^2\} \cup \{27\}$, density $\log 2$; entire lift $G_\pm(z)$	**Thms. 8.1–8.3, Prop. 8.4**, **Fig. 10** (Local proofs + [13]; §8.2 table finite; 2-pt occupancy open)

Section	Core Object & Local Coordinates	Principal Theorem / Identity	Proof Method & Scope
App. A. Carrier Budgets	Integer budget $M \geq 1$, excluded target $\mathbf{p}_* = \left(\frac{A^2-C^2}{D_0}, \frac{2AC}{D_0}\right)$, leg chart $\kappa_{\text{leg}} = \frac{r}{m+1}$	All-budget 45° Pell optimum; Bézout tail $M \geq M_{\text{cut}}$ with $ME_*(M)^2 \to 2/D_0$ & $(3,4)$ budget-17 exception $(3,5)$; two-chart $m_{0,j} - 1$ advance	**Thms. A.1–A.3**, **Fig. A.1** (Algebraic & descent proofs)
App. B. Stack Ω_n	$\Omega_n = \bigcup_{j=0}^{n}[-j-\frac{1}{2}, j+\frac{1}{2}]^2 \times [j, j+1]$, viewing vector $\boldsymbol{v} = (A, C, D)$	Exact union area law; hiding cone $\max(\lvert A\rvert, \lvert C\rvert) \leq \lvert D\rvert$; extrema $[(n+1)^2, (2n+1)\sqrt{(2n+1)^2+2}]$; mean $(1+\sqrt{2})n^2 + (4+\chi)n + C_* + \varepsilon_n$; sharp $\tau = \frac{1}{2}$	**Thms. B.1–B.3**, **Fig. B.1** (Geometric & analytic proofs)

1. The Address, Its Chambers, and Phase Centering Conventions

1.1 Enumerating the Positive Quadrant

Let the triangular polynomial be defined for every complex argument $z \in \mathbb{C}$, and write its integer values with subscripts:

$$T(z) = \frac{z(z+1)}{2}, \qquad T_n = T(n) \quad (n \in \mathbb{Z}), \qquad N(r,c) = T_{r+c-2} + r \quad (r, c \in \mathbb{Z}_{\geq 1}). \quad (1.1)$$

For each fixed anti-diagonal sum $r + c$, the term r counts the sites along that anti-diagonal. Define the **chamber index** m, the **row offset** V, and the **centered odd legs** $(\widetilde{r}, \widetilde{c})$ by

$$m = r + c - 1, \qquad V = r - c, \qquad \widetilde{r} = 2r - 1 = m + V, \qquad \widetilde{c} = 2c - 1 = m - V. \quad (1.2)$$

For each fixed chamber $m \geq 1$, the rows $r = 1, \ldots, m$ (with $c = m + 1 - r$) carry the consecutive integer addresses $T_{m-1} + 1, \ldots, T_m$. The first chamber ($m = 1$) contains 1; the second ($m = 2$) contains 2 and 3; the third ($m = 3$) contains $4, 5$, and 6. These disjoint consecutive intervals partition $\mathbb{Z}_{\geq 1}$ without gaps. We distinguish the integer address N written in a cell, its row and column (r, c), and its chamber m; none is a substitute for the others.

Proposition 1.1 (Exact Chamber Wedge and Parity Lattice). *A positive integer cell $(r, c) \in \mathbb{Z}^2_{\geq 1}$ of address $N = N(r, c)$ satisfies*

$$2N = m^2 + V + 1, \qquad r = \frac{m + V + 1}{2}, \qquad c = \frac{m - V + 1}{2}. \quad (1.3)$$

Conversely, an integer pair $(m, V) \in \mathbb{Z}^2$ represents a positive integer cell $(r, c) \in \mathbb{Z}^2_{\geq 1}$ if and only if

$$m \geq 1, \qquad |V| \leq m - 1, \qquad m + V \equiv 1 \pmod 2. \quad (1.4)$$

Proof. In chamber m, $N = T_{m-1} + r = \frac{m(m-1)}{2} + r$. Multiplying by 2 and substituting $2r = m + V + 1$ yields $2N = m^2 - m + (m + V + 1) = m^2 + V + 1$, and solving $r + c = m + 1, r - c = V$ gives the coordinate recovery formulas in (1.3). Conversely, given $(m, V) \in \mathbb{Z}^2$, the parity condition $m + V \equiv 1 \pmod 2$ makes r and c integers, and the inequalities $m \geq 1, -m + 1 \leq V \leq m - 1$ make $r \geq 1$ and $c \geq 1$. Substituting (r, c) into (1.1) recovers N. Thus (1.4) is both necessary and sufficient. In particular, any algebraic curve in the (m, V) plane represents actual positive grid cells only where it meets both the parity lattice and the chamber wedge (1.4). □

1.2 Two Exact Inverse Formulas and the Origin Convention

Proposition 1.2 (Inverse Address Recovery). *For each positive integer address $N \in \mathbb{Z}_{\geq 1}$, its unique chamber m and cell coordinates (r, c) are given by*

$$T_{m-1} < N \le T_m, \qquad m = \left\lceil \frac{\sqrt{8N+1}-1}{2} \right\rceil, \qquad r = N - T_{m-1}, \qquad c = m + 1 - r. \quad (1.5)$$

Equivalently, the chamber m is recovered by nearest-integer rounding of $\sqrt{2N}$:

$$m - \frac{1}{2} < \sqrt{2N} < m + \frac{1}{2}, \qquad m = \left\lfloor \sqrt{2N} + \frac{1}{2} \right\rfloor. \quad (1.6)$$

Proof. Because the chamber intervals $(T_{m-1}, T_m] \cap \mathbb{Z}$ partition $\mathbb{Z}_{\ge 1}$, the unique chamber m satisfies $\frac{(m-1)m}{2} < N \le \frac{m(m+1)}{2}$. Completing the square $8T_m + 1 = (2m+1)^2$ gives $2m - 1 < \sqrt{8N+1} \le 2m + 1$, which is equivalent to (1.5). Within chamber m, integrality of N strengthens the lower inequality $N \ge T_{m-1} + 1$ to

$$2N \ge m^2 - m + 2 = \left(m - \frac{1}{2}\right)^2 + \frac{7}{4} > \left(m - \frac{1}{2}\right)^2,$$

while the upper inequality $N \le T_m$ gives

$$2N \le m^2 + m = \left(m + \frac{1}{2}\right)^2 - \frac{1}{4} < \left(m + \frac{1}{2}\right)^2.$$

Taking positive square roots yields the strict inequalities in (1.6) and the floor formula $m = \lfloor \sqrt{2N} + \frac{1}{2} \rfloor$. A nearest-integer tie $\sqrt{2N} = m \pm \frac{1}{2}$ can never occur for an integer N, because $2N$ is an integer whereas $(m \pm \frac{1}{2})^2 = m^2 \pm m + \frac{1}{4} \notin \mathbb{Z}$. □

As a worked address, $N = 25$ lies between $T_6 = 21$ and $T_7 = 28$. By (1.5)–(1.6), it has chamber $m = 7$, cell $(r, c) = (4, 4)$, and offset $V = 0$. The identity $2 \cdot 25 = 7^2 + 1$ describes its chamber position $(m = 7, V = 0)$, whereas $25 = 5^2$ describes its square address $(Q = 5)$. Keeping the chamber index m and the address root Q separate is essential in §§4–5.

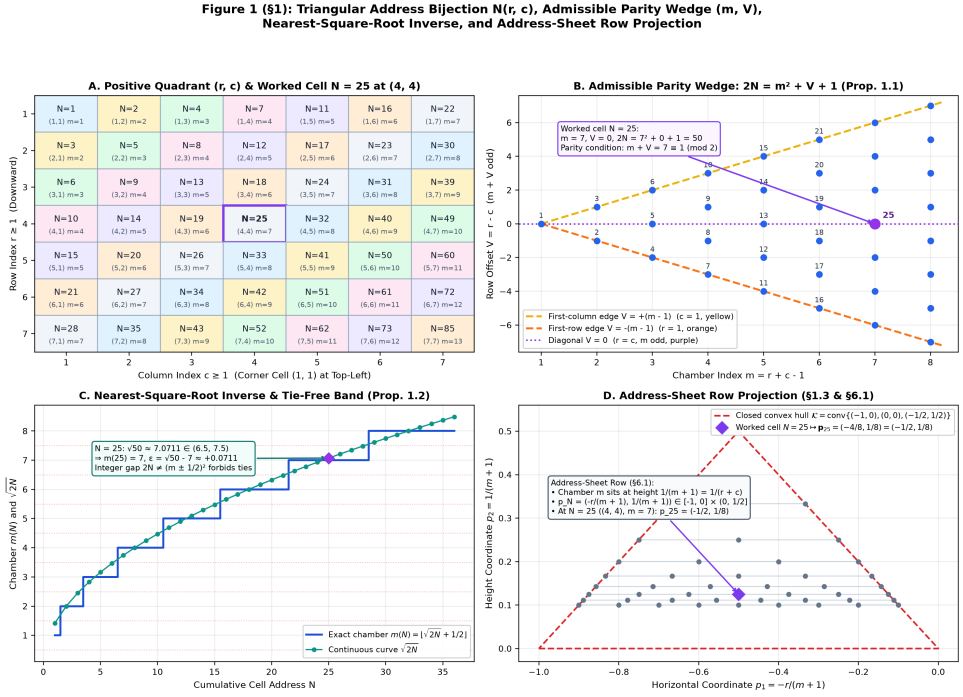


Figure 1 (Positive quadrant address, chamber wedge, and inverse recovery): **A.** Positive quadrant cells $(r, c) \in \mathbb{Z}^2_{\ge 1}$ colored by triangular chamber bands $m = r + c - 1 \le 7$ with cumulative addresses $N(r, c) = T_{m-1} + r$ and worked diagonal cell $N = 25$ at $(r, c) = (4, 4), m = 7, V = 0$. **B.** Admissible chamber-offset lattice (m, V) in Proposition 1.1 (`2N = m^2+V+1`, $|V| \le m - 1$, $m + V \equiv 1 \pmod 2$), bounded by the first-column edge $V = m - 1$ ($c = 1$, yellow) and the first-row edge $V = 1 - m$ ($r = 1$, orange), showing the odd-m diagonal center $V = 0$ (purple) and the even-m superdiagonal center $V = -1$ (teal). **C.** Nearest-integer root inverse $m = \lfloor \sqrt{2N} + 1/2 \rfloor$ in Proposition 1.2, showing $\sqrt{2N} \in (m - 1/2, m + 1/2)$ strictly inside each chamber band with no half-integer ties.

Origin Convention. The positive grid has its corner cell at $(r, c) = (1, 1)$, holding $N(1, 1) = 1$. Translating the drawing's corner to a Cartesian origin $(0, 0)$ replaces (r, c) by $(r', c') = (r - 1, c - 1) \in \mathbb{Z}^2_{\geq 0}$:

$$r' = r - 1, \qquad c' = c - 1, \qquad N(r' + 1, c' + 1) = T_{r'+c'} + r' + 1 \quad (r', c' \geq 0). \quad (1.7)$$

This coordinate translation changes where the axes sit in a drawing without creating a cell of address 0 in the positive Grid. Extending $T(z)$ to $z = 0$ or negative arguments (such as the vertex $z = -1/2$ where $T(-1/2) = -1/8$) is a separately declared polynomial operation.

1.3 Relation to Rational Triangular Coordinates and Centering Conventions

The cumulative address (1.1) shares its indexing with the rational triangular-fractional coordinate studied in [4, 11], where chamber $m \geq 1$ carries the m entries

$$a(m, r) = m - 1 + \frac{r}{m} \qquad (1 \leq r \leq m), \quad (1.8)$$

and the rank of the entry $a(m, r)$ in this enumeration is exactly the address $N(r, c) = T_{m-1} + r$ with $c = m + 1 - r$ [7]. Two structural distinctions are maintained throughout this paper:

1. **Native Row Centering vs. Cell-Midpoint Centering:** Using the affine centering map $\mathcal{J}(w) = 2w - 1$ and quadratic fold $\mathfrak{f}(w) = w(1 - w) = (1 - \mathcal{J}(w)^2)/4$ [5], centering a chamber by its native row phase $\kappa_{\text{row}} = r/m$ yields the integer displacement

$$j_{\text{row}} = 2r - m = V + 1, \qquad \mathcal{J}(\kappa_{\text{row}}) = \frac{V + 1}{m}. \quad (1.9)$$

   By contrast, cell-transpose symmetry $(r, c) \leftrightarrow (c, r)$ centers a chamber by its cell-midpoint phase $\kappa_{\text{mid}} = (r - \frac{1}{2})/m = \widetilde{r}/(2m)$, for which

$$\mathcal{J}(\kappa_{\text{mid}}) = \frac{\widetilde{r} - \widetilde{c}}{2m} = \frac{V}{m}, \qquad 4\mathfrak{f}(\kappa_{\text{mid}}) = \frac{\widetilde{r}\widetilde{c}}{m^2} = 1 - \left(\frac{V}{m}\right)^2 = 1 - 4\left(\kappa_{\text{mid}} - \frac{1}{2}\right)^2. \quad (1.10)$$

   Consequently, the native half-row center $\mathcal{J}(\kappa_{\text{row}}) = 0$ is the **superdiagonal** cell $V = -1$ (occurring only in **even** chambers $m = 2a$, at $r = a, c = a + 1, N = 2a^2$), whereas the midpoint fixed center $\mathcal{J}(\kappa_{\text{mid}}) = 0$ is the **diagonal** cell $V = 0$ (occurring only in **odd** chambers $m = 2k - 1$, at $r = c = k, N = k^2 + (k - 1)^2$). This unit shift $j_{\text{row}} = V + 1$ explains why the two centering conventions select opposite chamber parities.
2. **Signed Binomial Arrays vs. Positive Quadrant Addresses:** Companion studies of alternating binomial coefficient arrays $(-1)^j \binom{k}{j}$ and their row-reversal involutions [4] act on finite polynomial coefficient tables rather than on the positive integer cell addresses $N(r, c)$ and fixed-chamber spatial reflections proved in §3 below.

2. Straight Cell Paths, Five Rails, and Parity

2.1 Every Affine Cell Path Has a Quadratic Address

Proposition 2.1 (Affine Path Polynomial). *Fix a baseline cell $(r_0, c_0) \in \mathbb{Z}^2_{\geq 1}$, integer increments $(\Delta_r, \Delta_c) \in \mathbb{Z}^2$, and an integer parameter $k \in \mathbb{Z}$, retaining precisely the indices k for which $r(k) = r_0 + \Delta_r k \geq 1$ and $c(k) = c_0 + \Delta_c k \geq 1$. Set $L = r_0 + c_0 - 2$ and $D = \Delta_r + \Delta_c$. Then*

$$N(r_0 + \Delta_r k,\, c_0 + \Delta_c k) = \frac{D^2}{2}k^2 + \left(\frac{D(2L + 1)}{2} + \Delta_r\right)k + T_L + r_0. \quad (2.1)$$

Proof. Along the path, the triangular index is $r(k) + c(k) - 2 = L + Dk$. Expanding $T(L + Dk) = T_L + \frac{D(2L+1)}{2}k + \frac{D^2}{2}k^2$ and adding $r(k) = r_0 + \Delta_r k$ yields (2.1). □

Every affine cell path therefore traces an address polynomial in k of degree at most 2. When $D = \Delta_r + \Delta_c = 0$, the path remains inside a single chamber $m = L + 1$ and its quadratic term vanishes, leaving a linear function of k.

2.2 The Five Distinguished Rails

Five affine rays carry most of the structure below. We name them by position; the colors are the keys used in the figures (and in the original notebook). Each is indexed by an integer parameter $k \geq 1$:

Rail (figure color)	**Cell** (r, c)	**Chamber** m **and Offset** V	**Exact Address** $N(r, c)$	**Line in** $(m, \widetilde{r})$
First-row edge (orange)	$(1, k)$	$m = k, \quad V = 1 - k$	$T_{k-1} + 1$	$\widetilde{r} = 1$
First-column edge (yellow)	$(k, 1)$	$m = k, \quad V = k - 1$	T_k	$\widetilde{r} = 2m - 1$
Diagonal (purple)	(k, k)	$m = 2k - 1, \quad V = 0$	$k^2 + (k-1)^2 = 4T_{k-1} + 1$	$\widetilde{r} = m$
Superdiagonal (teal)	$(k, k+1)$	$m = 2k, \quad V = -1$	$2k^2 = \frac{m^2}{2}$	$\widetilde{r} = m - 1$
Subdiagonal (pink)	$(k+1, k)$	$m = 2k, \quad V = +1$	$2k^2 + 1 = \frac{m^2+2}{2}$	$\widetilde{r} = m + 1$

In chamber and odd-row coordinates $(m, \widetilde{r})$, all five families are straight lines:

$$\widetilde{r} = 1, \qquad \widetilde{r} = 2m - 1, \qquad \widetilde{r} = m, \qquad \widetilde{r} = m - 1, \qquad \widetilde{r} = m + 1. \quad (2.2)$$

As functions of the chamber m, however, the three interior rails carry quadratic addresses:

$$N(k, k) = \frac{m^2 + 1}{2} = 4T_{k-1} + 1, \qquad N(k, k+1) = \frac{m^2}{2}, \qquad N(k+1, k) = \frac{m^2 + 2}{2}. \quad (2.3)$$

Thus a statement that the diagonal is "linear" requires naming the horizontal axis: in $(m, \widetilde{r})$ it is the line $\widetilde{r} = m$; against the triangular input T_{k-1} its address is $4T_{k-1} + 1$; against the chamber m its address is the quadratic $(m^2 + 1)/2$.

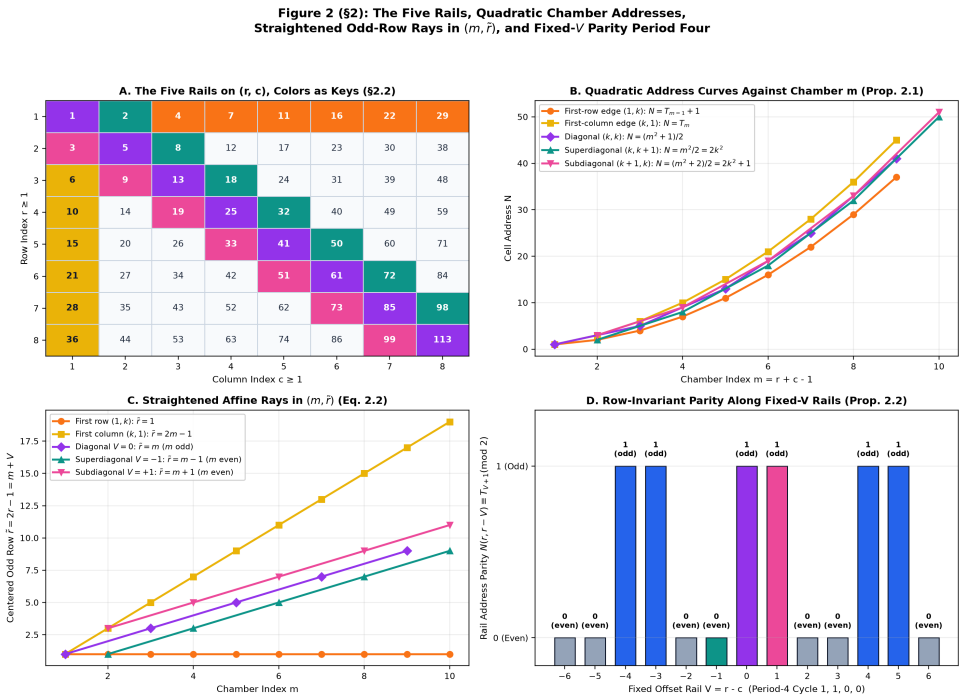


Figure 2 (The five rails, straight odd-row rays vs. quadratic chamber addresses, and fixed-V parity 4-cycle): **A.** The 8×8 positive quadrant (r, c) showing the five rails on the Grid: the first-row edge $(1, k)$ (orange, $N = T_{k-1} + 1$), the first-column edge $(k, 1)$ (yellow, $N = T_k$), the diagonal (k, k) (purple, $V = 0$, $N = 4T_{k-1} + 1$), the superdiagonal $(k, k+1)$ (teal, $V = -1$, $N = 2k^2$), and the subdiagonal $(k+1, k)$ (pink, $V = +1$, $N = 2k^2 + 1$). **B.** In chamber and odd-row coordinates $(m, \widetilde{r})$, all five rails are straight lines (2.2), whereas against the chamber m the interior rails carry the quadratic addresses (2.3). **C.** Constant address parity $N(r, r - V) \equiv T_{V+1} \pmod 2$ along each fixed-V rail (Proposition 2.2), repeating with period 4 in the pattern $(1, 1, 0, 0)$ from $V = 0, 1, 2, 3$ and inducing the one-dimensional four-state Gray cycle of Remark 2.3.

2.3 Fixed-Offset Rails, Parity Period Four, and Odd Powers of Two

Proposition 2.2 (Constant Parity of Fixed-V Rails). *Fix an integer offset $V \in \mathbb{Z}$, and let $r \in \mathbb{Z}$ vary over $r \geq \max(1, V+1)$ with $c = r - V \geq 1$. Then*

$$N(r, r-V) = 2r^2 - 2(V+1)r + T_{V+1}, \qquad N(r, r-V) \equiv T_{V+1} \pmod 2. \quad (2.4)$$

Consequently, every fixed-V rail has constant address parity throughout the positive quadrant, and as V increases by 1 that rail parity repeats with period 4 in the pattern $(1,1,0,0)$ starting at $V = 0,1,2,3$.

Proof. In (1.1), $r + c - 2 = 2r - V - 2$, so

$$N(r, r-V) = \frac{(2r-V-2)(2r-V-1)}{2} + r = 2r^2 - 2(V+1)r + \frac{(V+1)(V+2)}{2} = 2r^2 - 2(V+1)r + T_{V+1}.$$

The polynomial identity $T(-V-2) = T(V+1)$ holds for all $V \in \mathbb{Z}$. Since $2r^2 - 2(V+1)r$ is even for every integer r, $N(r, r-V) \equiv T_{V+1} \pmod 2$. Moreover, $T_{V+5} - T_{V+1} = 4V + 14 \equiv 0 \pmod 2$, giving period 4 with values $T_1 = 1, T_2 = 3 \equiv 1, T_3 = 6 \equiv 0, T_4 = 10 \equiv 0 \pmod 2$ at $V = 0,1,2,3$. □

Remark 2.3 (Connection to the One-Dimensional Gray Cycle and the Modular Coefficient Rows). In one dimension, consecutive triangular parities form the adjacent pair $(T_{n-1} \bmod 2, T_n \bmod 2)$, which traverses the four-state Gray cycle $00 \to 01 \to 11 \to 10 \to 00$ by the quarter-turn $F(a,b) = (b, 1-a)$, while index reflection $n \mapsto -1-n$ acts by $E(a,b) = (1-a, b)$, together generating D_4. That one-dimensional index-cycle reflection on modular rising-factorial rows $\Pi_n(y) = \prod_{j=1}^{n}(1+jy) \bmod (B, y^{K+1})$ [7] acts across consecutive triangular indices n and is distinct from the fixed-chamber spatial reflections in §3 below.

Finally, the odd powers of two lie exactly on the even-parity superdiagonal $V = -1$:

$$2^{2j+1} = 2(2^j)^2 \implies (r,c) = (2^j, 2^j+1), \quad m = 2^{j+1}, \quad V = -1 \qquad (j \in \mathbb{Z}_{\geq 0}). \quad (2.5)$$

This sparse exponential subsequence lies inside the quadratic rail $N = 2k^2$ $(k = 2^j)$ and must not be confused with the piecewise parabolic branches traced by even powers of two $(4^j = (2^j)^2)$ in §4.

3. Three Reflections and Their Surviving Integer Domains

3.1 Three Ways to Center and Reflect a Chamber

Hold an integer chamber $m \geq 1$ fixed. Within chamber m, the **native row phase** κ_{row}, the **cell-midpoint phase** κ_{mid}, and the **square-root phase** κ_{root} (with local root displacement ε) are defined by

$$\kappa_{\mathrm{row}} = \frac{r}{m}, \qquad \kappa_{\mathrm{mid}} = \frac{r - 1/2}{m} = \frac{\widetilde{r}}{2m}, \qquad \varepsilon = \sqrt{2N} - m, \qquad \kappa_{\mathrm{root}} = \varepsilon + \frac{1}{2} = \sqrt{2N} - m + \frac{1}{2}. \quad (3.1)$$

On a positive cell (r,c) in chamber m, $\kappa_{\mathrm{row}} = r/m \in (0,1]$ is a **right-endpoint step phase** (attaining 1 on the first-column edge $r = m, c = 1$, whereas the address-sheet coordinate $-p_1 = \kappa_{\mathrm{leg}} = r/(m+1) = r/(r+c) \in [1/(m+1), m/(m+1)] \subset (0,1)$ of §6.1 divides by $m+1 = r+c$ so both coordinates remain strictly positive inside the open unit interval), while both $\kappa_{\mathrm{mid}} = (r-1/2)/m$ and $\kappa_{\mathrm{root}} = \sqrt{2N} - m + 1/2$ are **interior cell phases** lying strictly in $(0,1)$ by Proposition 1.2 $(-\frac{1}{2} < \varepsilon < \frac{1}{2})$. Consequently, at the first-column endpoint $r = m, c = 1$ $(N = T_m)$, the involution $\kappa_{\mathrm{row}} \mapsto 1 - \kappa_{\mathrm{row}}$ sends $\kappa_{\mathrm{row}} = 1$ to 0, mapping $R_{\mathrm{row}}(T_m) = m^2 - T_m = T_{m-1}$ out of chamber m into the preceding chamber $m-1$ (or to 0 at $m = 1$). Although all three coordinates represent positions across chamber m, applying the scalar involution $\kappa \mapsto 1 - \kappa$ while holding m fixed induces three different address maps.

Theorem 3.1 (Three Reflection Maps and Their Domains). *Fix an integer chamber $m \geq 1$. Reflecting κ_{row}, κ_{mid}, and κ_{root} by $\kappa \mapsto 1 - \kappa$ induces the following address transformations on chamber m:*

Selected Phase	**Induced Address Map**	**Same-Chamber Positive Cell Domain & Action**	**Fixed Positive Cells in Chamber m**
$\kappa_{\mathrm{row}} \mapsto 1-\kappa_{\mathrm{row}}$	$R_{\mathrm{row}}(N) = m^2 - N$	$(r,c) \mapsto (c-1, r+1)$; preserves chamber m iff $c > 1$ ($1 \le r \le m-1$, empty for $m = 1$)	Even $m = 2a$: superdiagonal cell $(a, a+1)$, $V = -1$, $N = m^2/2 = 2a^2$
$\kappa_{\mathrm{mid}} \mapsto 1-\kappa_{\mathrm{mid}}$	$R_{\mathrm{mid}}(N) = m^2 + 1 - N$	$(r,c) \mapsto (c,r)$; permutes every positive cell of chamber m	Odd $m = 2k-1$: diagonal cell (k,k), $V = 0$, $N = (m^2+1)/2$
$\kappa_{\mathrm{root}} \mapsto 1-\kappa_{\mathrm{root}}$	$R_{\mathrm{root}}(N) = \frac{(2m-\sqrt{2N})^2}{2}$	Continuous involution on $\sqrt{2N} \in (m-\frac{1}{2}, m+\frac{1}{2})$; integer image iff fixed superdiagonal cell	Even $m = 2a$: superdiagonal cell $(a, a+1)$, $V = -1$, $N = m^2/2 = 2a^2$

Moreover, in terms of the offset $V = 2m\varepsilon + \varepsilon^2 - 1$, the transformed offsets and the exact nonlinear difference between R_{root} and R_{row} are

$$V'_{\mathrm{row}} = -V - 2, \qquad V'_{\mathrm{mid}} = -V, \qquad V'_{\mathrm{root}} = -V - 2 + 2\varepsilon^2, \qquad R_{\mathrm{root}}(N) - R_{\mathrm{row}}(N) = \varepsilon^2. \quad (3.2)$$

Proof. Under $\kappa_{\mathrm{row}} \mapsto 1-\kappa_{\mathrm{row}}$, the row $r = m\kappa_{\mathrm{row}}$ maps to $r' = m - r = c - 1$, giving address $T_{m-1} + (m-r) = m^2 - N$ and column $c' = m + 1 - r' = r + 1$. This image lies in chamber m with positive coordinates iff $1 \le r \le m-1$ ($c > 1$). At the first-column endpoint $r = m, c = 1$ ($N = T_m$), $R_{\mathrm{row}}(T_m) = m^2 - T_m = T_{m-1}$, which is a positive address in the preceding chamber $m-1$ when $m \ge 2$ and equals 0 (outside the positive grid) when $m = 1$.

Under $\kappa_{\mathrm{mid}} \mapsto 1-\kappa_{\mathrm{mid}}$, $r - \frac{1}{2}$ maps to $m - (r - \frac{1}{2})$, so $r' = m + 1 - r = c$, $c' = r$, and $R_{\mathrm{mid}}(N) = T_{m-1} + (m+1-r) = m^2 + 1 - N$, which is a bijection on $\{1, \dots, m\}$.

Under $\kappa_{\mathrm{root}} \mapsto 1-\kappa_{\mathrm{root}}$, $\varepsilon = \kappa_{\mathrm{root}} - \frac{1}{2}$ maps to $-\varepsilon$, so $\sqrt{2N} = m + \varepsilon$ maps to $m - \varepsilon = 2m - \sqrt{2N} \in (m - \frac{1}{2}, m + \frac{1}{2})$, giving $R_{\mathrm{root}}(N) = (2m - \sqrt{2N})^2/2$. Expanding $2N = (m+\varepsilon)^2 = m^2 + 2m\varepsilon + \varepsilon^2$ and comparing with $2N = m^2 + V + 1$ gives $V + 1 = 2m\varepsilon + \varepsilon^2$, so

$$R_{\mathrm{root}}(N) = \frac{(m-\varepsilon)^2}{2} = \frac{m^2 - 2m\varepsilon + \varepsilon^2}{2} = \frac{m^2 - (V + 1 - \varepsilon^2) + \varepsilon^2}{2} = m^2 - N + \varepsilon^2 = R_{\mathrm{row}}(N) + \varepsilon^2,$$

which establishes all relations in (3.2). □

Single-Cell Distinguishing Witness. For address $N = 5$ in chamber $m = 3$ (cell $(2,2)$, $V = 0$), the three reflections give

$$R_{\mathrm{row}}(5) = 4, \qquad R_{\mathrm{mid}}(5) = 5, \qquad R_{\mathrm{root}}(5) = 23 - 6\sqrt{10} \approx 4.026334, \quad (3.3)$$

with $4 < 23 - 6\sqrt{10} < 5$. This single cell rules out any identification of the three reflections.

3.2 Integer-Image Rigidity and Root–Midpoint Discrepancy

Proposition 3.2 (Integer-Image Rigidity of Root Reflection). *Among positive integer cells, $R_{\mathrm{root}}(N)$ is an integer if and only if the cell lies on the superdiagonal:*

$$m = 2a, \qquad N = 2a^2, \qquad (r,c) = (a, a+1), \qquad \varepsilon = 0 \qquad (a \in \mathbb{Z}_{\ge 1}), \quad (3.4)$$

and every such cell is fixed by R_{root}.

Proof. Expanding $R_{\mathrm{root}}(N) = 2m^2 + N - 2m\sqrt{2N}$ shows that if $R_{\mathrm{root}}(N) \in \mathbb{Z}$, then $\sqrt{2N} \in \mathbb{Q}$. Because $2N \in \mathbb{Z}$, a rational square root of $2N$ must be an integer. By Proposition 1.2, $m - \frac{1}{2} < \sqrt{2N} < m + \frac{1}{2}$, so the only integer in this open interval is m. Hence $\sqrt{2N} = m$, so $2N = m^2$ and $\varepsilon = 0$. Integrality of $N = m^2/2$ forces $m = 2a$ even, giving $N = 2a^2$ and $(r,c) = (a, a+1)$. Conversely, $\varepsilon = 0$ gives $R_{\mathrm{root}}(2a^2) = 2a^2$. □

Proposition 3.2 proves without any unbounded search that R_{root} never exchanges distinct integer Pell families: off the fixed superdiagonal, $R_{\mathrm{root}}(N)$ is always irrational. Even the affine map R_{row} need not preserve squares (in chamber $m = 7$, $R_{\mathrm{row}}(25) = 49 - 25 = 24$).

Proposition 3.3 (Root–Midpoint Phase Discrepancy Bounds). *On every positive integer cell (r,c) in chamber $m \ge 1$,*

$$m(\kappa_{\text{root}} - \kappa_{\text{mid}}) = \frac{1-\varepsilon^2}{2}, \qquad \frac{3}{8m} < \kappa_{\text{root}} - \kappa_{\text{mid}} \le \frac{1}{2m}. \quad (3.5)$$

Equality at the upper bound $\frac{1}{2m}$ *holds if and only if the cell is a superdiagonal cell (3.4), and the lower bound* $\frac{3}{8m}$ *is strict on every positive cell.*

Proof. Since $V = 2m\varepsilon + \varepsilon^2 - 1$, we have

$$\kappa_{\text{mid}} = \frac{1}{2} + \frac{V}{2m} = \frac{1}{2} + \varepsilon + \frac{\varepsilon^2 - 1}{2m} = \kappa_{\text{root}} - \frac{1-\varepsilon^2}{2m},$$

which gives $m(\kappa_{\text{root}} - \kappa_{\text{mid}}) = (1-\varepsilon^2)/2$. Proposition 1.2 gives $0 \le \varepsilon^2 < \frac{1}{4}$, which yields $\frac{3}{8m} < \kappa_{\text{root}} - \kappa_{\text{mid}} \le \frac{1}{2m}$, with upper equality iff $\varepsilon = 0$. □

Remark 3.4 (Anti-Diagonal Pair Correspondence and Even-Chamber Midpoint Reflection). For any integer $p \ge 2$ and step $1 \le k \le p-1$ (no primality condition on p is required), the anti-diagonal pair $(r, c) = (k, p-k)$ studied in the companion sum–difference geometry [15] lies on the Notebook Grid at

$$(r, c) = (k,\, p-k), \qquad m = p-1, \qquad V = 2k - p, \qquad N(k,\, p-k) = T_{p-2} + k. \quad (3.6)$$

Exchanging the pair $(k, p-k) \mapsto (p-k, k)$ sends $N = T_{p-2} + k$ to $N' = T_{p-2} + (p-k)$. Since $2T_{p-2} + p = (p-2)(p-1) + p = (p-1)^2 + 1 = m^2 + 1$, we have $N' = m^2 + 1 - N = R_{\text{mid}}(N)$: coordinate exchange on $(k, p-k)$ is identically the **midpoint reflection** R_{mid} on chamber $m = p-1$. When p is odd, the chamber $m = p-1$ is **even** and every offset $V = 2k - p$ is **odd**, so the diagonal center $V = 0$ is absent from chamber m and the central adjacent pair $\left(\frac{p-1}{2}, \frac{p+1}{2}\right), \left(\frac{p+1}{2}, \frac{p-1}{2}\right)$ occupies the superdiagonal and subdiagonal offsets $V = -1$ and $V = +1$. Equation (3.6) records the discrete pair correspondence; the companion polar scalar of [15], the exchange-commuting 2×2 Gram family $B_a = I + aE$ (characterized in §6.6, Remark 6.6b(1)), and Gaussian-integer lattice squares live in distinct ambient spaces and are not identified as a single point set, nor is this even chamber $m = p-1$ (for odd p) identified with the odd-chamber ($m = 2M+1$) midpoint prime-pair setting of §7.1.

Figure 3 (§3): Three Chamber Reflections, Distinguishing Witness N = 5 in Chamber m = 3, Superdiagonal Double-Square Integer Rigidity, and Exact Root-Midpoint Phase Parabola

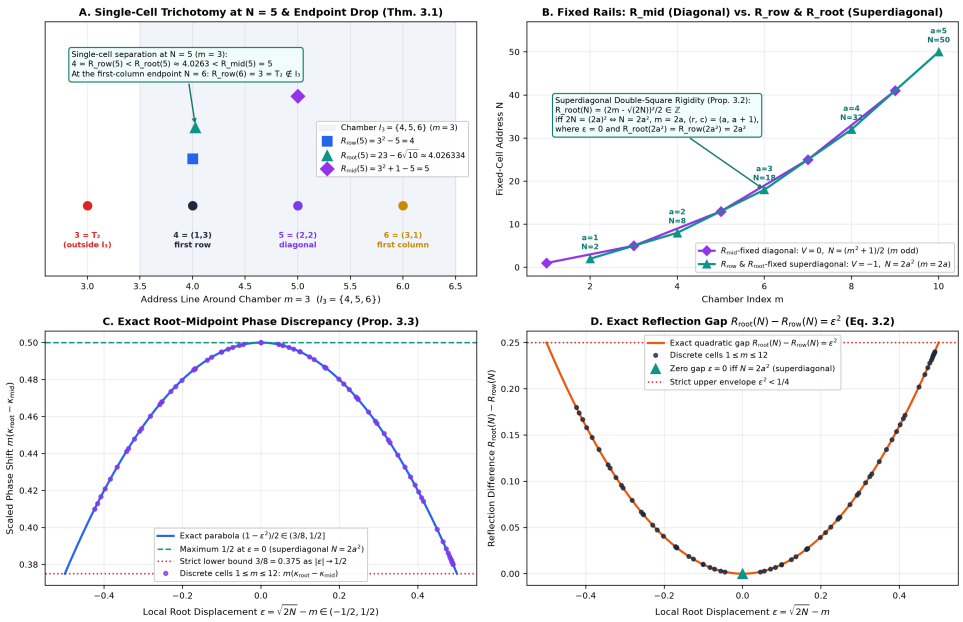


Figure 3 (Three chamber reflections, distinguishing witness $N = 5$*, and root–midpoint phase discrepancy):* **A.** In chamber $m = 3$ (addresses $\{4, 5, 6\}$), the diagonal cell $N = 5$ at $(2, 2)$ separates all three reflections (3.3): $R_{\text{row}}(5) = 4 < R_{\text{root}}(5) = 23 - 6\sqrt{10} \approx 4.026334 < R_{\text{mid}}(5) = 5$, while at the first-column endpoint $N = 6$ ($c = 1$) the native map $R_{\text{row}}(6) = 3 = T_2$ drops into chamber $m = 2$. **B.** Fixed-cell parity split (Theorem 3.1) and root-reflection integrality rigidity (Proposition 3.2): R_{mid} fixes the diagonal $V = 0$ (purple) in odd chambers $m = 2k - 1$, whereas R_{row} fixes the superdiagonal $V = -1, N = 2a^2$ (teal) in

even chambers $m = 2a$, which is also the unique positive locus where $R_{\mathrm{root}}(N) \in \mathbb{Z}$. **C.** Scaled phase discrepancy $m(\kappa_{\mathrm{root}} - \kappa_{\mathrm{mid}}) = (1 - \varepsilon^2)/2 \in (3/8, 1/2]$ across $\varepsilon = \sqrt{2N} - m \in (-1/2, 1/2)$ (Proposition 3.3).

4. Scaled-Square Branches, Pell Seams, and Classical Powers

4.1 Exact Floor-Selected Polynomial Branches

Proposition 4.1 (Floor-Branch Dictionary). *Fix positive integers $A, Q \in \mathbb{Z}_{\geq 1}$, and let $P \in \mathbb{Z}_{\geq 1}$ be the unique nearest integer to $Q\sqrt{2A}$. For each integer $k \geq 1$, define*

$$N_k = A(Qk)^2, \qquad \varepsilon = Q\sqrt{2A} - P, \qquad \delta = P^2 - 2AQ^2, \qquad \ell_k = \left\lfloor \frac{1}{2} + k\varepsilon \right\rfloor. \quad (4.1)$$

Then the chamber m_k, offset V_k, and cell coordinates (r_k, c_k) of N_k are given exactly by

$$m_k = Pk + \ell_k, \qquad V_k = -\delta k^2 - 2Pk\ell_k - \ell_k^2 - 1, \qquad (r_k, c_k) = \left(\frac{m_k + V_k + 1}{2}, \frac{m_k - V_k + 1}{2} \right). \quad (4.2)$$

Proof. By Proposition 1.2, $m_k = \lfloor \sqrt{2N_k} + \frac{1}{2} \rfloor = \lfloor k(P + \varepsilon) + \frac{1}{2} \rfloor = Pk + \ell_k$ because $Pk \in \mathbb{Z}$. Substituting $m_k = Pk + \ell_k$ and $2AQ^2 = P^2 - \delta$ into $V_k = 2N_k - m_k^2 - 1 = 2AQ^2k^2 - (Pk + \ell_k)^2 - 1$ yields (4.2). □

On any interval of integer indices k where the integer floor $\ell_k = L$ remains constant, m_k is linear in k and V_k is quadratic in k. That polynomial formula applies only on the floor-selected domain $L - \frac{1}{2} \leq k\varepsilon < L + \frac{1}{2}$.

Proposition 4.2 (Asymmetric First-Branch Criterion). *For the scaled-square path (4.1), a positive integer index $k \geq 1$ lies on the initial branch $\ell_k = 0$ if and only if*

$$\ell_k = 0 \quad \Longleftrightarrow \quad -P \leq \delta k < P. \quad (4.3)$$

Proof. The condition $\ell_k = 0$, i.e. $m_k = Pk$, holds iff $T_{Pk-1} < A(Qk)^2 \leq T_{Pk}$. Multiplying by 2 gives $(Pk)^2 - Pk < (P^2 - \delta)k^2 \leq (Pk)^2 + Pk$. Subtracting P^2k^2 and dividing by $k > 0$ yields $-P < -\delta k \leq P$, or equivalently $-P \leq \delta k < P$. □

The strict upper bound $\delta k < P$ (for $\delta > 0$) versus the closed lower bound $|\delta| k \leq P$ (for $\delta < 0$) comes directly from the half-open chamber interval $T_{m-1} < N \leq T_m$. On the first branch $\ell_k = 0$, the offset simplifies to $V_k + 1 = -\delta k^2$.

4.2 The Zero-Norm Domain

Proposition 4.3 (Zero-Norm Characterization). *For positive integers $A, Q \in \mathbb{Z}_{\geq 1}$ and $P = \mathrm{round}(Q\sqrt{2A})$,*

$$\delta = 0 \quad \Longleftrightarrow \quad A = 2b^2 \text{ and } P = 2bQ \text{ for some } b \in \mathbb{Z}_{\geq 1}, \qquad N_k = 2(bQk)^2. \quad (4.4)$$

In that case $\ell_k = 0$, $m_k = 2bQk$, and $V_k = -1$ for all $k \geq 1$ (the straight superdiagonal).

Proof. If $\delta = P^2 - 2AQ^2 = 0$, then $(P/Q)^2 = 2A \in \mathbb{Z}$, so P/Q is an integer whose square is even, hence $P/Q = 2b$ for some $b \in \mathbb{Z}_{\geq 1}$. Thus $A = 2b^2$ and $P = 2bQ$. The converse is immediate. □

In particular, $(A, P, Q) = (8, 4, 1)$ has $\delta = 0$. Stating that $\delta = 0$ occurs "only for $A = 2$" requires restricting A to be squarefree.

4.3 The Worked 181/128 Square Branch, First Departure, and Phase-Linearity Shift

Take $A = 1, P = 181, Q = 128$, for which $\delta = 181^2 - 2 \cdot 128^2 = 32761 - 32768 = -7$. By Proposition 4.2, the first branch $\ell_k = 0$ holds iff $7k \leq 181$, so its exact integer domain is $1 \leq k \leq 25$:

$$N_k = (128k)^2, \qquad m_k = 181k, \qquad V_k = 7k^2 - 1 \qquad (1 \le k \le 25). \quad (4.5)$$

The powers of four $4^7, 4^8, 4^9, 4^{10}, 4^{11}$ appear along this branch at $k = 1, 2, 4, 8, 16$ at cells $(94, 88), (195, 168), (418, 307), (948, 501)$, and $(2344, 553)$. The **first integer departure** of the full branch $N_k = (128k)^2$ occurs at $k = 26$, where $\ell_{26} = 1$, $m_{26} = 4707$, and $(r_{26}, c_{26}) = (13, 4695)$. By contrast, the **next sampled power of four** (4^{12}) occurs later at $k = 32$, where $\ell_{32} = 1$, $m_{32} = 5793$, $V_{32} = -4418$, and $(r_{32}, c_{32}) = (688, 5106)$. Distinguishing the full quadratic sequence from its sparse exponential subsequence prevents confusing $k = 26$ with $k = 32$.

Exact Phase-Linearity Shift on the First Branch. On $1 \le k \le 25$, substituting $m_k = 181k$ and $V_k = 7k^2 - 1$ into $2r_k = m_k + V_k + 1$ and $\widetilde{r}_k = m_k + V_k$ yields

$$2\kappa_{\mathrm{row}}(k) = \frac{2r_k}{m_k} = 1 + \frac{7}{181^2} m_k, \qquad 2\kappa_{\mathrm{mid}}(k) = \frac{\widetilde{r}_k}{m_k} = 1 + \frac{7}{181^2} m_k - \frac{1}{m_k} \qquad (1 \le k \le 25). \quad (4.6)$$

Thus the native row normalization $2\kappa_{\mathrm{row}}$ is strictly linear in the chamber m_k across the entire first branch, whereas the centered odd-row normalization $2\kappa_{\mathrm{mid}} = \widetilde{r}_k/m_k$ carries the exact reciprocal offset $-1/m_k$.

Remark 4.3a (Cross-Reference: The $(7, 180, 181)$ Reciprocal Bridge and the Ramanujan–Nagell Solutions). The arithmetic parameters of the 181/128 floor branch in (4.5)–(4.6) align with two structural bridges developed in [4, 16]:

1. **Grid 181/128 Branch Parameters ($\delta = -7,\ m_1 = 181 = 180{+}1$):** At the base step $k = 1$, the Ramanujan–Nagell relation $181^2 - 2 \cdot 128^2 = -7$ ($181^2 + 7 = 2^{15}$) places $N_1 = 128^2 = 16384 = 4^7$ in chamber $m_1 = 181 = 180 + 1$ immediately above $T_{180} = \frac{180 \cdot 181}{2} = 16290$, at $(r_1, c_1) = (94, 88)$ and offset $V_1 = 6$. In (4.6), the phase-linearity slope is $\frac{7}{181}$ per step k ($\frac{7}{181^2}$ per chamber unit m_k), governed by $|\delta| = 7$, while $2\kappa_{\mathrm{mid}}(k) - 2\kappa_{\mathrm{row}}(k) = -\frac{1}{m_k} = -\frac{1}{181k}$. Because $P = 181 = 180 + 1$ is prime, all $\varphi(181) = 180$ proper interior row phases $\kappa_{\mathrm{row}} = r/181$ ($1 \le r \le 180$) in chamber $m_1 = 181$ are reduced fractions, and at $n = 180$ the rising-factorial interior gcd of Theorem 8.3(5) evaluates to $g_{180} = 181$.
2. **Reciprocal, Catalan, and Degree-to-Radian π-Phase Bridge at $n = 7$ [4]:** At the third Mersenne index $n = 7 = 2^3 - 1$, the triangular number is $T_7 = 28$ ($2T_7 = 56 = 7 \cdot 8$). Because $n + 1 = 8$ is composite, $T_7/7! = 1/180$ with reduced denominator $b_7 = \frac{7!}{T_7} = \frac{5040}{28} = 180 = (3!)^2 C_3$ (the $j = 3$ odd-slice Catalan denominator in $T_{2j+1}/(2j+1)! = 1/[(j!)^2 C_j]$), giving
$$\frac{1}{7} \xrightarrow{\div 4} \frac{1}{T_7} = \frac{1}{28} \xrightarrow{\div 180} \frac{1}{7!} = \frac{1}{5040}, \qquad \left(\frac{1}{T_7}\right)^{\circ} = \frac{1}{7} \cdot \frac{1}{4} \cdot \frac{\pi}{180}\,\mathrm{rad} = \frac{\pi}{180\,T_7}\,\mathrm{rad} = \frac{\pi}{7!}\,\mathrm{rad} = \frac{\pi}{5040}\,\mathrm{rad},$$
while across dyadic halvings $i \ge 0$, $\frac{1}{7 \cdot 2^i} = 100^{-i}(A_i + \frac{1}{7})$ with $A_i = (50^i - 1)/7 \in \mathbb{Z}$ ($50 \equiv 1 \pmod 7$).
3. **The Value $u = 1/8$ and the Rational π Bracket [4]:** In the genus-zero triangular cosine product $\Pi_{\triangle}(u) = \prod_{n \ge 1}(1 - u/T_n) = -\frac{\cos(\frac{\pi}{2}\sqrt{1+8u})}{2\pi u}$ of [4] (Remark 6.6a), the value $u = 1/8$ gives the first-factor ratio $\frac{u}{T_1 - u} = \frac{1}{8T_1 - 1} = \frac{1}{7}$ and rational bounds $\frac{1}{8} < \pi - 3 < \frac{1}{7} \iff \frac{25}{8} < \pi < \frac{22}{7}$, with $\frac{11}{4} - \frac{7\pi}{8} = \frac{7}{8}\left(\frac{22}{7} - \pi\right)$. *Scope:* On the 181/128 floor branch, $(7, 180, 181)$ arises from $\delta = 181^2 - 2 \cdot 128^2 = -7$ and prime chamber $m_1 = 181$, whereas at $n = 7$ it arises from $7!/T_7 = 180$ and degree-to-radian conversion $\pi/180$; spatial chamber phase $\kappa_{\mathrm{row}} = r/m$ and angular radian conversion are kept distinct.
4. **The Complete Ramanujan–Nagell Solution Set [1, 16]:** Writing the odd chamber index as $m_1 = 2n + 1$ so $m_1^2 = 8T_n + 1$, the binary-square condition $m_1^2 + 7 = 8(T_n + 1) = 2^{\mu}$ is Nagell's Mersenne-triangular equation $M^2 + 7 = 2^{\mu} \iff T_n = 2^{\mu - 3} - 1$ [1], whose complete nonnegative integer solution set is
$$(n,\ M = 2n + 1,\ T_n,\ \mu) \in \big\{(0, 1, 0, 3),\ (1, 3, 1, 4),\ (2, 5, 3, 5),\ (5, 11, 15, 7),\ (90, \mathbf{181}, 4095, 15)\big\}.$$
   - *The largest solution $n = 90$ ($2n = 180,\ M = 181,\ T_{90} = 4095 = 2^{12} - 1,\ \mu = 15$):* Here $181^2 + 7 = 32768 = 2^{15}$, so on $1 \le k \le 25$, $2N(r_k, c_k) = m_k^2 + V_k + 1 = (181^2 + 7)k^2 = 2^{15}k^2 \iff N(r_k, c_k) = (128k)^2$, and $1 + \frac{7}{181^2} = \frac{2^{15}}{181^2} = \left(\frac{128\sqrt{2}}{181}\right)^2$.
   - *The solution $n = 5$ ($M = 11,\ T_5 = 15 = 2^4 - 1,\ \mu = 7$):* The solution $M = 11$ ($11^2 + 7 = 2^7$) yields the penultimate $V = 6$ binary square $N = 64 = 4^3$ in chamber $m = 11$ (Eq. 4.13), the unique nontrivial iterated triangular-factorial identity $T_{T_5} = T_{15} = 120 = 5!$ (since $T_{T_n} = n!$ fails for $n \in \{1, 2, 3, 4\}$ and for $n \ge 6$ Stirling's bound gives $n! > \frac{1}{8}n^4 \ge T_{T_n}$ for all $n \ge 7$ with $T_{21} = 231 \ne 720 = 6!$), and the largest pure power of 3 on the subdiagonal at $k = 11$, where $2(11)^2 + 1 = 243 = 3^5$ in chamber $m = 22$ (Eq. 4.14).

- *The reciprocal-π product:* In $\Pi_\triangle(-1/8) = \prod_{n\geq 1} \frac{(2n+1)^2}{8T_n} = \frac{4}{\pi}$ (§6.6, Theorem 6.5), the four positive solutions $n \in \{1, 2, 5, 90\}$ ($M \in \{3, 5, 11, 181\}$) are the unique stages where numerator $(2n+1)^2 = 2^\mu - 7$ and denominator $8T_n = 2^\mu - 8$ are simultaneously shifted powers of two.

4.4 Norm-One Seams, $k = 2P$ Returns, and the Square-Triangular Converse

Proposition 4.4 (Norm-One Launch and Triangular Seams). *Assume $\delta = P^2 - 2AQ^2 \in \{-1, +1\}$. Then the per-step root drift is*

$$\varepsilon = -\frac{\delta}{P + Q\sqrt{2A}}, \qquad \frac{1}{|\varepsilon|} = P + Q\sqrt{2A}. \quad (4.7)$$

At $k = 1$, the path launches at $m_1 = P, V_1 = -\delta - 1$. At $k = P$, the path lands on an exact triangular seam:

$$N_P = A(PQ)^2 = \begin{cases} T_{P^2} & \text{if } \delta = -1 \quad (\text{in chamber } m_P = P^2,\ \ell_P = 0), \\ T_{P^2-1} & \text{if } \delta = +1 \quad (\text{in chamber } m_P = P^2 - 1,\ \ell_P = -1). \end{cases} \quad (4.8)$$

Proof. Multiplying $(P - Q\sqrt{2A})(P + Q\sqrt{2A}) = \delta$ gives (4.7). At $k = P$, $2N_P = P^2(2AQ^2) = P^2(P^2 - \delta)$, so $N_P = \frac{P^2(P^2+1)}{2} = T_{P^2}$ when $\delta = -1$ and $N_P = \frac{(P^2-1)P^2}{2} = T_{P^2-1}$ when $\delta = +1$. By Proposition 4.2, $k = P$ satisfies $-P \leq \delta P < P$ for $\delta = -1$ ($\ell_P = 0$) and violates it by one chamber for $\delta = +1$ ($\ell_P = -1$). □

Proposition 4.5 (Exact Algebraic Return at $k = 2P$). *Under $\delta = P^2 - 2AQ^2 = \pm 1$, set $M = P^2 + 2AQ^2$. At $k = 2P$,*

$$m_{2P} = M = P^2 + 2AQ^2, \qquad V_{2P} = -2, \qquad (r_{2P}, c_{2P}) = \left(\frac{M-1}{2}, \frac{M+3}{2}\right), \quad (4.9)$$

corresponding to the quadratic-unit squaring identity $(P + Q\sqrt{2A})^2 = M + 2PQ\sqrt{2A}$.

Proof. Expanding $M^2 - 2A(2PQ)^2 = (P^2 - 2AQ^2)^2 = \delta^2 = 1$ gives $2N_{2P} = 2A(2PQ)^2 = M^2 - 1$. Since $M = 2P^2 - \delta \geq 3$ is odd, $(M - \frac{1}{2})^2 < M^2 - 1 < (M + \frac{1}{2})^2$, so Proposition 1.2 gives $m_{2P} = M$ and Proposition 1.1 gives $V_{2P} = 2N_{2P} - M^2 - 1 = -2$. □

Proposition 4.6 (Complete Square-Triangular Converse). *Every positive square-triangular number $T_n = L^2$ ($n, L \in \mathbb{Z}_{\geq 1}$) arises as an $A = 1$ norm-one seam (4.8): there exist unique positive integers $P, Q \in \mathbb{Z}_{\geq 1}$ with $P^2 - 2Q^2 = \delta \in \{-1, +1\}$ such that $L = PQ$ and $n = P^2$ ($\delta = -1$) or $n = P^2 - 1$ ($\delta = +1$).*

Proof. In $n(n+1) = 2L^2$, $\gcd(n, n+1) = 1$, so the odd member of $\{n, n+1\}$ is a square P^2 and the even member is twice a square $2Q^2$. Then $L = PQ$ and $P^2 - 2Q^2 = \mp 1$. Since $|Q\sqrt{2} - P| = 1/(P + Q\sqrt{2}) < 1/2$, $P = \text{round}(Q\sqrt{2})$, placing (P, Q) in the $A = 1$ branch family (4.8). □

4.5 Square Addresses on the Diagonal and the Subdiagonal

Proposition 4.7 (Diagonal-Square Pell Equivalence). *For any square address $N = Q^2$ ($Q \in \mathbb{Z}_{\geq 1}$) in chamber $m = \lfloor Q\sqrt{2} + \frac{1}{2} \rfloor$, its offset is $V = 2Q^2 - m^2 - 1$. Consequently:*

1. *$N = Q^2$ lies on the **diagonal** ($V = 0$) if and only if*

$$m^2 - 2Q^2 = -1, \qquad m = 2k - 1, \qquad Q^2 = k^2 + (k-1)^2 \quad (k = r = c). \quad (4.10)$$

2. *$N = Q^2$ lies on the **subdiagonal** ($V = +1$) if and only if*

$$m^2 - 2Q^2 = -2, \qquad m = 2k, \qquad Q^2 = 2k^2 + 1 \quad (r = k+1,\ c = k), \quad (4.11)$$

whose first positive instances are $(m, Q) = (4, 3), (24, 17), (140, 99)$ with square addresses $N = 9, 289, 9801$.

Proposition 4.8 (Complete Negative-Pell Descent for Diagonal Squares). *Every positive integer solution of* $m^2 - 2Q^2 = -1$ *is generated from the base solution* $(m_0, Q_0) = (1, 1)$ *by iterating*

$$(m, Q) \longmapsto (3m + 4Q,\ 2m + 3Q). \quad (4.12)$$

Proof. The map (4.12) preserves $m^2 - 2Q^2 = -1$ and positivity. Conversely, let (m, Q) be a positive solution with $Q > 1$. Testing $Q \in \{2, 3, 4\}$ gives $2Q^2 - 1 \in \{7, 17, 31\}$, none of which is a square, so $Q \geq 5$. Hence $\frac{4}{3} < \frac{m}{Q} = \sqrt{2 - 1/Q^2} < \frac{3}{2}$. Applying the inverse integral matrix gives

$$(m', Q') = (3m - 4Q,\ 3Q - 2m),$$

which satisfies $m' > 0$, $Q' > 0$, $(m')^2 - 2(Q')^2 = -1$, and $Q' < Q$ (since $m > Q \implies 3Q - 2m < Q$). Iterating this strict positive-integer descent must terminate at $Q = 1, m = 1$. Reversing the steps yields (4.12). □

The first five diagonal-square solutions are $(m, Q) = (1, 1), (7, 5), (41, 29), (239, 169), (1393, 985)$, with diagonal row indices $k = (m + 1)/2 \in \{1, 4, 21, 120, 697\}$ and square addresses $N = Q^2 \in \{1, 25, 841, 28561, 970225\}$.

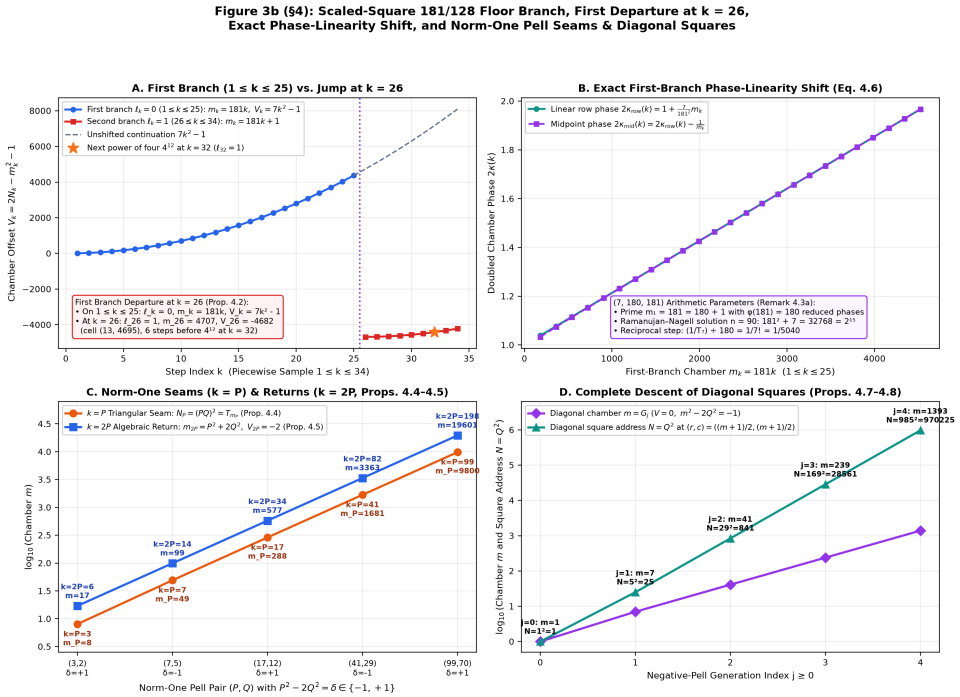


Figure 3b (Scaled-square 181/128 *floor branch, phase-linearity shift, and Pell seams/descent):* **A.** Piecewise sample across $1 \leq k \leq 34$ along $N_k = (128k)^2$ $(A = 1, P = 181, Q = 128, \delta = -7)$: the first polynomial branch $\ell_k = 0$ $(m_k = 181k, V_k = 7k^2 - 1$, Eq. (4.6)) holds strictly on $1 \leq k \leq 25$ (carrying $4^7, \ldots, 4^{11}$ at $k = 1, 2, 4, 8, 16$), departs first at $k = 26$ $(\ell_{26} = 1, m_{26} = 4707, (13, 4695))$, and reaches the next power sample 4^{12} at $k = 32$ $(m_{32} = 5793, V_{32} = -4418)$. **B.** On the first branch $1 \leq k \leq 25$, native row phase $2\kappa_{\text{row}}(k) = 1 + \frac{7}{181^2} m_k$ is strictly linear in m_k, whereas $2\kappa_{\text{mid}}(k) = 2\kappa_{\text{row}}(k) - 1/m_k$ carries the reciprocal offset $-1/m_k$ (4.6). **C.** Logarithmic chamber growth of diagonal squares $(m^2 - 2Q^2 = -1$, Proposition 4.8), subdiagonal squares $(m^2 - 2Q^2 = -2)$, and norm-one first-column-edge triangular seams $T_n = (PQ)^2$ at $k = P$ (Propositions 4.4–4.6).

4.6 Classical Classifications of Powers on the Rails

Several visually prominent power intersections on the rails reduce to classical exponential Diophantine equations:

- **Powers of 2 on the First-Row Edge and Offset $V = 6$:** On the first-row edge $(1, c)$, $N = 2^j$ $(j \geq 0)$ is equivalent to $T_{c-1} + 1 = 2^j$, or

$$(2c - 1)^2 + 7 = 2^{j+3}. \quad (4.13)$$

By Nagell's theorem [1], the positive odd solutions $2c-1$ are $1, 3, 5, 11, 181$, giving $j \in \{0, 1, 2, 4, 12\}$ and addresses $N \in \{1, 2, 4, 16, 4096\}$. Similarly, since odd powers of 2 sit on $V = -1$ (2.5), an even power 4^k sits at offset $V = 6$ iff $P^2 + 7 = 2^{2k+1}$ with $P = \text{round}(2^k\sqrt{2})$; Nagell's list intersected with the nearest-integer bound leaves $P \in \{11, 181\}$, so **only** 64 **($m = 11$) and** 16384 **($m = 181$) are powers of** 2 **with** $V = 6$.

- **Powers of** 3 **on the Subdiagonal:** On the subdiagonal $(k+1, k)$, $N = 3^j$ $(k, j \geq 1)$ is

$$2k^2 + 1 = 3^j. \quad (4.14)$$

By Leu and Li [2], the only positive solutions are $(k, j) \in \{(1, 1), (2, 2), (11, 5)\}$, giving addresses $N \in \{3, 9, 243\}$.

- **Powers of** 5 **on the Diagonal:** On the diagonal (k, k), $N = 5^j$ $(k, j \geq 1)$ is

$$(2k-1)^2 + 1 = 2 \cdot 5^j. \quad (4.15)$$

Cohn's perfect-Pell-power lemma [3] excludes $j > 2$ for base 5, leaving $(k, j) \in \{(2, 1), (4, 2)\}$, diagonal chambers $m = 2k - 1 \in \{3, 7\}$, and diagonal addresses $N = N(k, k) = 5^j \in \{5, 25\}$ (where $(2k-1)^2 + 1 = 2N \in \{10, 50\}$; Cohn's exceptional higher-power solution for an arbitrary base gives $(239^2 + 1)/2 = 28561 = 13^4$ at $k = 120$). Moreover, for the fixed base 5 in (4.15), **no appeal to Ljunggren's $k = 4$ theorem is required**, using two short self-contained prerequisites: (i) in $\mathbb{Z}[\sqrt{10}]$, any integral unit $\omega = A + C\sqrt{10} > 1$ of norm $A^2 - 10C^2 = \pm 1$ has positive integers $A, C \geq 1$, where $C = 1$ gives $A = 3$ ($\varepsilon_{10} = 3 + \sqrt{10}$ of norm -1) and $C \geq 2$ gives $A + C\sqrt{10} \geq 1 + 2\sqrt{10} > \varepsilon_{10}$, so choosing $a \geq 1$ with $\varepsilon_{10}^a \leq \omega < \varepsilon_{10}^{a+1}$ places $\omega\varepsilon_{10}^{-a} \in [1, \varepsilon_{10})$ and forces $\omega = \varepsilon_{10}^a$ (with a odd whenever $\text{Norm}(\omega) = -1$); and (ii) for the Pell recurrence matrix $G = \left(\begin{smallmatrix} 2 & 1 \\ 1 & 0 \end{smallmatrix}\right)$, $G^3 = \left(\begin{smallmatrix} 12 & 5 \\ 5 & 2 \end{smallmatrix}\right) \equiv 2I \pmod 5$, so $P_{3a+i} \equiv 2^a P_i \pmod 5$ $(i \in \{0, 1, 2\})$ with $P_0 = 0, P_1 = 1, P_2 = 2$, whence $5 \mid P_n \iff 3 \mid n$. Consequently:

  - When $j = 2b + 1$ is odd, (4.15) is $(2k-1)^2 - 10(5^b)^2 = -1$, so Prerequisite (i) gives $5^b = C_{2a+1} = \sum_{i=0}^{a} \binom{2a+1}{2i+1} 3^{2(a-i)} 10^i$ in $(3 + \sqrt{10})^{2a+1}$ $(a \geq 0)$. Using $\binom{2a+1}{2i+1} = \frac{2a+1}{2i+1}\binom{2a}{2i}$ and $v_5(2i+1) \leq i - 1 < i$ for all $i \geq 1$, the i-th summand has valuation $\geq v_5(2a+1) + i - v_5(2i+1) \geq v_5(2a+1) + 1 > v_5(2a+1)$ (a sharp one-unit gap, attained at $a = 1, i = 1$ where $(3 + \sqrt{10})^3 = 117 + 37\sqrt{10}$ has $37 = 27 + 10$ with $v_5(10) = 1$). Thus the $i = 0$ term $(2a+1)3^{2a}$ strictly dominates the 5-adic valuation, forcing $v_5(C_{2a+1}) = v_5(2a+1)$ and hence $5^b \mid (2a+1)$. Since $C_{2a+1} \geq (2a+1)3^{2a} > 2a + 1$ for all $a \geq 1$, this holds only at $a = 0, b = 0, j = 1$ ($k = 2$, chamber $m = 3$, diagonal address $N = 5$).
  - When $j = 2b$ is even ($b \geq 1$), (4.15) is $(2k-1)^2 - 2(5^b)^2 = -1$, so **Proposition 4.8** and Prerequisite (ii) give $(2k-1) + 5^b\sqrt{2} = (1 + \sqrt{2})^{2n+1}$ with $5^b = P_{2n+1}$ ($P_0 = 0, P_1 = 1, P_{i+2} = 2P_{i+1} + P_i$) and $3 \mid (2n+1)$. Writing $2n + 1 = 3(2a+1)$ $(a \geq 0)$ and expanding $(1 + \sqrt{2})^{3(2a+1)} = (7 + 5\sqrt{2})^{2a+1}$ gives $P_{3(2a+1)} = 5\sum_{i=0}^{a} \binom{2a+1}{2i+1} 49^{a-i} 50^i$. Because $50^i = 2^i \cdot 5^{2i}$ and $v_5(2i+1) \leq i-1$ implies $2i - v_5(2i+1) \geq i+1 \geq 2$ for all $i \geq 1$, each $i \geq 1$ summand has valuation $\geq 1 + v_5(2a+1) + 2i - v_5(2i+1) \geq 1 + v_5(2a+1) + 2$, so $v_5(P_{3(2a+1)}) = 1 + v_5(2a+1)$, forcing $5^{b-1} \mid (2a+1)$. Since $P_{3(2a+1)}/5 \geq (2a+1)49^a > 2a + 1$ for all $a \geq 1$, this holds only at $a = 0, b = 1, j = 2$ ($k = 4$, chamber $m = 7$, diagonal address $N = 25$).

Sources. The completeness statements (4.13) and (4.14) are taken from [1, 2]; (4.15) for base 5 follows both from [3] and from the self-contained 5-adic argument above. In (4.14), factoring $(1 + k\sqrt{-2})(1 - k\sqrt{-2}) = (1 + \sqrt{-2})^j(1 - \sqrt{-2})^j$ in the Euclidean domain $\mathbb{Z}[\sqrt{-2}]$ reduces $2k^2 + 1 = 3^j$ to $\text{Re}\big((1 + \sqrt{-2})^j\big) = \pm 1$ $(j \in \{1, 2, 5\})$.

5. Rational Carriers, the Route to 5, and the Diagonal Bridge

5.1 The Midpoint Fold Circle Map and Unique Rational Carrier Parameterization

In [5, §2.1], the analytic fold operator $\mathfrak{f}(w) = w(1-w) = (1 - \mathcal{J}(w)^2)/4$ is applied to the complex argument s of $\xi(s)$ to produce $q = \mathfrak{f}(s)$. On the discrete address grid, applying the same operators $(\mathcal{J}, \mathfrak{f})$ to the cell-midpoint phase $\kappa_{\text{mid}} = \widetilde{r}/(2m)$ defines the **centered carrier map** on the open upper unit semicircle:

$$\mathcal{C}(r, c) = \Big(\mathcal{J}(\kappa_{\text{mid}}),\, 2\sqrt{\mathfrak{f}(\kappa_{\text{mid}})}\Big) = \left(\frac{\widetilde{r} - \widetilde{c}}{\widetilde{r} + \widetilde{c}},\, \frac{2\sqrt{\widetilde{r}\widetilde{c}}}{\widetilde{r} + \widetilde{c}}\right) = \left(\frac{V}{m},\, \frac{\sqrt{\widetilde{r}\widetilde{c}}}{m}\right). \quad (5.1)$$

Because $r, c \geq 1$, both odd legs $\widetilde{r} = 2r - 1$ and $\widetilde{c} = 2c - 1$ are positive, so the second coordinate of $\mathcal{C}(r, c)$ is strictly positive and the boundary endpoints $(\pm 1, 0)$ are excluded. This is a specified algebraic map on positive grid cells, distinct from polar-shell embeddings $Z = \sqrt{d}\, e^{2\pi i h/d}$ and from κ_{root}.

Theorem 5.1 (Unique Rational Carrier Classification). *For a positive integer cell $(r,c) \in \mathbb{Z}^2_{\geq 1}$, the circle point $\mathcal{C}(r,c)$ in (5.1) belongs to $\mathbb{Q}^2$ if and only if there exist* ***unique*** *positive odd integers $U, W, \lambda \in \mathbb{Z}_{\geq 1}$ with $\gcd(U,W) = 1$ such that*

$$(\widetilde{r}, \widetilde{c}) = \lambda(U^2, W^2). \quad (5.2)$$

Equivalently, the cell (r,c), its chamber m, its primitive first chamber m_0, its carrier point $\mathbf{p}(U,W) = \mathcal{C}(r,c)$, and its midpoint phase κ_{mid} are given by

$$(r,c) = \left(\frac{\lambda U^2 + 1}{2}, \frac{\lambda W^2 + 1}{2}\right), \qquad m = \lambda m_0, \qquad m_0 = \frac{U^2 + W^2}{2}, \quad (5.3)$$

$$\mathbf{p}(U,W) = \left(\frac{U^2 - W^2}{2m_0}, \frac{UW}{m_0}\right), \qquad \kappa_{\mathrm{mid}} = \frac{U^2}{U^2 + W^2}. \quad (5.4)$$

Here $\lambda = \gcd(\widetilde{r}, \widetilde{c})$ is the odd ray-repeat scale, the reduced denominator of κ_{mid} is $2m_0$, and the primitive first chamber satisfies

$$m_0 \equiv 1 \pmod 4, \qquad \left(\frac{U^2 - W^2}{2}, UW, m_0\right) \text{ is a primitive Pythagorean triple} \quad (5.5)$$

(with signed first leg, reducing to the degenerate triple $(0,1,1)$ at $(U,W) = (1,1)$).

Proof. Since $V/m \in \mathbb{Q}$ for every cell, $\mathcal{C}(r,c) \in \mathbb{Q}^2$ iff $\sqrt{\widetilde{r}\widetilde{c}} \in \mathbb{Q}$, which holds iff the odd integer $\widetilde{r}\widetilde{c}$ is a perfect square. Let $\lambda = \gcd(\widetilde{r}, \widetilde{c})$, which is a positive odd integer. Then $\widetilde{r}/\lambda$ and $\widetilde{c}/\lambda$ are coprime positive odd integers whose product $(\widetilde{r}\widetilde{c})/\lambda^2$ is a rational square, hence an integer square. By coprimality, $\widetilde{r}/\lambda = U^2$ and $\widetilde{c}/\lambda = W^2$ for unique positive odd coprime integers U, W. Conversely, (5.2) makes $\sqrt{\widetilde{r}\widetilde{c}} = \lambda UW \in \mathbb{Z}$. For a fixed oriented point $\mathbf{p} = (p_1, p_2)$, $p_2/(1-p_1) = U/W$ determines the coprime positive pair (U,W) uniquely, while $\lambda = m/m_0$ runs over all positive odd integers. Since any odd square is $\equiv 1 \pmod 8$, $U^2 + W^2 \equiv 2 \pmod 8$, so $m_0 = (U^2 + W^2)/2 \equiv 1 \pmod 4$. □

5.2 First Chambers $5, 13, 17$, the Route to 5, and Multi-Ray Chambers

The only primitive diagonal carrier has $U = W = 1$, giving $\mathbf{p}(1,1) = (0,1)$ at first chamber $m_0 = 1$, cell $(1,1)$. For any nontrivial primitive carrier ($U \neq W$), the smallest unordered pair of distinct positive odd coprime integers is $\{3,1\}$. Therefore, **the least nontrivial rational carrier chamber in the centered chart is** $m_0 = (3^2 + 1^2)/2 = 5$, realized at cell $(5,1)$ with $\mathbf{p}(3,1) = (4/5, 3/5)$ and its transpose $(1,5)$ with $\mathbf{p}(1,3) = (-4/5, 3/5)$.

Primitive Pair (U,W)	**First Chamber** $m_0 = \frac{U^2+W^2}{2}$	**First Cell** (r,c)	**Carrier Point** $\mathbf{p}(U,W)$	**Midpoint Phase** κ_{mid}	**Role in Classification**
$(1,1)$	1	$(1,1)$	(0, 1)	1/2	Unique diagonal carrier (45° record $j=0$)
$(3,1)$	5	$(5,1)$	(4/5, 3/5)	9/10	Least nontrivial chamber (45° record $j=1$)
$(5,1)$	13	$(13,1)$	(12/13, 5/13)	25/26	Second nontrivial chamber (not a 45° record)
$(5,3)$	17	$(13,5)$	(8/17, 15/17)	25/34	Third nontrivial chamber; its transpose $(3,5)$ wins for $(A,C) = (3,4)$ at $M = 17$
$(7,1)$	25	$(25,1)$	(24/25, 7/25)	49/50	First composite primitive carrier chamber
$(7,3)$	29	$(25,5)$	(20/29, 21/29)	49/58	Second nontrivial 45° Pell record ($j=2$)

Three scope clarifications govern this classification:

1. **Prime vs. Composite First Chambers:** By (5.5) and Fermat's two-square theorem ($p = A^2 + C^2 \implies U = A + C, W = |A - C|$), an odd prime p occurs as a primitive first chamber m_0 if and only if $p \equiv 1 \pmod 4$. However, m_0 is not a prime generator: $(U, W) = (7, 1)$ gives the composite first chamber $m_0 = 25$.
2. **Non-Injectivity of m_0 Across Distinct Rays:** A primitive first chamber m_0 need not determine a unique carrier ray, even up to transpose. At $m_0 = 65 = 5 \cdot 13$, the two coprime odd pairs $(U, W) = (11, 3)$ and $(9, 7)$ both satisfy $(11^2 + 3^2)/2 = (9^2 + 7^2)/2 = 65$, yielding first cells $(61, 5)$ and $(41, 25)$ and distinct non-mirror points $(56/65, 33/65)$ and $(16/65, 63/65)$.
3. **Exclusion of Opposite-Parity Targets from $\mathcal{C}(r, c)$:** In the continuous extension $\kappa_{\text{mid}} = a^2/(a^2 + 1)$, setting $a = 2$ gives $(3/5, 4/5)$. Because rational centered cells require $a = U/W$ with U, W both odd, $(3/5, 4/5)$ is excluded from the centered rational carrier chart (whereas $(4/5, 3/5)$ is admitted at $m_0 = 5$ via $a = 3/1$). Appendix A gives the complete budget approximation theory for excluded targets and shows how adjoining the leg-sum phase $\kappa_{\text{leg}} = r/(m + 1)$ realizes $(3/5, 4/5)$ at cell $(4, 1)$, chamber 4.

5.3 The Bidirectional Carrier-to-Diagonal Square Bridge

The 45° Pell carrier record sequence begins at $(U_0, W_0) = (1, 1)$ and advances by

$$(U_{j+1}, W_{j+1}) = (2U_j + W_j,\, U_j) \qquad (j \geq 0). \quad (5.6)$$

Appendix A (Theorem A.1) proves that for every chamber budget $M \geq 1$, the last available ray in (5.6) with $m_{0,j} \leq M$ uniquely minimizes Euclidean chord distance on $\mathcal{C}(r, c)$ to the 45° point $\mathbf{p}_* = (1/\sqrt{2}, 1/\sqrt{2})$. Here we prove that this carrier sequence maps bijectively to the diagonal-square Pell sequence of Proposition 4.8.

Theorem 5.2 (Bidirectional Bridge Between Carrier First Chambers and Diagonal Squares). *For each primitive carrier pair (U, W), define its triangle legs and their sum by*

$$m_0 = \frac{U^2 + W^2}{2}, \qquad \ell_1 = \frac{U^2 - W^2}{2}, \qquad \ell_2 = UW, \qquad G = \ell_1 + \ell_2, \qquad \delta_{\text{leg}} = \ell_1 - \ell_2. \quad (5.7)$$

Then $G^2 + \delta_{\text{leg}}^2 = 2m_0^2$. In particular, $|\delta_{\text{leg}}| = 1$ holds if and only if $(U, W) = (U_j, W_j)$ (or its transpose for $j = 0$) in the Pell carrier recurrence (5.6), and in that case $G_j^2 + 1 = 2m_{0,j}^2$. The grid diagonal cell in diagonal chamber $m_{\text{diag}} = G_j$ at row and column $r_{\text{diag}} = c_{\text{diag}} = (G_j + 1)/2$ then carries the exact square address

$$N_{\text{diag}}(G_j) = \frac{G_j^2 + 1}{2} = m_{0,j}^2. \quad (5.8)$$

Conversely, every positive integer solution (m, Q) of the diagonal-square equation $m^2 - 2Q^2 = -1$ in (4.10) determines a unique primitive carrier pair (U, W) in (5.6) with first carrier chamber $m_0 = Q$ and leg sum $G = m$.

Proof. Direct expansion gives

$$G^2 + \delta_{\text{leg}}^2 = (\ell_1 + \ell_2)^2 + (\ell_1 - \ell_2)^2 = 2(\ell_1^2 + \ell_2^2) = 2\left(\frac{(U^2 - W^2)^2}{4} + U^2W^2\right) = \frac{(U^2 + W^2)^2}{2} = 2m_0^2.$$

Along (5.6), $\delta_{\text{leg},j+1} = \frac{(2U_j + W_j)^2 - U_j^2}{2} - (2U_j + W_j)U_j = -\left(\frac{U_j^2 - W_j^2}{2} - U_jW_j\right) = -\delta_{\text{leg},j}$, so $\delta_{\text{leg},j} = (-1)^{j+1}$ and $G_j^2 + 1 = 2m_{0,j}^2$. By Proposition 4.7, the diagonal cell in chamber $m_{\text{diag}} = G_j$ has address $N_{\text{diag}} = (G_j^2 + 1)/2 = m_{0,j}^2$.

Conversely, let (m, Q) be any positive integer solution of $m^2 + 1 = 2Q^2$. Set $G = m$ and $m_0 = Q$ (with $(U, W) = (1, 1)$ for $G = m_0 = 1$). For $G > 1$, choose $\delta_{\text{leg}} \in \{-1, +1\}$ so that $\ell_1 = (G + \delta_{\text{leg}})/2$ is even and $\ell_2 = (G - \delta_{\text{leg}})/2$ is odd. Then $\ell_1^2 + \ell_2^2 = (G^2 + 1)/2 = m_0^2$ and $\gcd(\ell_1, \ell_2) = 1$. Consequently $m_0 + \ell_1$ and $m_0 - \ell_1$ are coprime positive odd integers whose product is $m_0^2 - \ell_1^2 = \ell_2^2$, forcing $m_0 + \ell_1 = U^2$ and $m_0 - \ell_1 = W^2$ for unique coprime positive odd integers $U > W$ with $|\ell_1 - \ell_2| = 1$. By the descent in Theorem A.1, $(U, W) = (U_j, W_j)$. □

Record Index j	**Primitive Carrier Pair (U_j, W_j)**	**Carrier First Chamber $m_{0,j}$**	**First Carrier Cell (r, c)**	**Right-Triangle Legs $(\ell_{1,j}, \ell_{2,j})$**	**Grid Diagonal Chamber $m_{\text{diag}} = G_j$**	**Grid Diagonal Cell (r, r)**	**Diagonal Square Address $N_{\text{diag}} = m_{0,j}^2$**
0	$(1, 1)$	1	$(1, 1)$	$(0, 1)$ (degenerate)	1	$(1, 1)$	$1 = 1^2$
1	$(3, 1)$	5	$(5, 1)$	$(4, 3)$	7	$(4, 4)$	$25 = 5^2$
2	$(7, 3)$	29	$(25, 5)$	$(20, 21)$	41	$(21, 21)$	$841 = 29^2$
3	$(17, 7)$	169	$(145, 25)$	$(120, 119)$	239	$(120, 120)$	$28{,}561 = 169^2$
4	$(41, 17)$	985	$(841, 145)$	$(696, 697)$	1393	$(697, 697)$	$970{,}225 = 985^2$

The first nondegenerate bridge is the 3–4–5 triangle ($j = 1$): its hypotenuse is the **carrier first chamber** $m_{0,1} = 5$ (at carrier cell $(5, 1)$), its leg sum is the **grid diagonal chamber** $m_{\text{diag}} = 4 + 3 = 7$ (at diagonal cell $(4, 4)$), and the **diagonal square address is** $N_{\text{diag}} = 5^2 = 25$. Naming these three distinct roles resolves the index ambiguity between the sequence $1, 5, 29, 169, 985, \ldots$ and the diagonal chamber sequence $1, 7, 41, 239, 1393, \ldots$.

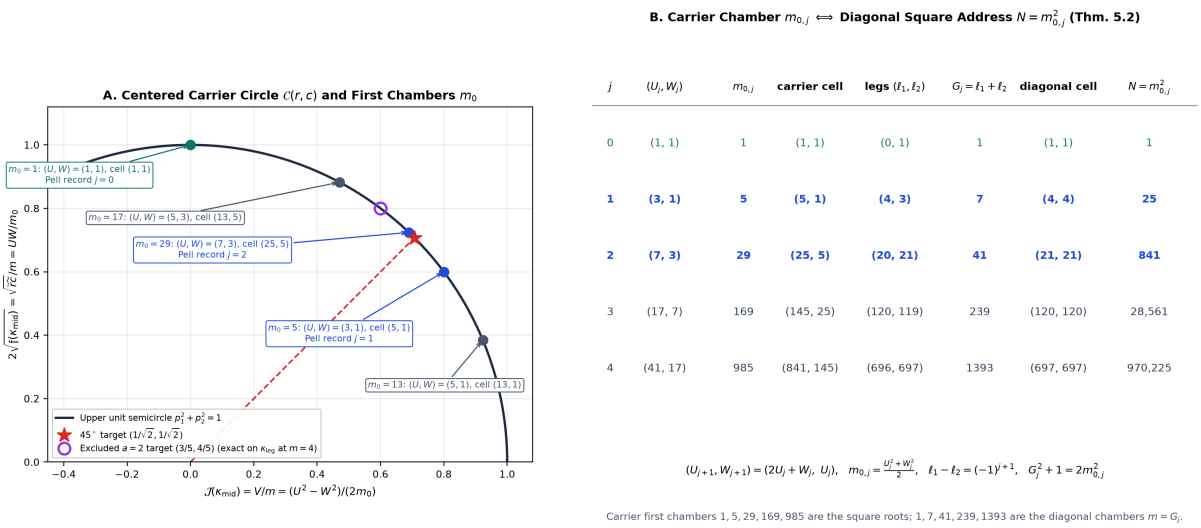


Figure 4 (Rational carriers and the carrier-to-diagonal bridge): The centered carrier map $\mathcal{C}(r, c)$ of (5.1) places the odd-square cells $(\widetilde{r}, \widetilde{c}) = \lambda(U^2, W^2)$ on rational points of the upper unit semicircle. The 45° Pell records $(U_j, W_j) = (1, 1), (3, 1), (7, 3), (17, 7), \ldots$ have first chambers $m_{0,j} = 1, 5, 29, 169, \ldots$, and Theorem 5.2 sends each to the diagonal chamber $G_j = 1, 7, 41, 239, \ldots$ whose diagonal cell carries the square address $N = m_{0,j}^2$.

6. A Bounded View of the Address Set

6.1 The Bounded Address Sheet, Closure, and Convex Hull

Dividing each row index by its chamber scale maps the infinite quadrant into a bounded planar region while preserving address order. Each address N, in chamber m with $m + 1 = r + c \geq 2$, maps to a planar site $\mathbf{p}_N$ in the second quadrant [7]:

$$m + 1 = \left\lfloor \sqrt{2N - \frac{3}{4}} + \frac{3}{2} \right\rfloor \geq 2, \qquad r = N - T_{m-1}, \qquad \mathbf{p}_N = (p_1, p_2) = \left(-\frac{r}{m+1}, \frac{1}{m+1} \right), \quad (6.1)$$

where $(p_1, p_2) \in \mathbb{R}^2$ are the coordinates of the **address sheet**. For each chamber $m \geq 1$, the address N satisfies $T_{m-1} < N \leq T_m$ and $1 \leq r \leq m$. At height $p_2 = 1/(m + 1) \in (0, \frac{1}{2}]$, the row's extreme sites are $(-p_2, p_2)$ (at $r = 1$) and $(p_2 - 1, p_2)$ (at $r = m$).

Proposition 6.1 (Discrete Sites, Topological Closure, and Isosceles Right Hull). *Every site $\mathbf{p}_N$ in (6.1) satisfies $0 < p_2 \leq \frac{1}{2}$ and $p_2 - 1 \leq p_1 \leq -p_2$. The topological closure of the infinite site set $\{\mathbf{p}_N : N \geq 1\}$ in $\mathbb{R}^2$ is precisely*

$$\overline{\{\mathbf{p}_N : N \geq 1\}} = \{\mathbf{p}_N : N \geq 1\} \cup \big([-1, 0] \times \{0\}\big), \quad (6.2)$$

so the sites are not dense in the interior of the triangle. The closed convex hull of the site set is the isosceles right triangle $\mathrm{conv}(A, B, C)$ *with vertices*

$$A = (-1, 0), \qquad B = (0, 0), \qquad C = \left(-\frac{1}{2}, \frac{1}{2}\right), \quad (6.3)$$

whose right angle is at the apex $C = \mathbf{p}_1$ *(*$AB^2 = 1$, $AC^2 = BC^2 = \frac{1}{2}$, $(A - C) \cdot (B - C) = 0$*).*

Proof. Any sequence of sites converging to a point with limiting height $p_2 > 0$ has bounded m, hence lies in a finite subset of $\{\mathbf{p}_N\}$ and is eventually constant. For $p_2 = 0$ and any $a \in [0, 1]$, choosing $r_m \in \{1, \ldots, m\}$ with $r_m/(m+1) \to a$ as $m \to \infty$ produces the limiting base point $(-a, 0)$. Since every $\mathbf{p}_N$ lies in $\mathrm{conv}(A, B, C)$ and A, B, C belong to the closure (6.2), the closed convex hull of the infinite site set is $\mathrm{conv}(A, B, C)$. (A finite prefix $m \leq m_{\max}$ has a smaller hull; at $m_{\max} = 1$ it is the singleton $\{C\}$.) □

Example (Primitive columns of the address sheet). In the finite crop $1 \leq r, c \leq L$, write $(r, c) = k(a, b)$, where $k = \gcd(r, c)$ and $\gcd(a, b) = 1$. Equations (1.1) and (6.1) give

$$N = T_{k(a+b)-2} + ka, \qquad \mathbf{p} = \left(-\frac{a}{a+b}, \frac{1}{k(a+b)}\right).$$

The primitive ordered pair fixes the vertical column; the common scale fixes the height. For $L = 6$, the cells $(2, 1), (4, 2), (6, 3)$ have addresses $3, 14, 34$ and heights $1/3, 1/6, 1/9$, all at $p_1 = -2/3$. Keeping the full point retains the pair. Discarding height identifies its common multiples. The conserved fraction is the leg-sum phase $\kappa_{\mathrm{leg}} = r/(r + c)$, distinct from the row and midpoint phases below and from the odd-leg gcd in Theorem 5.1.

Figure 5 (§6.1): One Primitive Ratio, Three Grid Addresses — keeping both coordinates recovers the cell; keeping only p_1 keeps the ratio 2:1 and loses the scale k

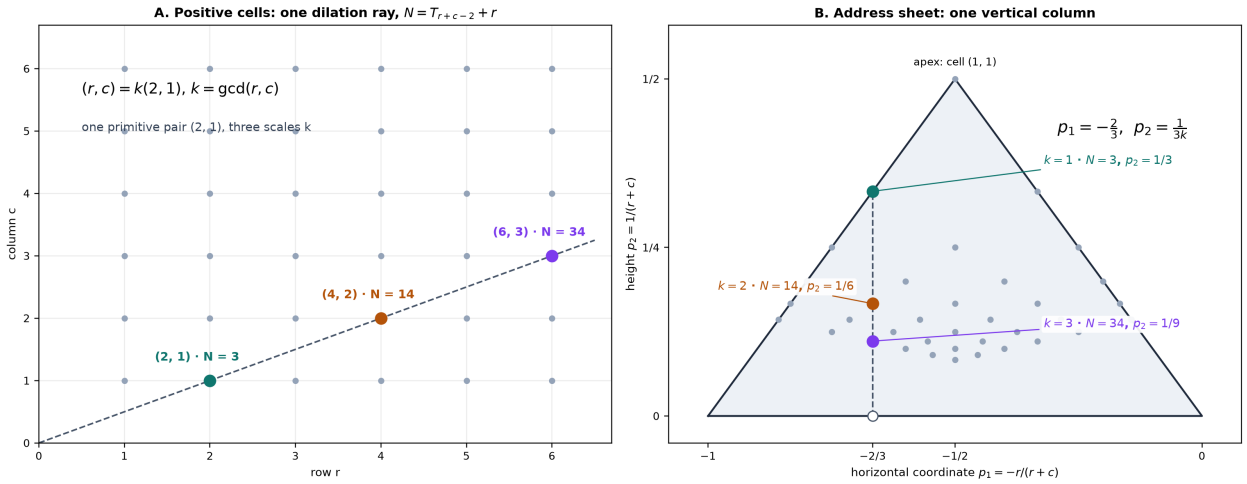


Figure 5 (Source map & coordinate recovery): On the finite crop $1 \leq r, c \leq 6$, writing $(r, c) = k(a, b)$ with $k = \gcd(r, c)$ and $\gcd(a, b) = 1$ places all common multiples of a primitive cell (a, b) on the vertical column $p_1 = -a/(a + b)$ at heights $p_2 = 1/[k(a + b)]$. For $(a, b) = (2, 1)$, the cells $(2, 1), (4, 2), (6, 3)$ carrying addresses $N = 3, 14, 34$ lie on $p_1 = -2/3$ at heights $1/3, 1/6, 1/9$; the open base marker $(-2/3, 0)$ is a limit point in the closure (6.2), not a discrete Grid cell.

Remark 6.1b (Euler Totient $\varphi(m + 1)$ *Chamber Bridge, Denominator-20 Partition, and Square Coprime Count).* Let Euler's totient $\varphi(M) = \#\{1 \leq j \leq M : \gcd(j, M) = 1\} = M \prod_{p|M}(1 - 1/p)$ count the positive integers up to M that are coprime to M ($\varphi(1) = 1$; φ counts coprime numerators, composite ones included, not primes). In chamber m, every cell satisfies $r + c = m + 1$ with $1 \leq r \leq m$ and $c = m + 1 - r$, so $\gcd(r, c) = \gcd(r, m + 1)$. Because the omitted endpoint $r = m + 1$ ($c = 0$) is not coprime to $m + 1$ for $m \geq 1$, the number of primitive cells (r, c) at height $1/(m + 1)$ of the address sheet (6.1) is exactly

$$\#\{(r,c)\in\mathbb{Z}^2_{\geq 1} : r+c=m+1,\ \gcd(r,c)=1\}=\varphi(m+1), \qquad \sum_{\substack{d\mid(m+1)\\ d>1}}\varphi(d)=m \quad (m\geq 1).$$

For $m=8$ ($r+c=9$), the $\varphi(9)=6$ primitive cells are $(1,8),(2,7),(4,5),(5,4),(7,2),(8,1)$ (including the composite coordinates 4 and 8 because $\gcd(4,9)=\gcd(8,9)=1$). For $m=19$ ($r+c=20$), reducing the twenty fractions $1/20,\dots,20/20$ partitions them by reduced denominator $d\mid 20$: $d=20$ retains the $\varphi(20)=20(1-1/2)(1-1/5)=8$ primitive cells $(1,19),(3,17),(7,13),(9,11),(11,9),(13,7),(17,3),(19,1)$ at height $p_2=1/20$ (paired by $r\leftrightarrow 20-r$ so complementary native abscissae sum to -1), while $d=10,5,4,2$ contribute $\varphi(10)+\varphi(5)+\varphi(4)+\varphi(2)=4+4+2+1=11$ scaled cells lifted from earlier primitive columns by $k=20/d$, and $d=1$ (20/20, i.e., $(20,0)$) lies outside the positive quadrant, giving $8+11=19=m$. Keep the predicates distinct: primitive cells in chamber m use the leg-sum denominator $m+1$ and count $\varphi(m+1)$, whereas asking which native row fractions $\kappa_{\mathrm{row}}=r/m$ are already in lowest terms requires $\gcd(r,m)=1$ and counts $\varphi(m)$ (and the odd-square carrier condition in Theorem 5.1 imposes the further restriction $(\widetilde{r},\widetilde{c})=\lambda(U^2,W^2)$). Separately, in the $L\times L$ square $1\leq a,b\leq L$, the lower triangle $1\leq b\leq a\leq L$ contains $\sum_{k=1}^{L}\varphi(k)$ coprime pairs and shares only $(1,1)$ with the upper triangle, so under independent uniform sampling on $\{1,\dots,L\}^2$,

$$C_2(L)=\#\{1\leq a,b\leq L:\gcd(a,b)=1\}=2\sum_{k=1}^{L}\varphi(k)-1, \qquad \Pr(\gcd(a,b)=1)=\frac{C_2(L)}{L^2}\underset{L\to\infty}{\longrightarrow}\frac{6}{\pi^2}=\frac{1}{\zeta(2)},$$

by standard Möbius inversion $\sum_{1\leq a,b\leq L,\,\gcd(a,b)=1}1=\sum_{i=1}^{L}\mu(i)\lfloor L/i\rfloor^2=\frac{6}{\pi^2}L^2+O(L\log L)$ [17].

Remark 6.1a (Unit-Square Frame, Half-Diagonal Length $1/\sqrt{2}$, Row vs. Midpoint Half-Phase Pencils, and Reflected Extension C_-). The address sheet (6.1) sits inside the unit square $Q=[-1,0]\times[0,1]$ with corners $O=B=(0,0)$, $A=(-1,0)$, $B_{\mathrm{ul}}=(-1,1)$, and $D=(0,1)$. Its first positive site ($m=r=c=N=1$) is the unit-square center $C_+=C=(-1/2,1/2)$. Holding $r=1$ fixes the square diagonal $p_1=-p_2$ (OB_{ul}, of length $\sqrt{2}$), which the native hull condition $p_1\geq p_2-1$ restricts to $0\leq p_2\leq 1/2$; hence the native fixed-row segment OC_+ has exact Euclidean length $\sqrt{2}/2=1/\sqrt{2}$ (which also equals the orthogonal projection $A\cdot\mathbf{e}=D\cdot\mathbf{e}=1/\sqrt{2}$ of the unit edges onto the unit diagonal $\mathbf{e}=(-1,1)/\sqrt{2}$, while $\mathrm{Area}(\mathrm{conv}(A,O,C_+))=1/4=\frac{1}{2}\,\mathrm{Area}(\mathrm{conv}(A,O,D))$). On this same chart, three distinct lines meet the square's geometry differently:

1. **Fixed-row ray ($r=1$):** $p_1=-p_2$ through $O=(0,0)$ and $C_+=(-1/2,1/2)$ (approaching O as $m\to\infty$).
2. **Row half-phase ($\kappa_{\mathrm{row}}=r/m=1/2$):** $p_1=(p_2-1)/2$ through the upper apex $D=(0,1)$ and the native site $P=(-1/3,1/3)$ ($(m,r,c)=(2,1,2),N=2$), crossing the fixed-row ray at $P\neq C_+$.
3. **Midpoint half-phase ($\kappa_{\mathrm{mid}}=(r-1/2)/m=1/2$):** the vertical line $p_1=-1/2$, which contains every positive diagonal site $r=c$ ($m=2r-1$, $\mathbf{p}_{2r-1,r}=(-1/2,1/(2r))$) including $C_+=(-1/2,1/2)$.

The row and midpoint half-phase lines share the boundary foot $F=(-1/2,0)$ (where their phase difference $p_2/[2(1-p_2)]$ vanishes as $p_2\to 0^+$), while the vertical line $p_1=-1/2$ continues downward through F to the horizontal-axis reflection $C_-=(-1/2,-1/2)$—an explicit reflected extension below the positive sheet with $|OC_+|=|OC_-|=1/\sqrt{2}$ and complex diagonal coincidence $i\omega_+=\overline{\omega_+}=\omega_-$ for $\omega_\pm=(-1\pm i)/2$ (whereas the row-half-phase line $p_1=(p_2-1)/2$ passes through $(-3/4,-1/2)\neq C_-$). This unit-square half-diagonal scale $1/\sqrt{2}$ is distinct from the $1/\sqrt{5}$ inner-square side arising in five-part equal-area dissections of a unit square [17].

Hull side lengths, angle bisector and the Pell target. In the unit-base normalization of (6.3), the hull $\mathcal{K}=\mathrm{conv}(A,B,C)$ has side lengths $1,1/\sqrt{2},1/\sqrt{2}$. Therefore

$$L_\triangle=1+\sqrt{2}, \qquad \mathrm{Area}(\mathcal{K})=\frac{1}{4}, \qquad R_{\mathrm{in}}=\frac{2\,\mathrm{Area}(\mathcal{K})}{L_\triangle}=\frac{1}{2L_\triangle}=\frac{\sqrt{2}-1}{2}.$$

The base-angle bisector gives $\tan(\pi/8)=2R_{\mathrm{in}}=L_\triangle^{-1}$. Write the centered rational carrier in (5.4) as $\mathbf{p}(U,W)=(C_1,C_2)=(\cos\psi,\sin\psi)$, reserving (p_1,p_2) for the address sheet here. Then

$$\frac{C_2}{1-C_1}=\frac{U}{W}=\cot(\psi/2).$$

Thus the 45° carrier target has $U/W = \cot(\pi/8) = L_\triangle$. Under the existing Pell step $(U, W) \mapsto (2U + W, U)$, the signed error $E = U - L_\triangle W$ obeys $E' = -E/L_\triangle$. This connects the hull's side-length constant to the carrier's half-angle parameter and its Pell approximation. The native first site $(-1/2, 1/2)$ corresponds to cell $(1, 1)$, whose carrier (5.1) is the apex $(0, 1)$; the 45° point is the separate approximation target.

6.2 The Sloping Sides and Apex Circle vs. Circumcircle

Proposition 6.2 (Triangular Polynomial Difference and Sum on the Address Sheet). *In planar coordinates $(p_1, p_2) \in \mathbb{R}^2$, the difference and sum of $T(p_1)$ and $T(p_2 - 1)$ satisfy*

$$2\big(T(p_1) - T(p_2 - 1)\big) = (p_1 + p_2)(p_1 - p_2 + 1) = \frac{E_1^2 - E_2^2}{4}, \quad (6.4)$$

$$T(p_1) + T(p_2 - 1) = 0 \iff \left(p_1 + \frac{1}{2}\right)^2 + \left(p_2 - \frac{1}{2}\right)^2 = \frac{1}{2} \iff E_1^2 + E_2^2 = 2, \quad (6.5)$$

where $E_1 = 2p_1 + 1$ and $E_2 = 2p_2 - 1$ center the apex $C = (-1/2, 1/2)$ at the origin.

The locus $T(p_1) - T(p_2 - 1) = 0$ factors into the two sloping sides $p_1 = -p_2$ (BC) and $p_1 = p_2 - 1$ (AC). The circle $T(p_1) + T(p_2 - 1) = 0$ has **center at the apex** $C = (-1/2, 1/2)$ **and radius** $1/\sqrt{2}$; it passes through $A = (-1, 0)$ and $B = (0, 0)$, and its closed disk contains $\mathrm{conv}(A, B, C)$. It is **not** the triangle's circumcircle: the actual circumcircle passing through A, B, and C has center $(-1/2, 0)$ and radius $1/2$, with equation $(p_1 + \frac{1}{2})^2 + p_2^2 = \frac{1}{4}$.

6.3 The Scalene Affine Variant

Replacing the numerator r in (6.1) by $r - (m - 1) = N - \frac{(m+2)(m-1)}{2}$ defines the variant sites

$$\widetilde{\mathbf{p}}_N = \left(\frac{r - m + 1}{m + 1}, \frac{1}{m + 1}\right) \qquad (2 - m \le r - m + 1 \le 1). \quad (6.6)$$

Proposition 6.3 (Affine Involution and Scalene Hull). *The two bounded address sheets are related site-by-site by the area-preserving affine involution*

$$(p_1, p_2) \longmapsto (-p_1 + 2p_2 - 1,\, p_2) \qquad (\det = -1). \quad (6.7)$$

The closed convex hull of $\{\widetilde{\mathbf{p}}_N : N \ge 1\}$ is the scalene triangle with vertices $(-1, 0), (0, 0), (\frac{1}{2}, \frac{1}{2})$, bounding edges $p_2 = 0$, $p_1 = p_2$, and $p_1 = 3p_2 - 1$, and squared side lengths $1, \frac{1}{2}, \frac{5}{2}$.

6.4 Equilateral Lift and Regular k-Simplex Orthogonal Projection

The isosceles right triangle $\mathrm{conv}(A, B, C)$ in (6.3) is the orthogonal projection onto $p_3 = 0$ of the spatial equilateral triangle of side 1 with vertices $\widehat{A} = (-1, 0, 0)$, $\widehat{B} = (0, 0, 0)$, and $\widehat{C} = (-\frac{1}{2}, \frac{1}{2}, \frac{1}{\sqrt{2}})$, tilted from the horizontal plane by $\psi_2 = \arccos(1/\sqrt{3}) \approx 54.7356°$.

Proposition 6.4 (Regular k-Simplex Orthogonal Projection Factor). *In $\mathbb{R}^{k+1}$ ($k \ge 1$), let $\Delta_k = \mathrm{conv}(\mathbf{e}_0, \mathbf{e}_1, \ldots, \mathbf{e}_k)$ be the standard regular k-simplex of edge length $\sqrt{2}$, and let $\mathrm{proj}\,\Delta_k = \mathrm{conv}(0, \mathbf{e}_1, \ldots, \mathbf{e}_k)$ be its orthogonal projection onto the coordinate hyperplane orthogonal to $\mathbf{e}_0$. Then the edge vectors $\mathbf{e}_i - \mathbf{e}_0$ ($1 \le i \le k$) have Gram matrix $G = I_k + \mathbf{1}\mathbf{1}^\mathsf{T}$ with $\det G = k + 1$, and the intrinsic k-volumes satisfy*

$$\mathrm{Vol}_k(\Delta_k) = \frac{\sqrt{k+1}}{k!}, \qquad \mathrm{Vol}_k(\mathrm{proj}\,\Delta_k) = \frac{1}{k!}, \qquad \frac{\mathrm{Vol}_k(\mathrm{proj}\,\Delta_k)}{\mathrm{Vol}_k(\Delta_k)} = \cos\psi_k = \frac{1}{\sqrt{k+1}}. \quad (6.8)$$

Distinction Between Two Meanings of "Simplex Shadow". Proposition 6.4 projects a k-dimensional simplex orthogonally onto a k-dimensional hyperplane and tracks its intrinsic k-volume ratio $1/\sqrt{k+1}$ (with angles $\psi_k = 45°, 54.7356°, 60°, 63.4349°$ for $k = 1, 2, 3, 4$). By contrast, in *Reading the Fold* v1.3 (§3.2), a "simplex shadow" is the **pushforward of uniform probability measure** on an n-simplex to a **one-dimensional line**, producing the normalized Curry–Schoenberg B-spline density M_n on $[-n, 0]$ [6]. For $n = 2$, the graph of M_2 has vertices $(-2, 0), (-1, 1), (0, 0)$ and area 1; scaling both coordinates by $\frac{1}{2}$ produces the triangle $\mathrm{conv}(A, C, B)$ of area $\frac{1}{4}$, which is a geometric similarity of plane figures rather than a probability-preserving rescaling.

Remark 6.5 (Discrete Triangular Chamber Law on a Finite $L \times L$ Grid Crop and Weak Convergence to M_2). While the infinite positive quadrant $\mathbb{Z}^2_{\geq 1}$ has chamber sizes $\#\{(r, c) \in \mathbb{Z}^2_{\geq 1} : r + c - 1 = m\} = m$ that grow linearly without bound, restricting the grid to a **finite origin-anchored square crop**

$$\mathcal{Q}_L = \{1, 2, \ldots, L\}^2 \subset \mathbb{Z}^2_{\geq 1} \qquad (L \in \mathbb{Z}_{\geq 1})$$

equipped with uniform discrete probability weight $1/L^2$ on each of its L^2 cells produces an exact discrete triangular distribution for the chamber $m = r + c - 1 \in \{1, 2, \ldots, 2L - 1\}$ of a uniformly chosen cell (r, c):

$$\Pr_{\mathcal{Q}_L}(m = k) = \frac{\#\big\{(r, c) \in \{1, \ldots, L\}^2 : r + c - 1 = k\big\}}{L^2} = \frac{L - |k - L|}{L^2} \qquad (1 \leq k \leq 2L - 1). \quad (6.8a)$$

Indeed, for each $k \in \{1, \ldots, 2L - 1\}$, the admissible rows $r \in \{1, \ldots, L\}$ satisfying $1 \leq k + 1 - r \leq L$ form the interval $\max(1, k + 1 - L) \leq r \leq \min(L, k)$, which contains $\min(L, k) - \max(1, k + 1 - L) + 1 = L - |k - L|$ cells, and $\sum_{k=1}^{2L-1}(L - |k - L|) = L^2$.

Mapping m to the negative-support convention of [5, §3.2] via the rescaled chamber variable

$$A_L = -\frac{m - 1}{L} = -\frac{r - 1}{L} - \frac{c - 1}{L} \in \left\{0, -\frac{1}{L}, \ldots, -2 + \frac{2}{L}\right\} \subset [-2, 0], \quad (6.8b)$$

the independent discrete uniform coordinates $E_L = -(r - 1)/L$ and $F_L = -(c - 1)/L$ converge in distribution as $L \to \infty$ to independent $\mathrm{Unif}([-1, 0])$ variables, and $A_L = E_L + F_L$ converges weakly (and uniformly on the lattice mesh $z_k = -(k - 1)/L$ with $L \Pr(A_L = z_k) = M_2(z_k) + O(1/L)$) to the continuous two-fold Curry–Schoenberg tent density

$$M_2(z) = (M_1 * M_1)(z) = (1 - |z + 1|)_+ \qquad (z \in [-2, 0]). \quad (6.8c)$$

This finite-crop identity requires explicitly declaring the $L \times L$ square crop $\mathcal{Q}_L$, uniform $1/L^2$ cell weighting, and the additive chamber variable $m = r + c - 1$; the finite distribution (6.8a) is discrete, and it provides a concrete $n = 2$ bridge between the Notebook Grid and [5, §3.2] without implying that empirical Gaussian or moving-average bell plots in other parts of the archive belong to the M_n spline family. Moreover, on the same uniform finite square crop $\mathcal{Q}_L$, sorting (r, c) into the pair $Y = (\min(r, c), \max(r, c))$ (equivalently $(m, |V|)$) leaves the chamber $m = r + c - 1$ and its tent limit unchanged while mapping the L diagonal cells ($r = c$) to singleton fibers of mass $1/L^2$ and the $L^2 - L$ off-diagonal cells ($r \neq c$) to equiprobable two-element fibers of mass $2/L^2$, forming $T_{L-1} = L(L - 1)/2$ off-diagonal **sorted pairs**, so the exact conditional orientation information removed by sorting is $H(r, c \mid Y) = \big(1 - \frac{1}{L}\big) \ln 2$ (recovered by the single orientation bit $I = \mathbf{1}_{\{r>c\}}$). More generally, for an exchangeable pair (A, C) taking values in a finite or countable ordered set, define $Y_{AC} = (\min(A, C), \max(A, C))$, $I_{AC} = \mathbf{1}_{\{A>C\}}$, and $p_= = \Pr(A = C)$. Direct conditional entropy on the at-most-two-point fibers gives $H(A, C \mid Y_{AC}) = H(I_{AC} \mid Y_{AC}) = (1 - p_=) \ln 2$; this remains well-defined even when $H(A, C)$ or $H(Y_{AC})$ is infinite. Moreover, because the sorted pair Y is equivalent to $(m, |V|)$ and the address is $N = \big(m^2 + 1 + (2I - 1)|V|\big)/2$, retaining only the chamber m discards $|V|$ as well: with $L_m = L - |m - L|$, the additional conditional offset entropy lost in passing from Y to m is $H(Y \mid m) = \frac{1}{L^2}\sum_{m=1}^{2L-1} L_m \ln L_m - \big(1 - \frac{1}{L}\big) \ln 2$, which vanishes at $L \in \{1, 2\}$ and is strictly positive for all $L \geq 3$ (at $L = 3$, $H(Y \mid m) = \frac{1}{3} \ln 3 - \frac{2}{9} \ln 2 > 0$, witnessed by chamber $m = 3$ with cells $(1, 3), (2, 2), (3, 1)$ at addresses $4, 5, 6$), while $H(m) = \ln L + \frac{1}{2} + o(1)$ matches the continuous tent differential entropy $1/2$ after subtracting the $\ln L$ lattice scale.

Remark 6.4a (Tangent-Sphere Cone Ratio, Matched $2/\pi$ Inscribed Ratio, and $\mathrm{SO}^+(1, 1)$ Double-Pell Conjugacy [18]). Three three-dimensional geometric identities connect the simplex tilt $\cos \psi_2 = 1/\sqrt{3}$ in Proposition 6.4 to the Pell recurrences of §4:

1. **Axial Tangent-Sphere Cone Ratio:** In a right circular cone of half-apex angle $\alpha \in (0, \pi/2)$, two spheres of radii $R_1 > R_2 > 0$ tangent to the cone wall at apex distances $\delta_i = R_i/\sin\alpha$ and externally tangent to each other satisfy $\delta_1 - \delta_2 = R_1 + R_2$, whence $(R_1 - R_2)/\sin\alpha = R_1 + R_2$ and $\Lambda_{\text{cone}}(\alpha) := \frac{R_2}{R_1} = \frac{1-\sin\alpha}{1+\sin\alpha} = \tan^2(\frac{\pi}{4} - \frac{\alpha}{2})$. At $\alpha = 45^\circ$ ($\sin\alpha = 1/\sqrt{2}$), $\Lambda_{\text{cone}}(45^\circ) = 3 - 2\sqrt{2} = (\sqrt{2}-1)^2$, whose reciprocal $(1+\sqrt{2})^2 = 3 + 2\sqrt{2}$ generates the negative-Pell step $(m, Q) \mapsto (3m+4Q, 2m+3Q)$ of Proposition 4.8; at $\sin\alpha = 1/\sqrt{3}$, $\Lambda_{\text{cone}} = 2 - \sqrt{3} = (2+\sqrt{3})^{-1}$.
2. **Cube** $1:2:3$ **Squared-Radius Law and Matched Inscribed Ratio** $2/\pi$**:** A cube $[-a, a]^3$ of half-side $a > 0$ has insphere, midsphere, and circumsphere radii $(R_{\text{in}}, R_{\text{mid}}, R_{\text{out}}) = (a, a\sqrt{2}, a\sqrt{3})$ in squared ratio $1:2:3$. Under **matched inscribed orientation**, a square Q_2 inscribed in a disk $B_2(R)$ ($a = R/\sqrt{2}$, area $2R^2$) and a cube Q_3 inscribed in a sphere $B_3(R)$ ($a = R/\sqrt{3}$, surface area $6(2a)^2 = 8R^2$) share the exact ratio

$$\frac{\text{Area}(Q_2)}{\text{Area}(B_2(R))} = \frac{2R^2}{\pi R^2} = \frac{2}{\pi} = \frac{8R^2}{4\pi R^2} = \frac{\text{Area}(\partial Q_3)}{\text{Area}(\partial B_3(R))},$$

   whereas for the dual orientation (an inscribed disk in a square) $\text{Area}(B_2)/\text{Area}(Q_2) = \pi/4$.
3. **Double-Pell Integrality and Positive-Sheet** $\mathrm{SO}^+(1,1)$ **Boost Conjugacy:** In $\mathbb{R}^k$ ($k > 2$), mapping the body-diagonal seeds $1/\sqrt{k}$ and $1/\sqrt{k-1}$ by the Cayley map $\mu(\beta) = \frac{1+\beta}{1-\beta}$ gives $\mu(1/\sqrt{D}) = \frac{D+1}{D-1} + \frac{2}{D-1}\sqrt{D}$ on $P_1^2 - DQ_1^2 = 1$. Both coordinates $(D+1)/(D-1)$ and $2/(D-1)$ are integers iff $(D-1) \mid 2 \iff D \in \{2, 3\}$, singling out $k = 3$ as the unique dimension $k > 2$ where both $\mu(1/\sqrt{3}) = 2 + \sqrt{3}$ ($D = 3$) and $\mu(1/\sqrt{2}) = 3 + 2\sqrt{2}$ ($D = 2$) land on fundamental integer Pell units. Normalizing $A_\beta = \left(\begin{smallmatrix} 1 & \beta \\ \beta & 1 \end{smallmatrix}\right)$ ($|\beta| < 1$) to $\Lambda_\beta = (1-\beta^2)^{-1/2} A_\beta \in \mathrm{SO}^+(1,1)$ gives $\Lambda_\beta \Lambda_\gamma = \Lambda_{(\beta+\gamma)/(1+\beta\gamma)}$. For any Pell solution (P_1, Q_1) of $P_1^2 - DQ_1^2 = 1$ on the **positive Lorentz sheet** $P_1 > 0$, setting $C_D = \text{diag}(1, \sqrt{D})$, $L_D = \left(\begin{smallmatrix} P_1 & DQ_1 \\ Q_1 & P_1 \end{smallmatrix}\right)$, and $\beta_D = \frac{\sqrt{D}\,Q_1}{P_1} \in (-1, 1)$ gives $(1-\beta_D^2)^{-1/2} = P_1 > 0$ and the exact orthochronous conjugacy

$$C_D L_D C_D^{-1} = \begin{pmatrix} P_1 & \sqrt{D}\,Q_1 \\ \sqrt{D}\,Q_1 & P_1 \end{pmatrix} = \Lambda_{\beta_D} \in \mathrm{SO}^+(1,1)$$

   (whereas for $P_1 \neq 0$ in $\mathrm{O}(1,1)$, $(1-\beta_D^2)^{-1/2} = |P_1|$ gives $\text{sgn}(P_1)\Lambda_{\beta_D}$, witnessed at $(P_1, Q_1) = (-1, 0)$ where $C_D L_D C_D^{-1} = -I \neq +I = \Lambda_0$). For $D \in \{2, 3\}$, where $1/\sqrt{D}$ rationalizes to the primitive integer fundamental Pell solution $(P_1, Q_1) = \left(\frac{D+1}{D-1}, \frac{2}{D-1}\right) \in \{(3, 2), (2, 1)\}$, this gives the exact seed square $C_D L_D C_D^{-1} = \Lambda_{1/\sqrt{D}}^2 = \Lambda_{\beta_D}$. Moreover, for $\beta \neq 0$, $A_\beta^{\mathsf{T}} A_\beta = \left(\begin{smallmatrix} 1+\beta^2 & 2\beta \\ 2\beta & 1+\beta^2 \end{smallmatrix}\right)$ is not a scalar multiple of I, so A_β cannot lie in the Euclidean similarity group $\mathbb{R}^\times \cdot \mathrm{O}(2)$.

Remark 6.4b (Tetrahedral-to-Hexagonal Projection, Adjacent-Pair Conic Basis, D_8 **Fiber Centralizer, and Interstitial Volume Partition [18]):**

1. **Tetrahedral Midpoints, Homothetic Hexagons, and Conic Basis:** Partitioning $\{\pm 1\}^3$ by the sign of the product of the three coordinates into dual regular tetrahedra $\Delta_\pm$, the edge-midpoint map $M(\{v_i, v_j\}) = \frac{1}{2}(v_i + v_j)$ sends the 6 edges of Δ_+ bijectively onto $\{\pm\mathbf{e}_1, \pm\mathbf{e}_2, \pm\mathbf{e}_3\}$. Orthogonal projection $P(v) = v - (v \cdot \mathbf{e}_*)\mathbf{e}_*$ along $\mathbf{e}_* = \frac{1}{\sqrt{3}}(1,1,1)$ sends $\pm(1,1,1) \mapsto 0$, maps the remaining 6 cube vertices to a regular hexagon of squared radius $\|P(1,1,-1)\|^2 = 3 - \frac{1}{3} = \frac{8}{3}$, and maps $\{\pm\mathbf{e}_i\}$ to a homothetic regular hexagon of squared radius $\|P(\mathbf{e}_1)\|^2 = 1 - \frac{1}{3} = \frac{2}{3}$. Writing $\Sigma(z) = T(z) + T(z-1) = z^2$, $\delta(z) = T(z) - T(z-1) = z$, and $\beta(a,b) = \Sigma(a+b) - \Sigma(a) - \Sigma(b) = 2ab$ gives a triangular basis $(\Sigma(a), \beta(a,b), \Sigma(b), \delta(a), \delta(b), 1)$ for all bivariate quadratics, in which $\{\Sigma(a) + \Sigma(b) = 1\} \cap \{\beta(a,b) = \pm b\}$ reduces to $a^2 + b^2 = 1$ and $b(2a \mp 1) = 0$, cutting out the six sixth roots of unity $(\pm 1, 0)$ and $(\pm\frac{1}{2}, \pm\frac{\sqrt{3}}{2})$.
2. **Intrinsic** D_8 **Fiber Envelope:** On each 4-state fiber $Q_a = \{a, a+6, a+12, a+18\} \pmod{24}$ over the 6 projected rays ($\mu_{24} \xrightarrow{z \mapsto z^4} \mu_6$), cycling $L(i) \equiv i + 1 \pmod 4$ and odd reflection $A(i) \equiv b - i \pmod 4$ ($b \in \{1, 3\}$) satisfy $ALA = L^{-1}$ and $L^2 \equiv (\cdot) + 2$, generating $\langle A, L\rangle \cong D_8$ containing both the tetrahedral stabilizer $\langle A, L^2\rangle$ (a Klein four-group) and the cube rotation stabilizer $C_4 = \langle L\rangle$.
3. **Ball–Cube–Ball Volume Tuple:** Alternating inward in $\mathbb{R}^k$ between a k-ball $B_n(R_n)$, its inscribed cube Q_n (side $2R_n/\sqrt{k}$), and the inscribed ball $B_{n+1}(R_n/\sqrt{k})$ partitions unit ball volume as $1 = k^{-k/2} + \left(\frac{2^k}{k^{k/2}\omega_k} - k^{-k/2}\right) + \left(1 - \frac{2^k}{k^{k/2}\omega_k}\right)$; at $k = 3$ ($\omega_3 = \frac{4\pi}{3}$), the step ratios form $\left(\frac{\text{Vol}(Q_n)}{\text{Vol}(B_n)}, \frac{\text{Vol}(B_{n+1})}{\text{Vol}(Q_n)}, \frac{\text{Vol}(B_{n+1})}{\text{Vol}(B_n)}\right) = \left(\frac{2}{\pi\sqrt{3}}, \frac{\pi}{6}, \frac{1}{3\sqrt{3}}\right)$.

6.5 The Diagonal Staircase, Odd-Square Sectors, and Depth-Weighted Stack Projection

On the address sheet (6.1), where $\mathbf{p}(r,c) = \left(-\frac{r}{m+1}, \frac{1}{m+1}\right)$ satisfies $p_1 < 0 < p_2$ and the closed convex hull $\mathcal{K}$ meets the upper-left diagonal boundary at $p_1 = -p_2$, the affine line $p_2 = \frac{k-1}{k} + p_1$ ($k \in \mathbb{Z}_{\geq 1}$) crosses $p_1 = -p_2$ at $(p_1, p_2) = \left(-\frac{k-1}{2k}, \frac{k-1}{2k}\right)$. Equivalently,

$$-p_1 = p_2 = \frac{k-1}{2k} = \frac{T_{k-1}}{k^2} = \frac{1}{2} - \frac{1}{2k}, \qquad \frac{T_k}{k^2} + \frac{T_{k-1}}{k^2} = 1 \qquad \left(k = 3,4,5,6 \implies \frac{1}{3}, \frac{3}{8}, \frac{2}{5}, \frac{5}{12}\right). \tag{6.9}$$

(Note: Since a discrete site $\mathbf{p}(r,c) = (-r/(m+1), 1/(m+1))$ *on* $p_1 = -p_2$ *requires* $r = 1$ *and* $m+1 = 2k/(k-1) = 2 + 2/(k-1)$*, for integer* $k \geq 2$ *the crossing is a discrete site if and only if* $k \in \{2,3\}$*, giving cell* $(1,3), m = 3, N = 4$ *at* $k = 2$ *and cell* $(1,2), m = 2, N = 2$ *at* $k = 3$*.)* For $k > 1$, setting $\kappa_{\text{stair}} = T_k/k^2 = \frac{1}{2} + \frac{1}{2k}$ gives $\mathcal{J}(\kappa_{\text{stair}}) = \frac{1}{k}$ and $\mathfrak{f}(\kappa_{\text{stair}}) = \frac{T_k T_{k-1}}{k^4} = \frac{1}{4} - \frac{1}{4k^2}$, climbing to the fold vertex $\frac{1}{4}$ as $k \to \infty$ [5, §2.3].

Square split, $1/k$ normalization, quadratic fixed-point family, and the far edge of the address sheet. Because $T_k + T_{k-1} = k^2$ and $T_k - T_{k-1} = k$ ($k \in \mathbb{Z}_{\geq 1}$), dividing by k^2 gives the normalized gap $\chi_k^+ - \chi_k^- = 1/k$ between $\chi_k^\pm = \frac{1}{2} \pm \frac{1}{2k}$, with successive differences $\frac{1}{k} - \frac{1}{k+1} = \frac{1}{2T_k}$. Their common fold value $\mathfrak{f}(\chi_k^\pm) = \frac{1}{4} - \frac{1}{4k^2}$ factors $z^2 - z + \mathfrak{f}(\chi_k^\pm) = (z - \chi_k^-)(z - \chi_k^+)$, so $\chi_k^\pm$ are the real fixed points of the quadratic map $z \mapsto z^2 + \mathfrak{f}(\chi_k^\pm)$, whose parameter approaches the parabolic value $1/4$ (with multipliers $2\chi_k^\pm = 1 \pm 1/k$ and deficits $\frac{1}{4} - \mathfrak{f}(\chi_k^\pm) = \frac{1}{4k^2}$ summing to $\zeta(2)/4 = \pi^2/24$). On the address sheet (6.1), the far-edge site $\mathbf{p}_{m,m} = (-1 + \frac{1}{m+1}, \frac{1}{m+1}) \to (-1, 0)$ along $p_1 = p_2 - 1$, and its raw horizontal step $\frac{1}{m+1}$ rescales by the active m-step span $\frac{m}{m+1}$ to $\frac{1}{m}$ [17].

Figure 6 (§6.1): Diagonal Staircase Crossings and the Fixed Points of $z \mapsto z^2 + \mathfrak{f}(\chi_k^\pm)$

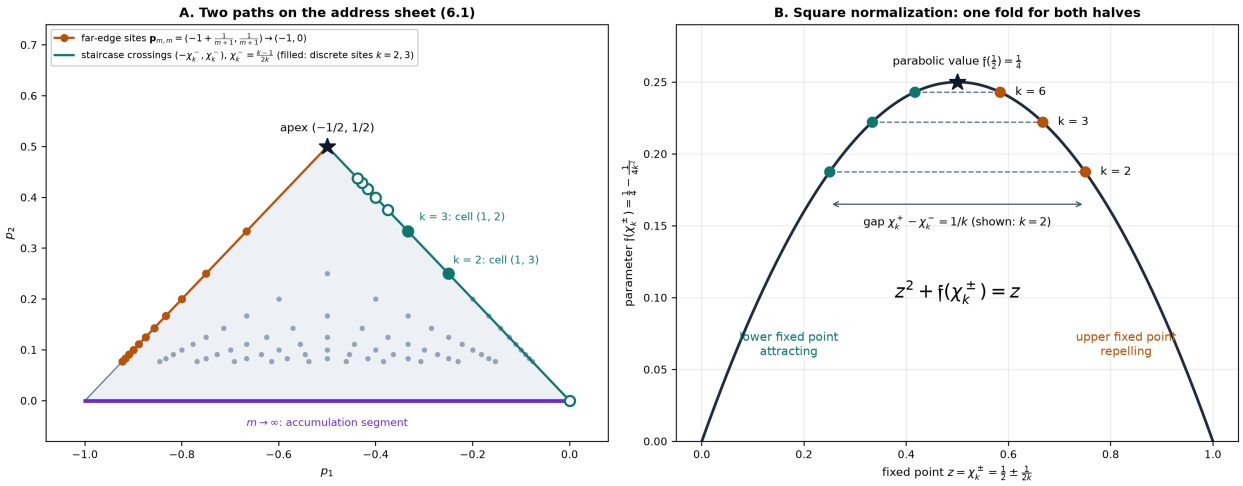


Figure 6 (Geometric locus vs. rescaled fixed points): Left: on the address sheet (6.1), the far-edge chamber site $\mathbf{p}_{m,m} = (-1 + \frac{1}{m+1}, \frac{1}{m+1})$ approaches $(-1, 0)$ along $p_1 = p_2 - 1$, while the diagonal staircase crossings $(-\chi_k^-, \chi_k^-)$ with $\chi_k^- = \frac{k-1}{2k}$ approach the apex $(-1/2, 1/2)$ along $p_1 = -p_2$. Right: active-span normalization of $1/(m+1)$ by $m/(m+1)$ gives $1/m$, whereas square normalization gives $\chi_k^+ - \chi_k^- = 1/k$ and the fixed-point pair $\chi_k^\pm = 1/2 \pm 1/(2k)$ of $z \mapsto z^2 + \mathfrak{f}(\chi_k^\pm)$ with $\mathfrak{f}(\chi_k^\pm) = 1/4 - 1/(4k^2)$.

Proposition 6.5 (Eight-Sector Lattice Congruence, Isometric Stack Fiber Multiplicity, and Atomic-to-Weak Screen Laws). *Let* $n \geq 1$ *and put* $j = 2n + 1$.

1. **Eight-Sector Decomposition in** $\mathrm{E}(2,\mathbb{Z}) = \mathbb{Z}^2 \rtimes \mathrm{O}(2,\mathbb{Z})$**:** *Centering* $\{1, \ldots, j\}^2$ *at* $(a,b) = (A' - n - 1, B' - n - 1) \in \{-n, \ldots, n\}^2$ *partitions the* $j^2 = 1 + 8T_n$ *lattice points into the origin* $(0,0)$ *and eight half-open max-norm sectors* $\Sigma_0, \ldots, \Sigma_7$ *obtained from* $\Sigma_0 = \bigcup_{k=1}^n \{(k,b) : 0 \leq b < k\}$ *and* $\Sigma_1 = \bigcup_{k=1}^n \{(a,k) : 0 < a \leq k\}$ *under the 4-fold rotation group* $C_4 \subset \mathrm{O}(2,\mathbb{Z}) \cong D_4$*. Each sector has cardinality* T_n *(indexed locally by* $N = T_{k-1} + r \in \{1, \ldots, T_n\}$*). In the lattice-preserving Euclidean semidirect product* $\mathrm{E}(2,\mathbb{Z}) = \mathbb{Z}^2 \rtimes \mathrm{O}(2,\mathbb{Z}) \subset \mathrm{E}(2) = \mathbb{R}^2 \rtimes \mathrm{O}(2)$ *with group law* $(\mathbf{b}_1, M_1)(\mathbf{b}_2, M_2) = (\mathbf{b}_1 + M_1\mathbf{b}_2, M_1M_2)$ *and action* $(\mathbf{b}, M) \cdot \mathbf{v} = M\mathbf{v} + \mathbf{b}$*, the lattice reflection-shift* $F = ((1,0), E) \in \mathrm{E}(2,\mathbb{Z})$*, with* E *the coordinate exchange,* $F(a,b) = (b+1, a)$*, maps* $\Sigma_0 \xrightarrow{\sim} \Sigma_1$ *bijectively, so all eight sectors are pairwise congruent as free Euclidean subsets while remaining non-equivalent under origin-fixing maps in* $\mathrm{O}(2)$ *(at* $n = 2$*,* Σ_0 *has origin squared-norm multiset* $\{1, 4, 5\}$ *whereas* Σ_1 *has* $\{2, 5, 8\}$*).*

2. **Oblique Fiber Multiplicity of the Bottom-Widest Point Stack S_n:** *Define the discrete point stack $S_n = \{(p_1,p_2,\ell) \in \mathbb{Z}^3 : 0 \le \ell \le n,\ |p_1|,|p_2| \le n-\ell\}$ of total cardinality $|S_n| = \sum_{\ell=0}^{n}(2(n-\ell)+1)^2 = \frac{(n+1)(2n+1)(2n+3)}{3} = \binom{2n+3}{3} = \binom{j+2}{3}$ (distinct from the solid cube union Ω_n of Appendix B). Along $\mathbf{e}_* = (1,1,1)/\sqrt{3}$, orthogonal projection $P = I - \mathbf{e}_*\mathbf{e}_*^{\mathsf{T}}$ maps (p_1,p_2,ℓ) to $(p_1-\ell)P\mathbf{e}_1 + (p_2-\ell)P\mathbf{e}_2$, indexed injectively by the oblique screen coordinate $(a,b) = (p_1-\ell, p_2-\ell) \in \{-n,\dots,n\}^2$ with exact fiber multiplicity*

$$w_n(a,b) := \#\big\{(p_1,p_2,\ell) \in S_n : (p_1-\ell, p_2-\ell) = (a,b)\big\} = 1 + \left\lfloor \frac{n-\max(a,b)}{2} \right\rfloor, \qquad \sum_{a=-n}^{n}\sum_{b=-n}^{n} w_n(a,b) = \binom{j+2}{3}. \quad (6.10)$$

3. **Finite Atomic Screen-Maximum PMFs vs. Rescaled Weak-Limit Densities:** *Set $M = \max(a+n+1, b+n+1) = \max(a,b)+n+1 \in \{1,\dots,j\}$. At every finite odd side $j = 2n+1$, M obeys the exact discrete atomic probability mass functions*

$$\Pr_{\text{flat}}(M=i) = \frac{2i-1}{j^2}, \qquad \Pr_{\text{stack}}(M=i) = \frac{(2i-1)\big(1+\lfloor (j-i)/2 \rfloor\big)}{\binom{j+2}{3}} \qquad (1 \le i \le j) \quad (6.11)$$

under uniform 2D screen sampling on $\{-n,\dots,n\}^2$ and uniform 3D stack sampling on S_n, respectively. As $j \to \infty$, the rescaled random variable $Y_j = M/j \in (0,1]$ satisfies the uniform local-limit bounds ($\omega = i/j$)

$$\max_{1\le i\le j} \big| j \Pr_{\text{flat}}(M=i) - 2\omega \big| = \frac{1}{j}, \qquad \max_{1\le i\le j} \big| j \Pr_{\text{stack}}(M=i) - 6\omega(1-\omega) \big| \le \frac{18}{j},$$

and hence converges weakly on $[0,1]$ to continuous laws with densities $p_{\text{flat}}(\omega) = 2\omega$ and $p_{\text{stack}}(\omega) = 6\omega(1-\omega) = 6\,\mathfrak{f}(\omega)$.

Proof. (1) For $(k,b) \in \Sigma_0$, $0 \le b < k \le n$ implies $1 \le b+1 \le k \le n$, so $F(k,b) = (b+1,k) \in \Sigma_1$ with inverse $(a,k) \mapsto (k, a-1)$, and $F \in \mathbb{Z}^2 \rtimes \mathrm{O}(2,\mathbb{Z})$ preserves Euclidean distances ($\|F(\mathbf{v}) - F(\mathbf{v}')\|_2 = \|E(\mathbf{v}-\mathbf{v}')\|_2 = \|\mathbf{v}-\mathbf{v}'\|_2$). Arbitrary rotations in $\mathrm{O}(2)$ do not preserve $\mathbb{Z}^2$, so $\mathrm{E}(2,\mathbb{Z})$ is written $\mathbb{Z}^2 \rtimes \mathrm{O}(2,\mathbb{Z})$ with normal translation subgroup $\mathbb{Z}^2$.

(2) Since $P\mathbf{e}_3 = -P\mathbf{e}_1 - P\mathbf{e}_2$ and $\{P\mathbf{e}_1, P\mathbf{e}_2\}$ is a basis of $\mathbf{e}_*^{\perp}$, $P(p_1,p_2,\ell) = (p_1-\ell)P\mathbf{e}_1 + (p_2-\ell)P\mathbf{e}_2$. Given $(a,b) \in \{-n,\dots,n\}^2$ and an integer $\ell \ge 0$, the lifted point $(a+\ell, b+\ell, \ell)$ belongs to S_n iff $\ell \le n$, $-(n-\ell) \le a+\ell \le n-\ell$, and $-(n-\ell) \le b+\ell \le n-\ell$. The lower bounds $a \ge -n$ and $b \ge -n$ already hold on $\{-n,\dots,n\}^2$, while the upper bounds reduce to $2\ell \le n-a$ and $2\ell \le n-b$, i.e., $0 \le \ell \le \lfloor (n - \max(a,b))/2 \rfloor \le n$, which has $1 + \lfloor (n-\max(a,b))/2 \rfloor$ integer solutions ℓ.

(3) Shifting $(A',B') = (a+n+1, b+n+1) \in \{1,\dots,j\}^2$ gives $n - \max(a,b) = j - M$. Exactly $i^2 - (i-1)^2 = 2i-1$ pairs (A',B') satisfy $\max(A',B') = i$, and w_n is constant on $\{M=i\}$ with value $1 + \lfloor (j-i)/2 \rfloor$, establishing both PMFs in (6.11). Writing $\omega = i/j \in (0,1]$, $j\Pr_{\text{flat}}(M=i) - 2\omega = -1/j$. For $\Pr_{\text{stack}}$, note $\frac{j-i+1}{2} \le 1 + \lfloor \frac{j-i}{2} \rfloor \le \frac{j-i+2}{2}$ and $\binom{j+2}{3} = \frac{j(j+1)(j+2)}{6}$. Multiplying by $6j/\big[j(j+1)(j+2)\big]$ gives

$$\big| j \Pr_{\text{stack}}(M=i) - 6\omega(1-\omega) \big| \le \frac{6\big|(2i-1)(1+\lfloor (j-i)/2 \rfloor) - i(j-i)\big|}{(j+1)(j+2)} + 6\omega(1-\omega)\frac{3j+2}{(j+1)(j+2)}.$$

Since $0 \le 1 + \lfloor (j-i)/2 \rfloor - (j-i)/2 \le 1$ and $2i-1 \le 2j$, the first numerator has magnitude at most $6\big[(2j)(1) + j/2\big] = 15j$, while $6\omega(1-\omega) \le \frac{3}{2}$ bounds the second term by $\frac{9j+6}{2(j+1)(j+2)} < \frac{3}{j}$, yielding total error $\le \frac{15}{j} + \frac{3}{j} = \frac{18}{j}$. Riemann-sum convergence over bounded continuous test functions on $[0,1]$ then yields weak convergence of $Y_j = M/j$ to $2\omega\,d\omega$ and $6\omega(1-\omega)\,d\omega$. □

For independent uniform stages $(A_n, C_n) \in \{1,\dots,j_n\}^2$ ($j_n = 2n+1$, center-hit event $E_n = \{A_n = C_n = n+1\}$ of probability j_n^{-2}), writing $\mathcal{S}_L = \prod_{n=1}^{L}(1 - j_n^{-2})$ for the probability of no center hit in the first L stages and $\Pi_{\triangle,L}(u) = \prod_{n=1}^{L}(1 - u/T_n)$ gives at every $L \ge 1$ [8]:

$$\mathcal{S}_L = \prod_{n=1}^{L} \frac{8T_n}{8T_n+1} \downarrow \frac{\pi}{4}, \qquad \Pi_{\triangle,L}\left(-\frac{1}{8}\right) = \prod_{n=1}^{L} \frac{8T_n+1}{8T_n} \uparrow \frac{4}{\pi}, \qquad \mathcal{S}_L\,\Pi_{\triangle,L}\left(-\frac{1}{8}\right) = 1, \quad (6.11a)$$

and since $\sum_{n\ge1}\Pr(E_n) < \infty$, the number of center hits $I = \sum_{n\ge1}\mathbf{1}_{E_n}$ is finite almost surely, with entire probability generating function

$$G(\tau)=\mathbb{E}[\tau^I]=\prod_{n=1}^{\infty}\left(1-\frac{1-\tau}{(2n+1)^2}\right)=\frac{\pi}{4}\,\Pi_{\triangle}\!\left(-\frac{\tau}{8}\right)=\frac{\cos\!\left(\frac{\pi}{2}\sqrt{1-\tau}\right)}{\tau}\quad(\tau\neq 0),\qquad G(0)=\frac{\pi}{4},\quad G(1)=1. \tag{6.11b}$$

Figure 7 (§6.5): Stack Projection and Declared Sampling Measures

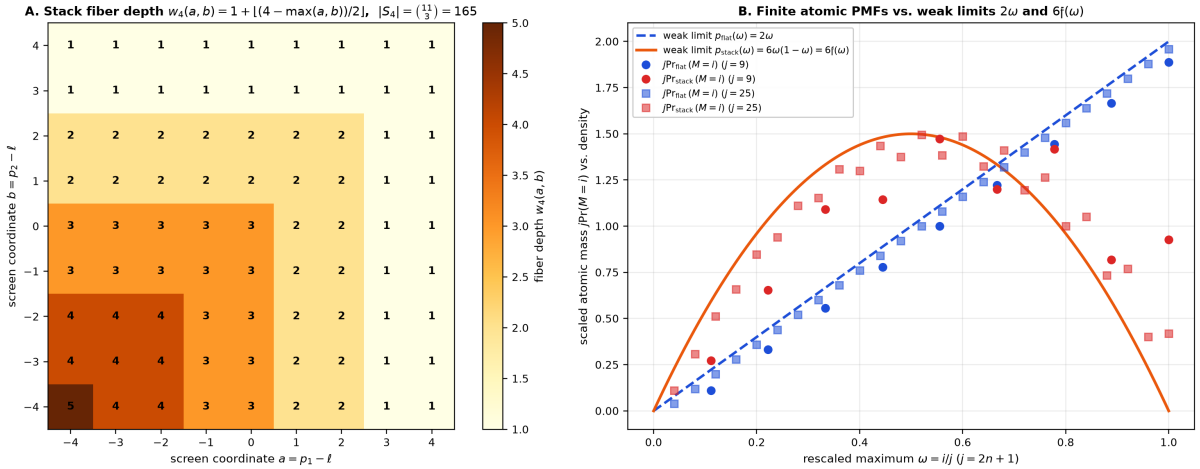


Figure 7 (Stack projection & declared sampling measures): **A.** Oblique fiber depth $w_4(a,b)=1+\lfloor(4-\max(a,b))/2\rfloor$ across $(a,b)\in\{-4,\dots,4\}^2$ summing to $|S_4|=\binom{11}{3}=165$. **B.** Finite odd-side discrete atomic scaled masses $j\,\Pr_{\mathrm{flat}}(M=i)$ and $j\,\Pr_{\mathrm{stack}}(M=i)$ $(j=9,25)$ converging weakly as $j\to\infty$ to 2ω and $6\omega(1-\omega)=6\mathfrak{f}(\omega)$.

6.6 Common Triangular / Odd-Square Factorization, Central-Binomial Closed Form, Euler Cosine PGF, and Fixed-Gap Gamma Family

The odd-square address geometry of §§1–5, the diagonal staircase value $\mathfrak{f}(\chi^{\pm}_{2n+1})=\frac{1}{4}-\frac{1}{4(2n+1)^2}$, and the eight-sector / stack decompositions of Proposition 6.5 all instantiate a single elementary integer identity, $(2n+1)^2=8T_n+1=4n(n+1)+1$, whose finite and asymptotic consequences we prove below [8, 10].

Lemma 6.5a (Rapidity Telescoping, Central-Binomial Product, and Polynomial Rigidity of FG). *For each integer $n\geq 1$, let $(F_n,G_n)=(n,n+1)$ be the balanced binary split of $j_n=2n+1$, with share $\chi_n=\frac{n}{2n+1}=\chi^{-}_{2n+1}$, contrast $\delta_n=1-2\chi_n=\frac{1}{2n+1}\in(0,1)$, odds ratio $O_n=\frac{G_n}{F_n}=\frac{n+1}{n}=\frac{1+\delta_n}{1-\delta_n}$, and rapidity $\varrho_n:=\operatorname{artanh}(\delta_n)=\frac{1}{2}\ln\frac{n+1}{n}$. Then:*

1. **Multiplicative Odds & Additive Rapidity Telescoping:** $\prod_{n=1}^{L}O_n=L+1$ and $\sum_{n=1}^{L}\varrho_n=\frac{1}{2}\ln(L+1)$.
2. **Variance-Fold Central-Binomial Product:** *Writing* $4\mathfrak{f}(\chi_n)=4\chi_n(1-\chi_n)=1-\delta_n^2=\frac{4n(n+1)}{(2n+1)^2}=\cosh^{-2}(\varrho_n)$, *at every finite* $L\geq 1$,

$$\mathcal{S}_L=\prod_{n=1}^{L}4\mathfrak{f}(\chi_n)=\prod_{n=1}^{L}\cosh^{-2}(\varrho_n)=\frac{L+1}{(2L+1)^2}\,\frac{16^L}{\binom{2L}{L}^2}. \tag{6.12a}$$

3. **Polynomial Rigidity of FG:** *Every symmetric polynomial $\Psi(F,G)=\Psi(G,F)$ over a commutative ring Λ satisfying $\Psi(F,0)=\Psi(0,G)=0$ factors uniquely as $\Psi(F,G)=FG\cdot Q(F+G,FG)$ for a polynomial Q over Λ.*

Proof. (1) $\prod_{n=1}^{L}\frac{n+1}{n}=L+1$, and $\operatorname{artanh}\!\left(\frac{1}{2n+1}\right)=\frac{1}{2}\ln\frac{n+1}{n}$ telescopes to $\frac{1}{2}\ln(L+1)$. (2) Using $\prod_{n=1}^{L}4n(n+1)=4^L(L+1)(L!)^2$ and $\prod_{n=1}^{L}(2n+1)=\frac{(2L+1)!}{2^L L!}=\frac{2L+1}{2^L}\binom{2L}{L}L!$, squaring the denominator and cancelling $(L!)^2$ gives $\frac{4^L(L+1)}{(2L+1)^2 4^{-L}\binom{2L}{L}^2}=\frac{L+1}{(2L+1)^2}\frac{16^L}{\binom{2L}{L}^2}$. (3) Viewing $\Psi\in(\Lambda[F])[G]$, $\Psi(F,0)=0$ implies $G\mid\Psi$, so $\Psi(F,G)=G\cdot\Psi_1(F,G)$; evaluating at $F=0$ gives $0=\Psi(0,G)=G\cdot\Psi_1(0,G)$ in $\Lambda[G]$, whence $\Psi_1(0,G)=0$ and $F\mid\Psi_1$, giving $\Psi(F,G)=FG\cdot\tilde{Q}(F,G)$ with $\tilde{Q}$ uniquely determined because FG is a monic regular element in each variable. Symmetry $\Psi(F,G)=\Psi(G,F)$ implies $FG(\tilde{Q}(F,G)-\tilde{Q}(G,F))=0$, so $\tilde{Q}$ is symmetric and by the fundamental theorem of symmetric polynomials equals a unique $Q(F+G,FG)$. □

Theorem 6.5 (Common Triangular / Odd-Square Factorization and Multi-Route Consequences). *For each integer $n \geq 1$, let $j_n = 2n+1$ and $T_n = n(n+1)/2$. All three routes below rest on $(2n+1)^2 = 8T_n + 1 = 4n(n+1)+1$ together with their stated route hypotheses:*

1. **Route 1 — Eight-Sector Partition, Balanced Split, and Finite Reciprocal Identity:** *The centered square $\{-n,\dots,n\}^2$ partitions into $(0,0)$ and eight $\mathrm{E}(2,\mathbb{Z})$-congruent half-open max-norm sectors $\Sigma_0,\dots,\Sigma_7$ of size T_n (Proposition 6.5(1)). In any discrete binary partition $F+G = 2n+1$ ($F,G \in \mathbb{Z}_{\geq 0}$), writing $(F,G) = (n-i, n+1+i)$ (or its swap) with imbalance $i \in \{0,\dots,n\}$ yields the exact triangular defect sequence $FG = (n-i)(n+1+i) = n(n+1) - i(i+1) = 2(T_n - T_i)$, which is uniquely maximized at $i=0$ by the balanced split $\{n, n+1\}$ (two oriented ordered states $(n,n+1),(n+1,n)$, and $\binom{2n+1}{n}$ labeled cuts of K_{2n+1}, all with $FG = 2T_n = \mathrm{ex}(2n+1;K_3)$). At $\chi_n = n/(2n+1)$,*

$$\mathfrak{f}(\chi_n) = \frac{n(n+1)}{(2n+1)^2} = \frac{2T_n}{8T_n+1} = \frac{1}{4} - \frac{1}{4(2n+1)^2}, \qquad \frac{1}{4\mathfrak{f}(\chi_n)} = 1 + \frac{1}{8T_n} = \left(1 - \frac{1}{(2n+1)^2}\right)^{-1},$$

and at every finite $L \geq 1$,

$$\mathcal{S}_L = \prod_{n=1}^{L} \frac{8T_n}{8T_n+1} = \frac{L+1}{(2L+1)^2}\,\frac{16^L}{\binom{2L}{L}^2} \downarrow \frac{\pi}{4}, \qquad \Pi_{\triangle,L}\left(-\frac{1}{8}\right) = \prod_{n=1}^{L} \frac{1}{4\mathfrak{f}(\chi_n)} = \frac{(2L+1)^2}{L+1}\,\frac{\binom{2L}{L}^2}{16^L} = \frac{1}{\mathcal{S}_L} \uparrow \frac{4}{\pi}.$$

2. **Route 2 — Euler Cosine Product and $\zeta(2)$ PGF Slope (Under Stage Independence):** *Under mutually independent Bernoulli center-hit indicators $\mathbf{1}_{E_n}$ with $\Pr(E_n) = (2n+1)^{-2}$, $I = \sum_{n=1}^{\infty} \mathbf{1}_{E_n}$ has entire generating function $G(\tau) = \mathbb{E}[\tau^I] = \prod_{n=1}^{\infty}\big(1 - \frac{1-\tau}{(2n+1)^2}\big)$, which by Euler's product $\cos(\frac{\pi z}{2}) = (1-z^2)\prod_{n=1}^{\infty}\big(1 - \frac{z^2}{(2n+1)^2}\big)$ at $z = \sqrt{1-\tau}$ satisfies*

$$G(\tau) = \frac{\cos\!\big(\frac{\pi}{2}\sqrt{1-\tau}\big)}{\tau} \quad (\tau \neq 0), \qquad G(0) = \lim_{z\to 1} \frac{\cos(\pi z/2)}{1-z^2} = \frac{\pi}{4} = \Pr(I=0), \qquad G'(1) = \sum_{n=1}^{\infty} \frac{1}{(2n+1)^2} = \big(1-2^{-2}\big)\,\zeta(2) - 1 = \frac{\pi^2}{8} - 1.$$

3. **Route 3 — Fixed-Gap Gamma Ratio and Isometric Stack Pushforward:** *For any real gap parameter $D = k-2 > 0$, setting $\nu_n^{(k)} = \frac{1}{2}n(n+D)$ ($\nu_n^{(3)} = T_n$) gives at every finite $L \geq 1$*

$$P_L^{(D)} := \prod_{n=1}^{L}\left(1 + \frac{D^2}{8\nu_n^{(k)}}\right) = \prod_{n=1}^{L} \frac{(n+D/2)^2}{n(n+D)} = \frac{\Gamma(D+1)}{\Gamma(1+D/2)^2}\,\frac{\Gamma(L+1+D/2)^2}{\Gamma(L+1)\,\Gamma(L+1+D)} \underset{L\to\infty}{\longrightarrow} \frac{\Gamma(D+1)}{\Gamma(1+D/2)^2},$$

evaluating to $4/\pi$ at $D=1$, $\frac{2(L+1)}{L+2} \to 2$ at $D=2$, and $\frac{32}{3\pi}$ at $D=3$. Separately, by Proposition 6.5(2)–(3), projecting S_n along $\mathbf{e}_* = (1,1,1)/\sqrt{3}$ weights screen coordinates by $w_n(a,b) = 1 + \lfloor \frac{n - \max(a,b)}{2} \rfloor$, carrying uniform 2D flat sampling and uniform 3D stack sampling from their exact finite-j atomic laws (6.11) to the weak-limit densities $p_{\mathrm{flat}}(\omega) = 2\omega$ and $p_{\mathrm{stack}}(\omega) = 6\omega(1-\omega) = 6\,\mathfrak{f}(\omega)$ on $[0,1]$.

Proof. Route 1 follows from Proposition 6.5(1), Lemma 6.5a(2), and Wallis's asymptotic $\binom{2L}{L} \sim \frac{4^L}{\sqrt{\pi L}}$ (so $\mathcal{S}_L \sim \frac{L}{4L^2}\cdot \pi L = \frac{\pi}{4}$), which also follows independently from $G(0) = \pi/4$ in Route 2. In Route 2, $\sum_{n\geq 1} \frac{|1-\tau|}{(2n+1)^2}$ converges locally uniformly on $\mathbb{C}$, so $G(\tau)$ is entire; L'Hôpital's rule at $z=1$ gives $\lim_{z\to 1} \frac{\cos(\pi z/2)}{1-z^2} = \frac{-\pi/2\sin(\pi/2)}{-2} = \frac{\pi}{4}$, and termwise logarithmic differentiation at $\tau = 1$ gives $G'(1) = \sum_{n\geq 1}(2n+1)^{-2} = \frac{3}{4}\frac{\pi^2}{6} - 1 = \frac{\pi^2}{8} - 1$. In Route 3, iterating $\Gamma(z+1) = z\Gamma(z)$ gives $\prod_{n=1}^{L}(n+a) = \frac{\Gamma(L+1+a)}{\Gamma(1+a)}$ for $a \in \{0, D/2, D\}$, establishing the exact finite Gamma identity for $P_L^{(D)}$, and Stirling's asymptotic $\frac{\Gamma(L+1+D/2)^2}{\Gamma(L+1)\Gamma(L+1+D)} = 1 + O(L^{-1}) \to 1$ yields the limit $\Gamma(D+1)/\Gamma(1+D/2)^2$; the stack pushforward is proved in Proposition 6.5(2)–(3). □

Table 6.1 — Hypotheses and Proved Scope of Each Route in Theorem 6.5

Component / Route	Required Hypotheses & Inputs	Exact Conclusion Proved	Explicit Nonclaim / Scope Boundary
Common Algebraic Core	Integer identity $(2n+1)^2 = 8T_n + 1 = 4n(n+1) + 1$.	Termwise reciprocity $\frac{8T_n}{(2n+1)^2}\left(1 + \frac{1}{8T_n}\right) = 1$, finite identity $\mathcal{S}_L \Pi_{\triangle,L}(-1/8) = 1$, and closed form $\mathcal{S}_L = \frac{L+1}{(2L+1)^2} \frac{16^L}{\binom{2L}{L}^2}$.	Evaluating the transcendental limit $\pi/4$ requires Wallis/Stirling or Euler's cosine product.
Route 1 (Balanced Split & 8-Sector Split)	Binary split $F + G = 2n + 1$ or centered square $\{-n, \ldots, n\}^2$.	Balanced split $\{n, n+1\}$ maximizes $FG = 2T_n$, defect sequence $2(T_n - T_i)$, rigidity of FG, and 8-sector split $(2n+1)^2 = 1 + 8T_n$ in $\mathbb{Z}^2 \rtimes \mathrm{O}(2, \mathbb{Z})$.	Sectors $\Sigma_0, \ldots, \Sigma_7$ are free-congruent in $\mathbb{Z}^2 \rtimes \mathrm{O}(2, \mathbb{Z}) \subset \mathbb{R}^2 \rtimes \mathrm{O}(2)$, not $\mathrm{O}(2)$-equivalent about $(0, 0)$; unlabeled $\{n, n+1\} \neq \binom{2n+1}{n}$ labeled cuts; forces $D = 1$.
Route 2 (Euler Product & PGF $G(\tau)$)	Euler's cosine product, removable limit at $\tau = 0$, and **mutual independence** of $\mathbf{1}_{E_n}$.	$G(\tau) = \cos((\pi/2)\sqrt{1-\tau})/\tau$ $(\tau \neq 0)$, removable $G(0) = \pi/4$, and $G'(1) = \sum_{n \geq 1} (2n+1)^{-2} = \frac{\pi^2}{8} - 1$.	Probabilistic interpretation $G(\tau) = \mathbb{E}[\tau^I]$ requires independent Bernoulli stages.
Route 3a (Fixed-Gap Gamma $P_L^{(D)}$)	Scalar sequence $\nu_n^{(k)} = \frac{1}{2} n(n+D)$ $(D = k - 2 > 0)$ and Gamma recurrence.	Exact finite ratio $P_L^{(D)}$ and limit $\Gamma(D+1)/\Gamma(1+D/2)^2$ for all $D > 0$.	For $D > 1$, matches scalar radial eigenvalues $\nu_n^{(k)}$; does **not** claim an operator intertwiner or full S^{k-1} spectral determinant with multiplicities.
Route 3b (Stack Pushforward)	Oblique projection $(p_1, p_2, \ell) \mapsto (p_1 - \ell, p_2 - \ell)$ of S_n, fiber depth $w_n(a, b)$, and two source measures at $j = 2n + 1$.	Finite-j atomic PMFs $\mathrm{Pr}_{\mathrm{flat}}, \mathrm{Pr}_{\mathrm{stack}}$ (6.11); rescaled $Y_j = M/j$ converges weakly (bounds $1/j, 18/j$) to 2ω and $6\omega(1-\omega) = 6\mathfrak{f}(\omega)$.	Viewing cosine $\cos\psi_2 = 1/\sqrt{3}$ (Prop. 6.4) is an area foreshortening factor; finite-j laws are atomic, and $6\mathfrak{f}(\omega)$ requires $w_n(a, b)$.

Figure 9 (§6.6, Theorem 6.5): Common Triangular / Odd-Square Factorization, $\mathbb{Z}^2 \rtimes \mathrm{O}(2, \mathbb{Z})$ Sector Congruence, Euler Cosine PGF, Fixed-Gap Gamma Family & Stack Limits

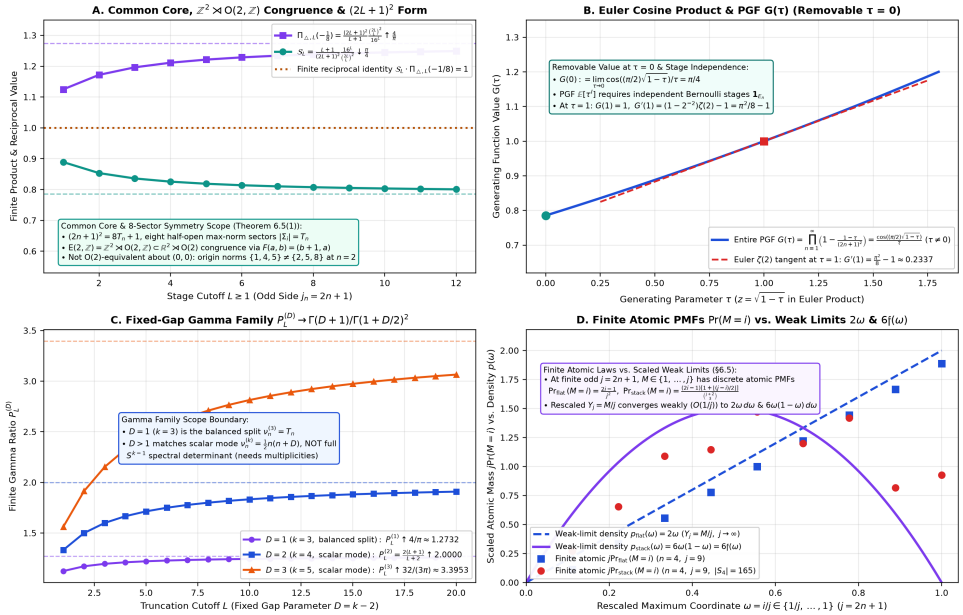


Figure 9 (Theorem 6.5 across four panels): **A.** Common algebraic core and finite closed form $\mathcal{S}_L = \frac{L+1}{(2L+1)^2} \frac{16^L}{\binom{2L}{L}^2} \downarrow \frac{\pi}{4}$ paired with $\Pi_{\triangle,L}(-1/8) = 1/\mathcal{S}_L \uparrow \frac{4}{\pi}$. **B.** Euler cosine product and entire PGF $G(\tau) = \cos((\pi/2)\sqrt{1-\tau})/\tau$ $(\tau \neq 0)$ with removable value $G(0) = \pi/4$ and tangent slope $G'(1) = \pi^2/8 - 1$ at $\tau = 1$. **C.** Fixed-gap Gamma family $P_L^{(D)} \uparrow \Gamma(D+1)/\Gamma(1+D/2)^2$. **D.** Finite-$j$ atomic masses vs. weak-limit densities $p_{\mathrm{flat}}(\omega) = 2\omega$ and $p_{\mathrm{stack}}(\omega) = 6\omega(1-\omega) = 6\mathfrak{f}(\omega)$.

Remark 6.6a (Triangular Canonical Product $\Pi_{\triangle}(u)$, Self-Contained Brouncker Continuant Defect Proof, and Completed-Zeta Scope). Because $\sum_{n \geq 1} T_n^{-1} = 2$, $\Pi_{\triangle}(u) = \prod_{n=1}^{\infty}(1 - u/T_n)$ is entire of genus 0, order $1/2$, and type $\pi\sqrt{2}$; writing $a(a+1) = 2u$ gives $1 - u/T_n = \frac{(n-a)(n+a+1)}{n(n+1)}$ and Euler's reflection closed form

$$\Pi_{\triangle}(u)=\frac{1}{\Gamma(1-a)\,\Gamma(a+2)}=\frac{\sin(\pi a)}{\pi a(a+1)},\qquad \Pi_{\triangle}\!\left(-\frac{1}{8}\right)=\frac{1}{\Gamma(3/2)^2}=\frac{4}{\pi}\quad\left(u=-\frac{1}{8}\iff a=-\frac{1}{2}\right).$$

For Brouncker's generalized continued fraction $B(s)=s+\mathrm{K}_{n=1}^{\infty}\frac{(2n-1)^2}{2s}=4\big[\frac{\Gamma((s+3)/4)}{\Gamma((s+1)/4)}\big]^2$ ($\operatorname{Re}s>0$, where $B(1)=4/\pi$ and $B(s)B(s+2)=(s+1)^2$) [16], define the continuant polynomials $P_L^{\mathrm{Br}}(s),Q_L^{\mathrm{Br}}(s)\in\mathbb{Z}[s]$ on all $s\in\mathbb{C}$ by the initial conditions

$$\big(P_{-1}^{\mathrm{Br}}(s),\,Q_{-1}^{\mathrm{Br}}(s)\big)=(1,0),\qquad \big(P_{0}^{\mathrm{Br}}(s),\,Q_{0}^{\mathrm{Br}}(s)\big)=(s,1),$$

and the three-term recurrence ($L\ge 1$)

$$P_L^{\mathrm{Br}}(s)=2s\,P_{L-1}^{\mathrm{Br}}(s)+(2L-1)^2P_{L-2}^{\mathrm{Br}}(s),\qquad Q_L^{\mathrm{Br}}(s)=2s\,Q_{L-1}^{\mathrm{Br}}(s)+(2L-1)^2Q_{L-2}^{\mathrm{Br}}(s).$$

For any $a,b\ge -1$ and $s\in\mathbb{C}$, put $\langle a,b\rangle_s:=(s+1)^2Q_a^{\mathrm{Br}}(s)Q_b^{\mathrm{Br}}(s+2)-P_a^{\mathrm{Br}}(s)P_b^{\mathrm{Br}}(s+2)$ and write $D_L^{\mathrm{Br}}(s):=\langle L,L\rangle_s$, $C_L^{-}(s):=\langle L,L-1\rangle_s$, and $C_L^{+}(s):=\langle L-1,L\rangle_s$ (with $(-1)!!:=1$). At $L=0$, $D_0^{\mathrm{Br}}(s)=(s+1)^2-s(s+2)=1$, $C_0^{-}(s)=-s$, and $C_0^{+}(s)=-(s+2)$; at $L=1$, $P_1^{\mathrm{Br}}(s)=2s^2+1$ and $Q_1^{\mathrm{Br}}(s)=2s$ give $C_1^{-}(s)=s-2$, $C_1^{+}(s)=s+4$, and $D_1^{\mathrm{Br}}(s)=4s(s+2)(s+1)^2-(2s^2+1)(2(s+2)^2+1)=-9=-(3!!)^2$. By induction on $L\ge 1$, expanding the first or second slot via the recurrence yields

$$C_L^{-}(s)=2s\,D_{L-1}^{\mathrm{Br}}(s)+(2L-1)^2C_{L-1}^{+}(s)=(-1)^{L-1}((2L-1)!!)^2\big[2s-(s+2L)\big]=(-1)^{L}((2L-1)!!)^2(2L-s),$$
$$C_L^{+}(s)=2(s+2)\,D_{L-1}^{\mathrm{Br}}(s)+(2L-1)^2C_{L-1}^{-}(s)=(-1)^{L-1}((2L-1)!!)^2\big[2(s+2)+(2L-2-s)\big]=(-1)^{L-1}((2L-1)!!)^2(s+2L+2),$$

and for $L\ge 2$, expanding $D_L^{\mathrm{Br}}(s)=2s\,C_L^{+}(s)+(2L-1)^2\big[2(s+2)C_{L-1}^{+}(s)+(2L-1)^2D_{L-2}^{\mathrm{Br}}(s)\big]$ gives

$$D_L^{\mathrm{Br}}(s)=(-1)^{L}((2L-1)!!)^2\Big[-2s(s+2L+2)+2(s+2)(s+2L)+(2L-1)^2\Big]=(-1)^{L}((2L-1)!!)^2(2L+1)^2=(-1)^{L}((2L+1)!!)^2.$$

Consequently, for every $L\ge 1$ and every $s\in\mathbb{C}$, $D_L^{\mathrm{Br}}(s)$ is independent of s and satisfies the exact finite-stage scalar normalization

$$\Pi_{\triangle,L}\!\left(-\frac{1}{8}\right)=\prod_{n=1}^{L}\frac{(2n+1)^2}{4n(n+1)}=\frac{((2L+1)!!)^2}{2^{2L}L!(L+1)!}=\frac{|D_L^{\mathrm{Br}}(s)|}{2^{2L}L!(L+1)!}=\frac{1}{\mathcal{S}_L}.$$

(Scope: This identity is an exact finite scalar normalization of $((2N+1)!!)^2$, not an operator intertwiner between the continuant recurrence and triangular multiplication. Likewise, under $u(s)=\frac{s(s-1)}{2}=-\frac{1}{8}+\frac{(s-1/2)^2}{2}$, the branch point $u(1/2)=-1/8$ and the Riemann–Siegel phase constant $-\pi/8$ in $\theta(t)=\frac{t}{2}\log\frac{t}{2\pi}-\frac{t}{2}-\frac{\pi}{8}+\frac{1}{48t}+O(t^{-3})$—giving $1-\frac{1}{8}=\frac{7}{8}$ in $N_0(t)=1+\frac{\theta(t)}{\pi}+S(t)$—share the half-shift $s-1/2$ as distinct polynomial and Gamma-phase operations. Writing $\Xi_{\triangle}(u):=\xi(s)=\frac{1}{2}s(s-1)\pi^{-s/2}\Gamma(s/2)\zeta(s)$ in $u=s(s-1)/2$, negative integers $s=-k$ ($k\ge 1$) evaluate at $u(-k)=T_k$ to $\Xi_{\triangle}(T_k)=\xi(k+1)$, which does not uniquely determine $\Xi_{\triangle}(u)$ inside its order-1/2 infinite-type class because $\Xi_{\triangle}(u)+b\,\Pi_{\triangle}(u)$ shares all triangular values $u=T_k$.)*

Remark 6.6b (The Commutant of the Exchange E and the Family $B_a=I+aE$, Projective Cayley / Möbius Group $\mathcal{M}\cong\mathbb{R}^{\times}$, and Self-Contained Euler-Transform Proof for S_+ [18, 19]):

1. **The Commutant of the Exchange E and the Family $B_a=I+aE$:** A 2×2 real matrix L commutes with the coordinate exchange $E=\left(\begin{smallmatrix}0&1\\1&0\end{smallmatrix}\right)$ iff $L\in\mathcal{A}=\mathbb{R}I\oplus\mathbb{R}E=\mathbb{R}P_+\oplus\mathbb{R}P_-$ ($P_\pm=\frac{1}{2}(I\pm E)$), on which $L\mapsto L\mathbf{e}_1$ is a linear isomorphism onto $\mathbb{R}^2$ intersecting the affine family $\left(\begin{smallmatrix}1&a\\a'&b\end{smallmatrix}\right)$ at the unique matrix $B_a=I+aE=(1+a)P_++(1-a)P_-$ ($a'=a,b=1$).
2. **Projective Cayley Conjugacies & Completed Möbius Group:** On $\mathbb{RP}^1$, the projective Cayley involution $C[a:b]=[b-a:b+a]$ ($C(a)=\frac{1-a}{1+a}$) satisfies $C(1/a)=-C(a)$ and $C(-a)=1/C(a)$, intertwining the Klein-four group $\{\mathrm{id},-a,1/a,-1/a\}\cong C_2\times C_2$ (with $\mathbb{RP}^1$ fixed sets $\{0,\infty\}$, $\{-1,1\}$, and $\varnothing$). Adjoining $M_\infty(a)=1/a$ to the open family $M_\beta(a)=\frac{a-\beta}{1-\beta a}$ ($\beta\in\mathbb{R}\setminus\{\pm1\}$, where $M_2M_{-1/2}=M_\infty$) yields the completed abelian group $\mathcal{M}=\{M_\beta:\beta\in\mathbb{RP}^1\setminus\{-1,1\}\}\cong\mathbb{R}^{\times}$ via the homomorphism $\mu_\beta=\frac{1+\beta}{1-\beta}$ ($\mu_\infty=-1$, $\mu_{\beta\star\gamma}=\mu_\beta\mu_\gamma$), in which $M_\infty(a)=1/a$ is the unique nonidentity involution.

3. **Telescoping Zeta Identity and Exact-Rational Euler Enclosure for S_+:** Define the positive telescoping series $S_+ := \sum_{n=1}^{\infty} \frac{\ln n}{n(n+1)}$ [19]. Using $\frac{1}{n(n+1)} = \frac{1}{n} - \frac{1}{n+1}$, partial summation on $1 \le n \le M$ gives $\sum_{n=1}^{M} \ln n\big(\frac{1}{n} - \frac{1}{n+1}\big) = \sum_{i=2}^{M} \frac{\ln i - \ln(i-1)}{i} - \frac{\ln M}{M+1}$. Letting $M \to \infty$ ($\frac{\ln M}{M+1} \to 0$), expanding $-\ln(1-1/i) = \sum_{k=1}^{\infty} \frac{1}{k\, i^k}$ (all terms positive for $i \ge 2$), and interchanging sums by Tonelli's theorem yields

$$S_+ = \sum_{i=2}^{\infty} \frac{-\ln(1-1/i)}{i} = \sum_{k=1}^{\infty} \frac{\zeta(k+1)-1}{k} = \int_0^1 \frac{1-\gamma-\psi(2-z)}{z}\, dz \approx 0.7885305659115090.$$

For rigorous rational enclosure without Euler–Maclaurin remainders, Euler's binomial transform of the alternating zeta function, $(1-2^{1-s})\zeta(s) = \sum_{n=0}^{\infty} 2^{-(n+1)} \Delta^n f_s(1)$ of the completely monotone sequence $f_s(j) = j^{-s}$ ($s = k+1 \ge 2$) satisfies $0 < (-1)^n \Delta^n f_s(1) \le 1$, so its L-term truncation has positive error bounded strictly by $\sum_{n=L}^{\infty} 2^{-(n+1)} = 2^{-L}$, while the outer tail beyond $K \ge 1$ satisfies $0 < \sum_{k=K+1}^{\infty} \frac{\zeta(k+1)-1}{k} \le \sum_{k=K+1}^{\infty} \frac{k+2}{k^2 2^{k+1}} \le \frac{K+3}{(K+1)^2 2^{K+1}}$ (at $L = 240, K = 200$, rational enclosure width $< 1.57 \times 10^{-63}$; by contrast, $S_- := \sum_{k=2}^{\infty} \frac{\ln k}{k(k-1)} \approx 1.2577468869443696$ gives $S_+ + S_- \approx 2.0462774528558786$ nats). Moreover, S_+ is strictly distinct from three elementary closed-form series whose values hold analytically by telescoping: (i) $S_{\text{tel}} := \sum_{n=2}^{\infty} \big[\ln(1 + \frac{1}{n^2-1}) - \frac{1}{n^2}\big] = 1 + \ln 2 - \frac{\pi^2}{6} \approx 0.0482131137$; (ii) $\sum_{i=1}^{\infty} \frac{2}{(4i-1)(4i+1)} = 1 - \frac{\pi}{4} \approx 0.2146018366$; and (iii) $\sum_{i=1}^{\infty} \frac{1}{(2i-1)(2i)(2i+1)} = \ln 2 - \frac{1}{2} \approx 0.1931471806$.

Figure 12 (§6.4–§6.6 & §8.2): Positive Lorentz Sheet & Seed Square, Balanced-Split Defect Ladder, Odd-Chamber Midpoint vs. n^2+1 Separation, and Exact-Rational Euler S_+ Series

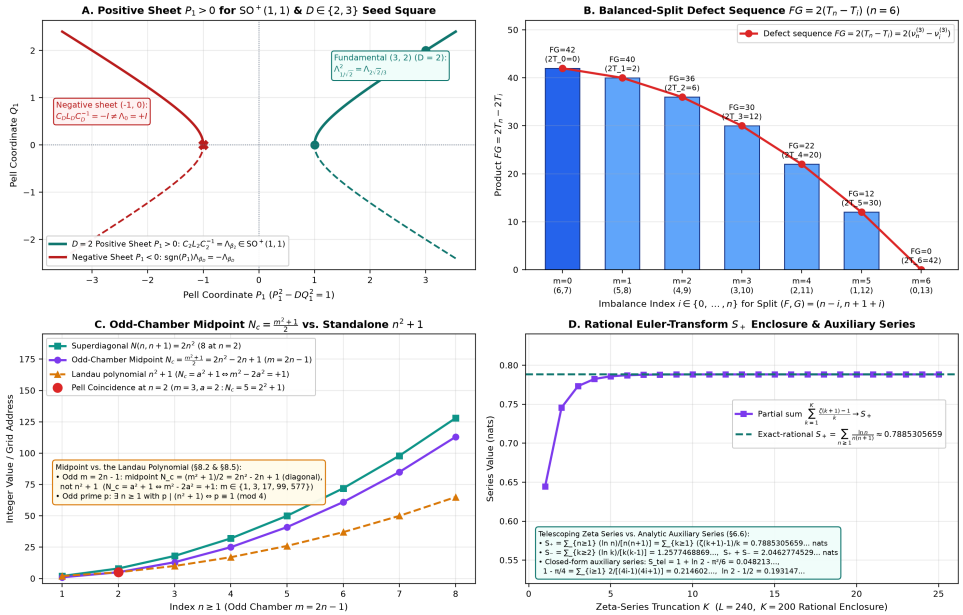


Figure 12 (Geometric and analytic scope separations across §§6.4–6.6 & §8.2): **A.** Positive Lorentz sheet $P_1 > 0$ for $C_D L_D C_D^{-1} = \Lambda_{\beta_D} \in \text{SO}^+(1,1)$ vs. the negative sheet $(-1, 0) \mapsto -I \ne \Lambda_0 = +I$, and the $D \in \{2, 3\}$ fundamental seed square. **B.** Balanced-split defect sequence $FG = 2(T_n - T_i)$ at $n = 6$ (Lemma 6.5a, Theorem 6.5). **C.** Odd-chamber diagonal midpoint $N_c = (m^2 + 1)/2 = 2n^2 - 2n + 1$ $(m = 2n - 1)$ vs. the superdiagonal address $2n^2$ and the standalone polynomial $n^2 + 1$ (odd primes $p \ge 3$). **D.** Exact-rational Euler-transform series for S_+ separated from the elementary closed-form series S_{tel}, $1 - \pi/4$, and $\ln 2 - 1/2$.

7. Scope Boundaries and Open Questions

7.1 Mirror-Prime Pairs in Odd Chambers (Finite Verification: $1403 \le m \le 20001$)

For an odd chamber $m = 2M + 1$, the midpoint reflection $R_{\text{mid}}(N) = m^2 + 1 - N$ fixes the diagonal address $N_c = (m^2 + 1)/2$, **exchanges** the ordered symmetric endpoints $N_c - k \leftrightarrow N_c + k$, and fixes the unordered pair $\{N_c - k, N_c + k\}$ setwise across the diagonal:

$$N_c = \frac{m^2+1}{2}, \qquad M = \frac{m-1}{2}, \qquad (a,b) = (N_c - k,\ N_c + k) \quad (1 \le k \le M). \quad (7.1)$$

Here $a + b = m^2 + 1$ and $2 \le b - a = 2k \le m - 1$. Using **distinct unordered prime pairs** ($a < b$, i.e., $k \ge 1$), direct sieve computation [9] verifies that every odd chamber in the finite interval $1403 \le m \le 20001$ contains at least one mirror-prime pair (beginning at $m = 1403$, $N_c = 984{,}205$ with $k_{\min} = 6$, pair $\{984{,}199, 984{,}211\}$). Proving existence for all odd $m \ge 1403$ requires controlling prime pairs in the short moving interval $[N_c - M, N_c + M]$ of length $m - 1 \approx \sqrt{2N_c}$ around N_c, which remains open.

7.2 Specific Record-Set Intersection Problem (Open Beyond $\{1, 5, 29\}$)

As shown in §5.2, generic distinct primitive carrier rays can share a first chamber (such as $(11, 3)$ and $(9, 7)$ at $m_0 = 65$). A narrower question concerns the two specific approximation record families in Appendix A: the 45° Pell record rays (U_j, W_j) (with $|U^2 - W^2 - 2UW| = 2$) and the $a = 2$ target $(3/5, 4/5)$ record rays (with $|U - 2W| = 1$). The only primitive rays belonging to *both* record families are $(1, 1), (3, 1)$, and $(7, 3)$, with first chambers $m_0 \in \{1, 5, 29\}$. Setting $\tau = 2U + W \equiv 3$ or $7 \pmod{10}$ and $\varepsilon = U - 2W = \pm 1$ on the $a = 2$ record chambers $m_k^- = 10k^2 + 6k + 1$ and $m_k^+ = 10k^2 + 14k + 5$ gives $10m_0 - 1 = \tau^2$, while Pell completeness ($G^2 - 2m_0^2 = -1$ for $m_0 = P_{2j+1}$, where $P_0 = 0, P_1 = 1, P_{n+2} = 2P_{n+1} + P_n$ and Q_n denotes the **half-Pell–Lucas sequence** $Q_0 = Q_1 = 1, Q_{n+2} = 2Q_{n+1} + Q_n$ with backward extension $Q_{-1} = -1$) reduces the value-set intersection $P_{2j+1} \in \{m_k^-, m_k^+\}$ to the quartic Diophantine equation $50G^2 = \tau^4 + 2\tau^2 - 49$, or equivalently via the companion identity $10P_{2j+1} - 1 = Q_{j+2}^2 + Q_{j-1}^2 - 1 = \tau^2$ (and via the generically degree-two unramified map $(\tau, G) \mapsto (A, C) = (2(\tau^2 + 1), 20G\tau) = (20m_0, 20G\tau)$—which is injective on $\tau, G > 0$—to positive integral points $(A, C) \in E(\mathbb{Z})$ on the smooth Weierstrass elliptic curve $E : C^2 = (A - 2)(A^2 - 200)$ of discriminant $\Delta(E) = 16 \cdot 4 \cdot 200 \cdot 196^2 = 491{,}724{,}800 = 2^{13} \cdot 5^2 \cdot 7^4$, where $(A, C) \in E(\mathbb{Z})$ represents a positive intersection iff $A > 0, C > 0, 20 \mid A$, $(A - 2)/2 = \tau^2$, and $(A^2 - 200)/200 = G^2$ for positive integers $\tau, G > 0$ with $\tau \equiv 3$ or $7 \pmod{10}$, recovering $m_0 = A/20$, $\varepsilon = -1$ if $\tau \equiv 3 \pmod{10}$ else $+1$, and $U = (2\tau + \varepsilon)/5, W = (\tau - 2\varepsilon)/5$). Because $Q_{j-1}^2 - 1 = 0$ iff $j \in \{0, 1, 2\}$, the three intersections $(m_0, G, \tau) \in \{(1, 1, 3), (5, 7, 7), (29, 41, 17)\}$ correspond to the particular square root $\tau = Q_{j+2}$ for $j = 0, 1, 2$ ($E_0 = (20, 60), E_1 = (100, 980), E_2 = (580, 13940)$). Direct finite enumeration confirms that the two record-chamber sets have no further intersection up to $m_0 \le 10^7$ (and modular quadratic-residue sieving excludes $0 \le j \le 1000$ beyond $j \in \{0, 1, 2\}$), while an all-index exclusion proof—either elementary or via a complete integral-point determination on $E(\mathbb{Z})$ with pullback filters—remains open.

Figure 8 (§7): Odd-Chamber Mirror-Prime Symmetry Across the Diagonal and Record-Set Intersection Pullback on $E : C^2 = (A-2)(A^2-200)$

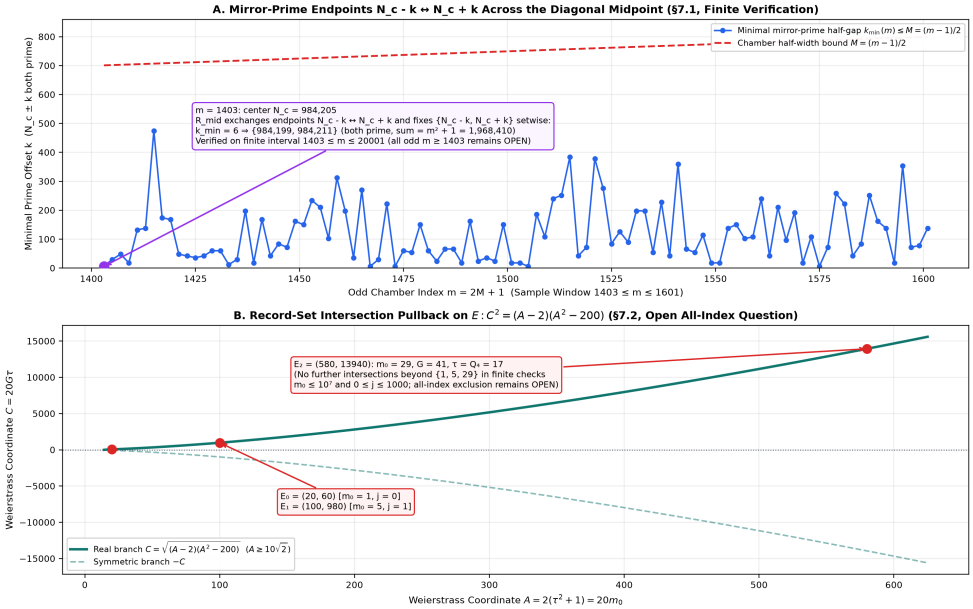


Figure 8 (Odd-chamber mirror-prime pairs and record-set intersection on E): **A.** Minimal mirror-prime half-gap $k_{\min}(m) \le M = (m-1)/2$ where midpoint reflection R_{mid} exchanges the prime endpoints $N_c - k \leftrightarrow N_c + k$ across $N_c = (m^2+1)/2$ and fixes $\{N_c - k, N_c + k\}$ setwise in odd chambers $m = 2M + 1$ (§7.1; verified across $1403 \le m \le 20001$, while existence for all odd $m \ge 1403$ remains open). **B.** Pullback of

shared $a = 2$ and 45° Pell record chambers $m_0 \in \{1, 5, 29\}$ to integral points $E_0 = (20, 60), E_1 = (100, 980), E_2 = (580, 13940)$ on $E : C^2 = (A-2)(A^2-200)$ ($A = 20m_0, C = 20G\tau$, §7.2; no further intersections occur in finite checks $m_0 \le 10^7$ and $0 \le j \le 1000$, while the all-index exclusion question remains open).

7.3 Separating Equations from Exploratory Notebook Sketches

Hand-drawn annotations on early working cards (such as reciprocal ratios $9/56 \leftrightarrow 56/9$ and Moessner striking diagrams) record heuristic motivation during the initial construction of the Grid [9]. Every theorem in this paper rests solely on the explicitly declared definitions, domains, and proofs given in the text.

8. Divisor Shells, Jordan Totients, and Factorial-Residual Arithmetic on the Grid Addresses

8.1 Relation to the Coordinate Layers and the Shared Identity Criterion

Because the address $N(r, c) = T_{m-1} + r$ in chamber $m = r + c - 1$ is exactly the rank of the rational triangular entry $a(m, r) = m - 1 + r/m$ (§1.3), the positive quadrant of §§1–7 serves directly as the coordinate system for three arithmetic structures [11, 12, 14]: (i) **divisor-band and shell-numerator progressions** (§8.2), (ii) ***k*-dimensional Jordan-totient shells and their three zeta limits** (§8.3), and (iii) **the triangular factorial-residual calculus and its entire-function Taylor lift** (§§8.4–8.4a). **Table 8.0** summarizes how the coordinate layers, the odd-square factorization of §6.6, and the arithmetic theorems below fit together logically:

Table 8.0 — Directional Implication Map Across the Coordinate, Factorization, and Arithmetic Layers

Structural Layer	Exact Mathematical Statement	Directional Logical Relation
Coordinate Layers (§§1–5)	Bijection $N(r, c) = T_{m-1} + r$, parity wedge $2N = m^2 + V + 1$ ($\widetilde{r} + \widetilde{c} = 2m$), phase reflections $(R_{\text{mid}}, R_{\text{row}}, R_{\text{root}})$, floor branches ℓ_k, and odd-square semicircle carriers $\mathcal{C}(r, c)$ with $(\widetilde{r}, \widetilde{c}) = \lambda(U^2, W^2)$.	**Supplies the address and phase coordinates** on which both the odd-square factorization and the divisor-shell / factorial-residual operators ($R_d(k, h)$, d_m, $Q(N)$) act.
Central Factorization (§6.6, Thm. 6.5)	**Triangular / Odd-Square Factorization and Reciprocal Identity:** $(2n+1)^2 = 8T_n + 1 = 4n(n+1) + 1 \iff \mathfrak{f}(\frac{n}{2n+1}) = \frac{2T_n}{8T_n+1} \iff (1 - j_n^{-2})(1 + \frac{1}{8T_n}) = 1$, tying $\mathcal{S}_L = \frac{L+1}{(2L+1)^2} \frac{16^L}{\binom{2L}{L}^2} \downarrow \frac{\pi}{4}$ to $\Pi_{\triangle, L}(-1/8) \uparrow \frac{4}{\pi}$.	**Unites the 8-sector odd-square partition**, the balanced split $\{n, n+1\}$ (two oriented states $(n, n+1), (n+1, n)$), the staircase value $\mathfrak{f}(\chi_{2n+1}^{\perp})$, and the Wallis product.
Analytic & Measure Pushforwards (§§6.5–6.6)	**(a)** Entire center-hit PGF $G(\tau) = \frac{\cos((\pi/2)\sqrt{1-\tau})}{\tau}$ ($G(0) = \frac{\pi}{4}, G'(1) = \frac{\pi^2}{8} - 1$); **(b)** Fixed-gap Gamma ratio $P_L^{(D)} \to \frac{\Gamma(D+1)}{\Gamma(1+D/2)^2}$; **(c)** stack fibers $w_n(a, b) = 1 + \lfloor \frac{n - \max(a,b)}{2} \rfloor$ pushing uniform stack measure forward to $p_{\text{stack}}(\omega) = 6\omega(1-\omega) = 6\mathfrak{f}(\omega)$ (vs. flat 2ω).	**Implied by Theorem 6.5 plus declared route hypotheses:** (a) requires stage independence + Euler's cosine product; (b) replaces $D = 1$ by scalar gap $D > 0$; (c) requires the stack fiber multiplicity $w_n(a, b)$ along $(1, 1, 1)/\sqrt{3}$.
Arithmetic on the Addresses (§§8.2–8.5)	**(d)** Shell numerators $R_d(k, h) = d^2k - d + h$ with the square-gap value $R_m(1, m-1) = m^2 - 1$ (Thm. 8.1); **(e)** Jordan conservation $\sum_{d \mid m} J_k(d) = m^k$ and three zeta limits (Thm. 8.2); **(f)** Factorial residual $Q(N) = N/\gcd(N, m!) \in \{1\} \cup \mathbb{P}$ with density $\log 2$ and entire lift $G_{\pm}(z)$ (Thm. 8.3, Prop. 8.4).	**Instantiates $N = T_{m-1} + r$ across divisor shells and factorials**, separating proved one-point / smooth density laws ($\frac{6}{\pi^2}, \log 2$) from open two-point prime occupancy (§7.1, §8.5).

Across all comparisons between geometric and arithmetic constructions, we enforce the following criterion [12]:

Principle 8.1 (Shared Identity Criterion). *A repeated numerical constant, exponent, or shape across two constructions is structurally meaningful if and only if both appearances instantiate an explicit common algebraic identity, coordinate transformation, generating function, or measure pushforward. Where no shared identity exists (such as a rational shell defect $-1/12$ vs. $\zeta(-1) = -B_2/2 = -1/12$, a 45° cone denominator 84 vs. $\zeta(-13) = -7/84$, or finite parameter counts vs. exponential-sum exponents), the coincidence is classified as a small-denominator collision and*

kept strictly separate. (All symbols are defined locally and summarized in Appendix C; the notation follows the corpus notation register [7].)

8.2 Divisor-Band Bijection, Shell Numerator Progressions, and Finite Shell Diagnostics

In the rational triangular grid [11], chamber $m \geq 1$ consists of the m rational numbers

$$a(m,r) = m - 1 + \frac{r}{m} = \frac{m(m-1)+r}{m}, \qquad 1 \leq r \leq m,$$

whose rank is the address $N(r,c) = T_{m-1} + r$ and whose fractional part r/m is the native row phase κ_{row}. Grouping entries by their reduced denominator $d = m/\gcd(m,r)$ gives the following exact progression structure [11, 14]:

Theorem 8.1 (Divisor-Band Bijection, Shell Numerator Progressions, and the Square-Gap Factorization). *For every integer $m \geq 1$ and row $1 \leq r \leq m$, set $k = \gcd(m,r)$, $d = m/k$, and $h = r/k$ so that $\gcd(h,d) = 1$ and $1 \leq h \leq d$. Then $m = dk$ and $r = hk$, and the reduced form of $a(m,r)$ has denominator d and numerator*

$$R_d(k,h) = \frac{m(m-1)+r}{\gcd(m,r)} = d^2k - d + h \equiv h - d \pmod{d^2}, \qquad \gcd(h-d, d^2) = 1.$$

Consequently:

1. **Divisor-Band Decomposition & Window Discrepancy:** *For each divisor $d \mid m$, exactly $\varphi(d)$ entries in chamber m reduce to denominator d, realizing $\sum_{d\mid m}\varphi(d) = m$. For any divisor subset $D \subseteq \mathrm{Div}(m)$ and $\beta \in [0,1]$, the coprime window discrepancy $\Delta_{m,D}(\beta) := \sum_{d\in D} \#\{1 \leq a \leq d\beta : \gcd(a,d) = 1\} - \beta\sum_{d\in D}\varphi(d)$ satisfies*

$$\Delta_{m,D}(\beta) = \sum_{d\in D}\sum_{i\mid d}\mu(i)\left(\left\lfloor \frac{d\beta}{i}\right\rfloor - \frac{d\beta}{i}\right), \qquad \sup_{0\leq\beta\leq 1}|\Delta_{m,D}(\beta)| \leq \sum_{d\in D} 2^{\omega(d)}, \qquad \sup_{0\leq\beta\leq 1}\left|\Delta_{p^a,\{p^a\}}(\beta)\right| = 1 - \frac{1}{p}.$$

2. **Strict Within-Shell Uniqueness & Progression Multiplier:** *For each fixed shell $d \geq 1$, $(k,h) \mapsto R_d(k,h)$ is injective on $\mathbb{Z}_{\geq 1} \times \{1 \leq h \leq d : \gcd(h,d) = 1\}$ (so no integer or prime value ever repeats within a single shell d, although cross-shell values such as $R_2(2,1) = R_3(1,1) = 7$ can coincide). As $k \geq 1$ varies, shell d traces $\varphi(d)$ residue classes $h - d \pmod{d^2}$, each coprime to d^2, and since d and d^2 have the same prime factors, $\varphi(d^2) = d\varphi(d)$, giving*

$$\frac{d^2}{\varphi(d^2)} = \frac{d^2}{d\,\varphi(d)} = \frac{d}{\varphi(d)}.$$

3. **Square Gap, the Factorization $m^2 - 1 = (m-1)(m+1)$, and the Midpoint vs. n^2+1:** *At $r = m-1$ ($\gcd(m, m-1) = 1$, $d = m$, $k = 1$, $h = m-1$), $m^2 - a(m,m-1)^2 = 2 - \frac{1}{m^2} = 4\left(\frac{1}{4} + \mathfrak{f}(\chi_m^{+})\right)$, and $R_m(1, m-1) = m^2 - 1 = (m-1)(m+1)$ is composite for every $m \geq 3$. On the Notebook Grid, the diagonal and superdiagonal addresses are $N(n,n) = 2n^2 - 2n + 1$ (**diagonal**, 5 at $n = 2$) and $N(n,n+1) = 2n^2$ (**superdiagonal**, 8 at $n = 2$), not n^2 and n^2+1; the Landau polynomial n^2+1 (where for an **odd prime** p there exists $n \geq 1$ with $p \mid (n^2+1)$ iff $\left(\frac{-1}{p}\right) = +1 \iff p \equiv 1 \pmod 4$) connects to the Grid via the odd-chamber midpoint sum $N + R_{\mathrm{mid}}(N) = 2N_c = m^2 + 1$ (§7.1 and §8.5(3)), not via $N(n,n+1)$.*

Proof. Since $\gcd(h,d) = 1$, $\gcd(R_d(k,h),d) = \gcd(d^2k - d + h, d) = \gcd(h,d) = 1$, so $R_d(k,h)/d$ is reduced and $\gcd(h-d, d^2) = 1$. (1) Each $r \in \{1,\ldots,m\}$ writes uniquely as $r = (m/d)h$ with $d \mid m$ and $\gcd(h,d) = 1$ ($1 \leq h \leq d$), giving $\varphi(d)$ entries per divisor $d \mid m$. By $\mathbf{1}_{\gcd(a,d)=1} = \sum_{i\mid\gcd(a,d)}\mu(i)$, $\#\{1 \leq a \leq d\beta : \gcd(a,d) = 1\} = \sum_{i\mid d}\mu(i)\lfloor d\beta/i\rfloor$; subtracting $\beta\varphi(d) = \sum_{i\mid d}\mu(i)(d\beta/i)$ gives the formula for $\Delta_{m,D}(\beta)$. Since each bracket $\lfloor\cdot\rfloor - (\cdot)$ lies in $(-1,0]$ and $\sum_{i\mid d}|\mu(i)| = 2^{\omega(d)}$, summing over $d \in D$ bounds $|\Delta_{m,D}(\beta)| \leq \sum_{d\in D} 2^{\omega(d)}$; for $D = \{p^a\}$, $\Delta_{p^a,\{p^a\}}(\beta) = (\lfloor p^a\beta\rfloor - p^a\beta) - (\lfloor p^{a-1}\beta\rfloor - p^{a-1}\beta)$, which approaches $-(1-1/p)$ as $\beta \uparrow 1/p^{a-1}$ and has supremum $1 - 1/p$. (2) Writing $R_d(k,h) - 1 = d^2(k-1) + \big(d(d-1) + h - 1\big)$ with $0 \leq h - 1 \leq d - 1$ places the remainder $d(d-1) + h - 1$ in $[d(d-1), d^2 - 1] \subset [0, d^2 - 1]$, so Euclidean division by d^2 uniquely recovers $k-1$ and $h-1$; $\varphi(d^2) = d^2\prod_{p\mid d^2}(1-1/p) = d\cdot d\prod_{p\mid d}(1-1/p) = d\varphi(d)$. (3) Direct substitution at $r = m-1$ gives $a(m,m-1) = m - 1/m$,

$m^2-(m-1/m)^2=2-1/m^2$, and $R_m(1,m-1)=m^2-1=(m-1)(m+1)\geq 8$ composite for $m\geq 3$; for an odd prime p, $a^2\equiv -1 \pmod p$ is solvable in $\mathbb{Z}$ iff $(-1)^{(p-1)/2}=1 \iff p\equiv 1 \pmod 4$ by Euler's criterion. □

Remark 8.1a (Finite Shell Diagnostics, Explicit Cohort, Like-for-Like CV Weightings, and Two Variance Conventions [14]). To compare finite prime counts across shells $1\leq d\leq M$ against the Dirichlet–PNT asymptotic heuristic without dividing by $\log 1=0$, define the active shell cells and cell weights by

$$S_M^*(d):=\big\{(k,h):1\leq k\leq \lfloor M/d\rfloor,\ 1\leq h\leq d,\ \gcd(h,d)=1,\ R_d(k,h)\geq 2\big\},\qquad w_d:=|S_M^*(d)|.$$

Because $R_d(k,h)=d^2k-d+h\geq 2$ for every cell except $(d,k,h)=(1,1,1)$ where $R_1(1,1)=1$, this cutoff excludes only $(1,1,1)$, giving $w_1=M-1$ and $w_d=\varphi(d)\lfloor M/d\rfloor$ for $d\geq 2$. Selecting the shell cohort

$$\mathcal{C}_M:=\{1\leq d\leq M: w_d\geq 100\}$$

gives $|\mathcal{C}_M|=153,479,1000,2000$ shells at $M=250,500,1000,2000$. Every integer threshold from 97 to 100 gives the same four cohorts; we fix $w_d\geq 100$. Define the observed active-cell prime density and the cellwise PNT-in-progressions predictor

$$\delta_M(d):=\frac{1}{w_d}\sum_{(k,h)\in S_M^*(d)}\mathbf{1}_{\mathbb{P}}\big(R_d(k,h)\big),\qquad \widehat{\delta}_M(d):=\frac{1}{w_d}\sum_{(k,h)\in S_M^*(d)}\frac{d}{\varphi(d)\log R_d(k,h)},$$

and compare the size-blind baseline $A_M(d):=\varphi(d)\delta_M(d)$ against the size-corrected ratio $Q_M(d):=\delta_M(d)/\widehat{\delta}_M(d)$ on $\mathcal{C}_M$. Here $d^2/\varphi(d^2)=d/\varphi(d)$ is exact, whereas $1/\log R_d(k,h)$ is an asymptotic prime-density heuristic (no uniform theorem for the growing moduli $d^2\leq M^2$ follows from a finite table). Using average ranks for Spearman ties and population variance, write $\mathrm{CV}_{\mathrm{eq}}(Y)=\sqrt{\frac{1}{|\mathcal{C}_M|}\sum_{d\in\mathcal{C}_M}(Y(d)-\overline{Y}_{\mathrm{eq}})^2}/\overline{Y}_{\mathrm{eq}}$ for equal-shell CV and $\mathrm{CV}_w(Y)=\sqrt{\sum_{d\in\mathcal{C}_M}w_d(Y(d)-\overline{Y}_w)^2/\sum_{d\in\mathcal{C}_M}w_d}/\overline{Y}_w$ for cell-weighted CV. The table reports **both** like-for-like weightings:

M	$\lvert\mathcal{C}_M\rvert$	**Spearman** (d,A_M)	**Spearman** (d,Q_M)	**Equal-Shell** $\mathrm{CV}_{\mathrm{eq}}(A_M)$	**Equal-Shell** $\mathrm{CV}_{\mathrm{eq}}(Q_M)$	**Cell-Weighted** $\mathrm{CV}_w(A_M)$	**Cell-Weighted** $\mathrm{CV}_w(Q_M)$
250	153	+0.959	+0.002	0.593	0.137	0.611	0.138
500	479	+0.979	−0.022	0.546	0.095	0.584	0.094
1000	1000	+0.984	+0.040	0.539	0.079	0.579	0.076
2000	2000	+0.991	+0.024	0.541	0.059	0.583	0.058

Under either identical weighting scheme ($\mathrm{CV}_{\mathrm{eq}}: 0.539\to 0.079$ or $\mathrm{CV}_w: 0.579\to 0.076$ at $M=1000$), dividing by $\widehat{\delta}_M(d)$ reduces shell dispersion substantially. Similarly, at $M=1000$, the two binomial-style standard-error conventions

$$\mathrm{SE}_d^{\mathrm{pred}}:=\sqrt{\frac{\widehat{\delta}_M(d)\big(1-\widehat{\delta}_M(d)\big)}{w_d}},\qquad \mathrm{SE}_d^{\mathrm{obs}}:=\sqrt{\frac{\delta_M(d)\big(1-\delta_M(d)\big)}{w_d}}$$

give 996/1000 **shells** satisfying $|\delta_M(d)-\widehat{\delta}_M(d)|\leq 2\ \mathrm{SE}_d^{\mathrm{pred}}$ (excluding $d\in\{450,464,680,956\}$) and 994/1000 **shells** satisfying $|\delta_M(d)-\widehat{\delta}_M(d)|\leq 2\ \mathrm{SE}_d^{\mathrm{obs}}$ (additionally excluding $d\in\{328,550\}$). These bands are descriptive diagnostics on deterministic prime data, not independent Bernoulli trials or confidence-coverage guarantees: higher shells reach larger numerators ($R_d(k,h)\sim d^2k\leq dM$), while $A_M(d)=\varphi(d)\delta_M(d)$ omits the factor d in $d/\varphi(d)$, explaining why shell stratification acts as a classical PNT-in-progressions coordinate lens rather than a new prime-distribution law.

8.3 The k-Dimensional Jordan Chamber Lift and Three Separate Zeta Limits

Lifting the row phases $\{r/m: 1\leq r\leq m\}$ to the k-dimensional cube $C_k(m)=\{(r_1/m,\dots,r_k/m): 1\leq r_i\leq m\}$ and assigning each tuple its reduced common denominator $d_m(r_1,\dots,r_k)=m/\gcd(m,r_1,\dots,r_k)$ connects Remark 6.1b directly to Jordan's totient $J_k(d)=d^k\prod_{p\mid d}(1-p^{-k})$ [12]:

Theorem 8.2 (Jordan Shell Conservation, Body-Shell Möbius Formula, and Three Separate Zeta Limits). *For every dimension $k\geq 1$ and chamber $m\geq 1$:*

1. **Jordan Shell Conservation, Separated Primitive Counts, and Punctured-Stack Möbius Sieve:** *For each divisor $d \mid m$, $\#\{(r_1,\dots,r_k) \in \{1,\dots,m\}^k : d_m(r_1,\dots,r_k) = d\} = J_k(d)$, so $\sum_{d|m} J_k(d) = m^k$. More generally, for any subset $\mathcal{W} \subseteq [0,1]^k$ with $L_{\mathcal{W}}(a) = \#\{\mathbf{r} \in \{1,\dots,a\}^k : \mathbf{r}/a \in \mathcal{W}\}$, $A_{\mathcal{W}}(d) := \#\{\mathbf{r} \in \{1,\dots,d\}^k : \mathbf{r}/d \in \mathcal{W}, \gcd(d, r_1,\dots,r_k) = 1\} = \sum_{i|d} \mu(i) L_{\mathcal{W}}(d/i)$. Row primitivity, common-denominator primitivity, and punctured-stack visibility carry distinct predicates: (a) on the address-sheet row of chamber m, with sites $(-r/(m+1), 1/(m+1))$ $(1 \le r \le m)$, the second coordinate forces $\gcd(m+1, r, 1) = 1$ for all m sites, whereas primitive columns require $\gcd(r, m+1) = 1$ (counting $\varphi(m+1)$); (b) on the punctured stack $S_n^* = S_n \setminus \{(0,0,0)\}$ of size $|S_n| - 1 = \binom{2n+3}{3} - 1$,*

$$A^{\mathrm{prim}}_{S_n^*} := \#\{(p_1,p_2,\ell) \in S_n^* : \gcd(|p_1|,|p_2|,\ell) = 1\} = \sum_{i=1}^{n} \mu(i) \left[\binom{2\lfloor n/i \rfloor + 3}{3} - 1 \right] \qquad (A^{\mathrm{prim}}_{S_1^*} = 9,\ A^{\mathrm{prim}}_{S_2^*} = 25,\ A^{\mathrm{prim}}_{S_3^*} = 65,\ A^{\mathrm{prim}}_{S_4^*} = 121).$$

2. **Three Separate Divisor-Support Limits:** *Setting $F_k(n) := \frac{J_k(n)}{n^k} = \sum_{i|n} \frac{\mu(i)}{i^k} = \prod_{p|n}(1 - p^{-k})$ (and primorial $P_\beta = \prod_{p \le \beta} p$) separates three distinct asymptotic objects:*

$$\text{(i) Fixed } n\text{: } F_k(n) = \sum_{i|n} \frac{\mu(i)}{i^k}, \qquad \text{(ii) Primorial } (k \ge 2)\text{: } \lim_{\beta \to \infty} F_k(P_\beta) = \frac{1}{\zeta(k)}, \qquad \text{(iii) Modulus-averaged } (k \ge 1)\text{: } \lim_{M \to \infty} \frac{1}{M} \sum_{n \le M} F_k(n) = \frac{1}{\zeta(k+1)}.$$

3. **Reconciliation of the Chamber Fraction $\frac{\varphi(n)}{n-1}$ and the One-Dimensional Density $\frac{\varphi(n)}{n}$:** *In chamber $m \ge 1$, put $n = m+1$; the m address-sheet sites $p_1 = -r/n$ $(1 \le r \le n-1)$ include $\varphi(n)$ with $\gcd(r,n) = 1$, so*

$$f_{\mathrm{native}}(m) = \frac{\varphi(m+1)}{m} = \frac{\varphi(n)}{n-1} = F_1(n) + \frac{\varphi(n)}{n(n-1)}, \qquad \frac{1}{M}\sum_{n=1}^{M} F_1(n) = \frac{6}{\pi^2} + O\Big(\frac{\log M}{M}\Big), \qquad \frac{1}{M-1}\sum_{n=2}^{M} \frac{\varphi(n)}{n-1} = \frac{6}{\pi^2} + O\Big(\frac{\log M}{M}\Big).$$

Proof. (1) Putting $a = \gcd(m, r_1,\dots,r_k) = m/d$ sets $(r_1,\dots,r_k) = a(r_1',\dots,r_k')$ with $\mathbf{r}' \in \{1,\dots,d\}^k$ and $\gcd(d, r_1',\dots,r_k') = 1$. Since $\mathbf{1}_{\gcd(d,r_1,\dots,r_k)=1} = \sum_{i|\gcd(d,r_1,\dots,r_k)} \mu(i)$, writing $\mathbf{r} = i\mathbf{v}$ ($\mathbf{v} \in \{1,\dots,d/i\}^k$) gives $A_{\mathcal{W}}(d) = \sum_{i|d} \mu(i) L_{\mathcal{W}}(d/i)$, which for $\mathcal{W} = [0,1]^k$ ($L_{\mathcal{W}}(a) = a^k$) evaluates to $\sum_{i|d} \mu(i)(d/i)^k = J_k(d)$. Similarly, $(p_1,p_2,\ell) \in S_n^*$ is divisible by $i \ge 1$ iff $(p_1,p_2,\ell) = i(p_1',p_2',\ell')$ with $0 \le i\ell' \le n \iff \ell' \le \lfloor n/i \rfloor$ and $|p_1'|, |p_2'| \le \lfloor (n - i\ell')/i \rfloor = \lfloor n/i \rfloor - \ell'$, bijecting onto $S^*_{\lfloor n/i \rfloor}$ of size $|S_{\lfloor n/i \rfloor}| - 1$. (2) For $k \ge 2$, $\sum_{i=1}^{\infty} i^{-k} < \infty$, so $F_k(P_\beta) = \prod_{p \le \beta}(1 - p^{-k}) \to \prod_p (1 - p^{-k}) = 1/\zeta(k)$. For $k \ge 1$, $\frac{1}{M}\sum_{n \le M} F_k(n) = \frac{1}{M}\sum_{i \le M} \frac{\mu(i)}{i^k} \lfloor M/i \rfloor = \sum_{i \le M} \frac{\mu(i)}{i^{k+1}} + O\big(\frac{1}{M}\sum_{i \le M} i^{-k}\big) \to \frac{1}{\zeta(k+1)}$, with error $O\big(\frac{\log M}{M}\big)$ at $k = 1$ and $O(M^{-1})$ for $k \ge 2$. (3) Since $0 < \frac{\varphi(n)}{n(n-1)} \le \frac{1}{n-1}$, $\frac{1}{M-1}\sum_{n=2}^{M} \frac{\varphi(n)}{n(n-1)} = O\big(\frac{\log M}{M}\big)$, giving the same Cesàro limit $\frac{6}{\pi^2}$. □

8.4 The Triangular Factorial-Residual Calculus on the Grid Addresses

On chamber $I_m = (T_{m-1}, T_m]$, with $m(N) = \lfloor \sqrt{2N} + 1/2 \rfloor$ the chamber of N, the factorial-residual operator $Q(N) := \frac{N}{\gcd(N, m!)}$ acts directly on the Notebook Grid address $N = N(r,c) = T_{m-1} + r$ [12]:

Theorem 8.3 (Complete Factorial-Residual Classification, the Exceptional Prime Powers $\{p^2\} \cup \{27\}$, the Successor-Prime Rule, the Rising-Factorial gcd, and the Dickman Density $\log 2$). *For every integer $N \ge 1$ in chamber $m = m(N)$, let $Q(N) = N/\gcd(N, m!)$. Then:*

1. **Prime-Residual Dichotomy & Complete Branch Classification:** *For every $N \ge 1$, $Q(N) \in \{1\} \cup \mathbb{P}$, and any prime p occurs as $Q(N) = p$ at most once in a chamber I_m. Moreover, $Q(N) > 1$ if and only if N belongs to one of three disjoint branches:*
   - *(i) Prime squares: $N = p^2$ for a prime p (lying in chamber $p \le m \le 2p-1$ where $v_p(m!) = 1$, giving $Q(p^2) = p$);*
   - *(ii) The exceptional cube: $N = 27 = 3^3$ in chamber $m = 7$ ($(r,c) = (6,2)$, $v_3(7!) = 2$, $Q(27) = 3$; every other prime power p^k with $k \ge 3$ satisfies $Q(p^k) = 1$);*
   - *(iii) High-prime multiples: $N = ap$ where $p > m$ is prime and $1 \le a < \frac{m+1}{2}$ (giving $Q(ap) = p$).*
2. **The Successor-Prime Rule on the First-Column Edge:** *On the first-column edge $c = 1$ ($r = m$, $N = T_m$), $Q(T_m) = \mathrm{den}(m!/T_m) = a_m$, the reduced numerator of $T_m/m!$ [4], satisfies*

$$a_m = Q(T_m) = \begin{cases} m+1, & \text{if } m+1 \text{ is an odd prime,} \\ 1, & \text{otherwise.} \end{cases}$$

3. **Pooled Dickman Density** $\log 2$ **& Abscissa** $\sigma_c = 2$**:** *Let* $F_{\mathrm{res}}(m) = \#\{N \in I_m : Q(N) > 1\}$ *and* $A_{\mathrm{res}}(M) = \sum_{m=1}^{M} F_{\mathrm{res}}(m)$*. For* $M \geq 7$*, the* m*-smooth count* $S_{\mathrm{sm}}(M) = \#\{N \leq T_M : P^+(N) \leq m(N)\}$ *and closed count* $C_{\mathrm{res}}(M) = T_M - A_{\mathrm{res}}(M)$ *satisfy* $S_{\mathrm{sm}}(M) - C_{\mathrm{res}}(M) = \pi(\sqrt{T_M}) + 1$*, and by de Bruijn's smooth-number theorem [13] (Dickman's function* ϱ *has* $\varrho(2) = 1 - \log 2$*),*

$$\lim_{M\to\infty} \frac{A_{\mathrm{res}}(M)}{T_M} = \log 2 \approx 0.693147, \qquad \mathcal{R}(s) := \sum_{m=1}^{\infty} \frac{F_{\mathrm{res}}(m)}{m^s} \sim \frac{\log 2}{s-2} \quad (s \downarrow 2).$$

4. **Half-Index Identity, Reciprocal-Triangular Sum, and the Golden Ratio at Address** $\frac{1}{2}$**:** *For odd* $j = 2n+1$*,* $8T_{(j-1)/2} + 1 = 8T_n + 1 = j^2$*;* $-\frac{1}{2} + \sum_{i=1}^{M} \frac{1}{T_i} = \frac{3}{2} - \frac{2}{M+1} \to \frac{3}{2} = \frac{T_2}{2!}$*; and the continuous inverse* $T^{-1}(a) = \frac{\sqrt{8a+1}-1}{2}$ *evaluates at* $a = 1/2$ *to* $T^{-1}(1/2) = \frac{\sqrt{5}-1}{2}$*, so* $T\big(\frac{\sqrt{5}-1}{2}\big) = \frac{1}{2}$*.*
5. **Successor Split, Rising-Factorial Interior gcd, and Denominator-Jump Trichotomy:** *For* $n \geq 2$*, write* $T_n/n! = a_n/b_n$ *in lowest terms, where* $a_n \in \{n+1, 1\}$ *(*$n+1$ *if* $n+1$ *is prime,* 1 *if* $n+1$ *is composite) and the cancelled part* $d_n := (n+1)/a_n = \gcd(n+1, 2(n-1)!) \in \{1, n+1\}$ *satisfy* $a_n d_n = n+1$ *and* $a_n + d_n = n+2$*. In the rising product* $\Pi_n(y) = \prod_{j=1}^{n}(1+jy) = \sum_{k=0}^{n} e_k(n)\, y^k$ *(*$e_0(n) = 1$*,* $e_1(n) = T_n$*,* $e_n(n) = n!$*), the interior coefficients satisfy* $g_n := \gcd(e_1(n), \ldots, e_{n-1}(n)) = a_n$ *for all* $n \geq 2$*. For* $n \geq 3$*, the denominator jump* $D_n := b_n/b_{n-1} = (n-1)d_{n-1}/d_n$ *obeys*

$$D_n = \begin{cases} n(n-1) = 2T_{n-1}, & n+1 \text{ prime,} \\ \dfrac{n-1}{n+1} < 1, & n \text{ prime,} \\ \dfrac{n(n-1)}{n+1} = n - 2 + \dfrac{2}{n+1} \notin \mathbb{Z}, & n,\, n+1 \text{ both composite,} \end{cases}$$

so $n+1$ *is prime iff* $D_n \in \mathbb{Z}$*, in which case* $\frac{2T_n + D_n}{2} = n^2$*,* $\frac{2T_n - D_n}{2} = n$*, and* $(2T_n)^2 - D_n^2 = 4n^3$*. (On the forward ratio* b_n/b_{n+1}*, the single composite-to-prime index* $n = 11$ *evaluates to* $\frac{1}{11\cdot 12} = \frac{1}{2T_{11}} = \frac{1}{132}$*, which coincides numerically at that single index with* $|\zeta(-9)| = B_{10}/10 = 1/132$ *under Principle 8.1.)*
6. **Primitive Triple Rank Bijection and the Unique Kummer Carry Excess at** $(j,p) = (5,3)$**:** *Writing* $(m,r) = k(d,h)$ *with* $k = \gcd(m,r)$ *and* $\gcd(d,h) = 1$*, the map* $(k,d,h) \mapsto N\big(kh,\, k(d-h)+1\big) = \frac{kd(kd-1)}{2} + kh$ *is a bijection onto* $\mathbb{Z}_{\geq 1}$*, and for a uniformly chosen address* $N \leq T_M$ *the scale satisfies* $\Pr(k = a) \to \frac{6}{\pi^2 a^2}$ *as* $M \to \infty$*. For* $\Lambda_j := \prod_{i=j}^{2j-1} i = \frac{(2j)!}{2\, j!}$*,* $\delta_p(j) := v_p(\Lambda_j) - 2v_p(j!) \leq 0$ *holds for every prime* $p \leq j$ *(*$j \geq 2$*) except at the unique pair* $(j,p) = (5,3)$*, where* $\delta_3(5) = +1$ *and* $\frac{\Lambda_5}{(5!)^2} = \frac{21}{20}$*.*

Proof. (1) Let $N \in I_m = (T_{m-1}, T_m]$, so $N \leq \frac{m(m+1)}{2} < \frac{(m+1)^2}{2}$, and suppose a prime p divides $Q(N)$, i.e., $k := v_p(N) > v_p(m!)$.

- *If* $p > m$*:* Then $v_p(m!) = 0$ and $N = ap$ with $1 \leq a = N/p \leq \frac{m(m+1)}{2(m+1)} = \frac{m}{2} < \frac{m+1}{2} \leq m$ (requiring $m \geq 2$). Every prime factor p' of a satisfies $p' \leq a < m$ and $v_{p'}(a) \leq v_{p'}(m!)$ (since $a \mid m!$), while $\gcd(p, m!) = 1$; thus $\gcd(ap, m!) = a$ and $Q(N) = p$ (Branch iii). Because $|I_m| = m < p$, at most one multiple of p lies in I_m.
- *If* $p \leq m$*:* Write $N = bp^k$ with $p \nmid b$; since $v_p(m!) \geq 1$, we have $k \geq 2$. If $k = 2$, then $v_p(m!) = 1 \implies p \leq m \leq 2p-1$, whence $N \leq T_{2p-1} = p(2p-1) < 2p^2$, forcing $b = 1$ and $N = p^2$ with $Q(p^2) = p$ (Branch i). If $k = 3$: for $p = 2$, $N \geq 8 > T_3 = 6 \implies m \geq 4 \implies v_2(m!) \geq 3 = k$, impossible; for $p \geq 5$, $m+1 > \sqrt{2}\, p^{3/2} \geq \sqrt{10}\, p > 3p \implies m \geq 3p \implies v_p(m!) \geq \lfloor m/p \rfloor \geq 3$, impossible; for $p = 3$, $N = 27b > T_6 = 21 \implies m \geq 7$, where $m \geq 9$ has $v_3(m!) \geq 4 > 3$ and $m \in \{7, 8\}$ has $N \leq T_8 = 36 < 54$, forcing $b = 1, N = 27 \in I_7$ ($v_3(7!) = 2, Q(27) = 3$, Branch ii; note $3^2 = 9 \notin I_7$). If $k \geq 4$: for $p = 2$, $N \geq 16 > T_5 \implies m \geq 6$ ($v_2(6!) = 4$), $N \geq 32 > T_7 \implies m \geq 8$ ($v_2(8!) = 7 \geq 5$), $N \geq 64 > T_{10} \implies m \geq 11$ ($v_2(11!) = 8 \geq 6$), and for $k \geq 7$, $m+1 > 2^{(k+1)/2} > 2k \implies v_2(m!) \geq \lfloor m/2 \rfloor + \lfloor m/4 \rfloor > k$; for $p \geq 3, k \geq 4$, $N \geq 81 > T_{12} \implies m \geq 13$ ($v_3(13!) = 5 \geq 4$), and in general $m+1 > \sqrt{2}\, p^{k/2}$ implies $\lfloor m/p \rfloor \geq \lceil \sqrt{2}\, p^{k/2} - 1 \rceil / p - 1 \geq k$ whenever $(p,k) \neq (3,4)$ (checked directly at $(3,5) : m \geq 22, v_3(22!) = 9$, and growing exponentially via $p^{k/2-1} \geq 3^{k/2-1}$). Because Branches (i)–(ii) are pure prime powers $p^2, 3^3$ and Branch (iii) has $a \mid m!$, no second prime can divide $Q(N)$, proving $Q(N) \in \{1\} \cup \mathbb{P}$ and within-chamber uniqueness.

(2) Since $m!/T_m = \frac{2(m-1)!}{m+1}$, $Q(T_m) = \frac{m+1}{\gcd(m+1,2(m-1)!)}$. At $m=1$ ($m+1=2$) and $m=3$ ($m+1=4$), $m+1$ divides $2(m-1)!$, so $Q(T_m)=1$. If $m+1$ is an odd prime ($m\geq 2$), $\gcd(m+1,2(m-1)!)=1$ so $Q(T_m)=m+1$. If $m+1\geq 6$ is composite, either $m+1=ab$ with $2\leq a<b\leq (m+1)/2\leq m-1$ (so $ab\mid (m-1)!$) or $m+1=p^2$ for an odd prime $p\geq 3$, where $2p\leq p^2-3<p^2-1=m$ for $p\geq 5$ and at $p=3$ ($m=8$) $3\cdot 6\mid 7!$, so $p^2\mid (m-1)!$ and $Q(T_m)=1$.

(3) By (1), $Q(N)=1$ iff $P^+(N)\leq m(N)$ and $N\notin\{p^2: p\in\mathbb{P}\}\cup\{27\}$. Every p^2 has $m(p^2)\geq p=P^+(p^2)$ and 27 has $m(27)=7>3$, so for $M\geq 7$, $S_{\mathrm{sm}}(M)-C_{\mathrm{res}}(M)=\pi(\sqrt{T_M})+1=O(M/\log M)$. Because $|m(N)-\sqrt{2N}|<\frac{1}{2}$, replacing $P^+(N)\leq m(N)$ by $P^+(N)\leq\sqrt{2T_M}$ alters at most $O(M^2/\log M)=o(T_M)$ integers (since $N\leq\varepsilon T_M$ contributes $\leq\varepsilon T_M$ and on $\varepsilon T_M<N\leq T_M$ primes in $[\sqrt{2\varepsilon T_M}-1,\sqrt{2T_M}+1]$ contribute $\ll T_M/\log M$ near the boundary). Applying de Bruijn's theorem $\Psi(A,A^{1/2})=(1-\log 2)A+O(A/\log A)$ [13] at $A=T_M$ gives $C_{\mathrm{res}}(M)/T_M\to 1-\log 2$, so $A_{\mathrm{res}}(M)/T_M\to\log 2$. Partial summation on $\sum_{m=1}^{M}F_{\mathrm{res}}(m)=(\frac{\log 2}{2}+o(1))M^2$ yields $(s-2)\mathcal{R}(s)\to\log 2$ as $s\downarrow 2$.

(4) $\sum_{i=1}^{M}\frac{1}{T_i}=\sum_{i=1}^{M}\left(\frac{2}{i}-\frac{2}{i+1}\right)=2-\frac{2}{M+1}$, and substituting $a=1/2$ in $T^{-1}(a)=\frac{\sqrt{8a+1}-1}{2}$ gives $\frac{\sqrt{5}-1}{2}$.

(5) Let $g_n=\gcd(e_1(n),\dots,e_{n-1}(n))$ for $n\geq 2$, and suppose a prime p divides g_n. If $p\leq n$, then $p\mid n!=e_n(n)$ as well, so $\Pi_n(y)=1+\sum_{k=1}^{n-1}e_k(n)y^k+n!\,y^n\equiv 1\pmod p$ as polynomials; evaluating at $y=-1$ gives $0=\Pi_n(-1)\equiv 1\pmod p$ (the factor $j=1$ vanishes), a contradiction. Hence **no prime $p\leq n$ divides g_n**. Since $g_n\mid e_1(n)=T_n=\frac{n(n+1)}{2}$ and every prime factor of n (and 2, since $n\geq 2$) is $\leq n$, g_n must divide $n+1$ and be odd. If $n+1$ is composite, every prime factor of $n+1$ is $\leq (n+1)/2<n$, forcing $g_n=1=a_n$. If $n+1=p$ is an odd prime ($n=p-1$), $\prod_{j=1}^{p-1}(1+jy)\equiv 1-y^{p-1}\pmod p$ in $\mathbb{F}_p[y]$, so $p\mid e_k(p-1)$ for $1\leq k\leq p-2$; since $v_p(T_{p-1})=1$, $g_{p-1}=p=a_n$. Next, $T_n/n!=\frac{n+1}{2(n-1)!}=\frac{a_n}{2(n-1)!/d_n}$ gives $b_n=\frac{2(n-1)!}{d_n}$, so for $n\geq 3$ (where n and $n+1$ cannot both be prime), $D_n=b_n/b_{n-1}=(n-1)d_{n-1}/d_n$ yields the three stated cases.

(6) Bijectivity of $(k,d,h)\mapsto N\big(kh,k(d-h)+1\big)$ follows from Proposition 1.2 and Theorem 8.1. Since $\frac{\Lambda_j}{(j!)^2}=\frac{\binom{2j}{j}}{2\,j!}$, Kummer's theorem ($v_p\binom{2j}{j}=C_p(j)$, the base-$p$ carry count of $j+j$) gives $\delta_2(j)=C_2(j)-1-v_2(j!)=2\,\mathrm{wt}_2(j)-1-j\leq 0$ for all $j\geq 2$, where $\mathrm{wt}_2(j)$ counts the ones in the binary expansion of j ($\delta_2(2)=\delta_2(3)=0$, and $2\,\mathrm{wt}_2(j)\leq 2\lfloor\log_2 j\rfloor+2\leq j+1$ for $j\geq 4$), and $\delta_p(j)=C_p(j)-v_p(j!)$ for odd primes $p\leq j$. Let $L=\lfloor\log_p j\rfloor+1$ be the number of base-p digits of j, so $C_p(j)\leq L$. If $j\geq p^2$ ($L\geq 3$), Legendre's sum gives $v_p(j!)\geq\sum_{i=1}^{L-1}p^{L-1-i}=\frac{p^{L-1}-1}{p-1}\geq\frac{3^{L-1}-1}{2}>L\geq C_p(j)$, so $\delta_p(j)<0$. If $p\leq j<p^2$ ($L=2$), write $j=ap+b$ ($1\leq a\leq p-1$, $0\leq b\leq p-1$): then $v_p(j!)=a$ and $C_p(j)\leq 2$, so $\delta_p(j)>0$ forces $a=1$ and $C_p(j)=2$. Adding $(1,b)_p+(1,b)_p$ produces two base-p carries iff $2b\geq p$ and $1+1+1\geq p$, forcing $p=3$, $b=2$, and $j=5$ ($\delta_3(5)=2-1=+1$, $\frac{\Lambda_5}{(5!)^2}=\frac{21}{20}$). □

8.4a Entire-Function Realization of the Triangular Coefficients

The factorial-weighted triangular sequence $T_n/n!$ of Theorem 8.3(5) admits an exact entire-function realization via the Euler differential operator [15]. Define on all $z\in\mathbb{C}$ the entire series and differential operators

$$E_{\mathrm{Ei}}(z):=\sum_{n=1}^{\infty}\frac{z^n}{n\,n!},\qquad \Theta_z:=z\frac{d}{dz},\qquad \mathcal{U}:=\frac{1}{2}\Theta_z^2(\Theta_z+1),\qquad \mathcal{L}:=\frac{1}{2}\Theta_z^2(\Theta_z-1).\quad (8.1)$$

Here $z\in\mathbb{C}$ is an analytic variable and $n\geq 1$ a Taylor coefficient index. In the notation of [20, §6.2], $E_{\mathrm{Ei}}(z)=-\operatorname{Ein}(-z)$; on any domain in $\mathbb{C}\setminus\{0\}$ with a consistent branch of the logarithm, $E_{\mathrm{Ei}}(z)=\mathrm{Ei}(z)-\gamma-\operatorname{Log} z$, and the power series in (8.1) is the branch-independent entire definition used throughout.

Proposition 8.4 (Triangular Coefficient Lift and Centered ODE). *For every $z\in\mathbb{C}$,*

$$G_+(z):=\mathcal{U}E_{\mathrm{Ei}}(z)=\sum_{n=1}^{\infty}\frac{T_n}{n!}z^n=\frac{z(z+2)}{2}e^z,\qquad G_-(z):=\mathcal{L}E_{\mathrm{Ei}}(z)=\sum_{n=1}^{\infty}\frac{T_{n-1}}{n!}z^n=\frac{z^2}{2}e^z.\quad (8.2)$$

Consequently, $G_+(z)+G_-(z)=z(z+1)e^z$ and $G_+(z)-G_-(z)=ze^z$, so $n![z^n](G_++G_-)=n^2$ and $n![z^n](G_+-G_-)=n$ for all $n\geq 1$. For every integer $n\geq 2$, Theorem 8.3(5) gives

$$\mathrm{num}\big([z^n]G_+(z)\big)=\begin{cases}n+1, & n+1\text{ prime},\\ 1, & n+1\text{ composite},\end{cases}\qquad [z^n]G_-(z)=\frac{1}{2(n-2)!}.\quad (8.3)$$

Moreover, the centered entire function $\widehat{E}(z) := e^{-z/2}E_{\mathrm{Ei}}(z)$ *satisfies* $\widehat{E}(0) = 0$ *and the linear differential equation*

$$\widehat{E}'(z) + \frac{1}{2}\widehat{E}(z) = \frac{2\sinh(z/2)}{z} \qquad (z \in \mathbb{C}), \quad (8.4)$$

where the right-hand side takes its removable value 1 *at* $z = 0$.

Proof. Because $E_{\mathrm{Ei}}(z)$ has infinite radius of convergence, termwise differentiation holds on $\mathbb{C}$. Since $\Theta_z(z^n) = nz^n$, applying $\mathcal{U}$ and $\mathcal{L}$ multiplies $\frac{z^n}{n\,n!}$ by $\frac{1}{2}n^2(n \pm 1)$, producing $\frac{n(n+1)}{2\,n!}z^n = \frac{T_n}{n!}z^n$ and $\frac{n(n-1)}{2\,n!}z^n = \frac{T_{n-1}}{n!}z^n$. Using $\sum_{n\geq 1}\frac{n}{n!}z^n = ze^z$ and $\sum_{n\geq 1}\frac{n(n-1)}{n!}z^n = z^2e^z$ gives $\sum_{n\geq 1}\frac{T_n}{n!}z^n = \frac{1}{2}(z^2e^z + ze^z) = \frac{z(z+2)}{2}e^z$ and $\sum_{n\geq 1}\frac{T_{n-1}}{n!}z^n = \frac{z^2}{2}e^z$, from which $G_+ \pm G_-$ and the $n \geq 2$ coefficient reduction (via Theorem 8.3(5), since $[z^n]G_+ = T_n/n!$) follow immediately (noting that at $n = 1$, $[z^1]G_+ = 1$ with $n + 1 = 2$, so the reduced-numerator dichotomy requires $n \geq 2$). Finally, $E'_{\mathrm{Ei}}(z) = \sum_{n\geq 1}\frac{z^{n-1}}{n!} = \frac{e^z-1}{z}$ (equal to 1 at $z = 0$), so $\widehat{E}'(z) + \frac{1}{2}\widehat{E}(z) = e^{-z/2}E'_{\mathrm{Ei}}(z) = \frac{e^{z/2}-e^{-z/2}}{z} = \frac{2\sinh(z/2)}{z}$. □

Scope. Proposition 8.4 is an exact analytic realization of the triangular Taylor coefficients $T_n/n!$ and the sums n^2 and n. Passing from a rational Taylor coefficient $[z^n]G_+$ to its lowest-terms numerator $\mathrm{num}(T_n/n!)$ is a nonlinear arithmetic operation on the discrete index $n \geq 2$; no interchange with infinite zeta-zero explicit-formula sums, prime-distribution theorem, or statement concerning the Riemann hypothesis is implied.

8.5 Residue Sieves, Odd-Prime Wheel Counts, and the Quadratic Characters of the Diagonal and the Subdiagonal

Comparing primitive lattice visibility (§8.3), shell-numerator progressions (§8.2), and symmetric prime-pair configurations (§7.1) isolates the distinction between **local congruence obstruction** and **global prime occupancy** [12]:

1. **One-Point Visibility vs. Two-Point Odd-Prime Wheels ($3 \leq p \leq \beta$):** Removing ν_p forbidden residue classes modulo each prime p leaves local survival factor $1 - \nu_p/p$ (or $1 - p^{-k}$ on $\mathbb{Z}^k$). For one-point primitive lattice visibility ($k \geq 2$), inclusion-exclusion converges unconditionally to $1/\zeta(k)$ ($6/\pi^2$ at $k = 2$). For two-point prime patterns—twin pairs $\{n, n+2\}$ ($\nu_p = 2$ for odd primes $p \geq 3$) and Goldbach midpoint pairs $\{M-k, M+k\}$ ($\nu_\ell = 2$ for odd primes $\ell \nmid M$, collapsing to $\nu_\ell = 1$ when $\ell \mid M$)—the Chinese Remainder Theorem gives the exact survivor counts modulo the odd-prime wheel $P_\beta^{\mathrm{odd}} = \prod_{3\leq p\leq\beta} p$:

$$A_\beta = \prod_{3\leq p\leq\beta}(p-2), \qquad A_\beta(2M) = \left(\prod_{\substack{3\leq\ell\leq\beta\\ \ell\nmid M}}(\ell-2)\right)\left(\prod_{\substack{3\leq\ell\leq\beta\\ \ell\mid M}}(\ell-1)\right) = A_\beta \prod_{\substack{3\leq\ell\leq\beta\\ \ell\mid M}}\frac{\ell-1}{\ell-2},$$

   recovering the exact local factor $\frac{\ell-1}{\ell-2}$ of the Hardy–Littlewood singular series $\mathfrak{S}(2M) = 2C_2\prod_{\ell\mid M,\ell\geq 3}\frac{\ell-1}{\ell-2}$, while global prime occupancy remains obstructed by the classical sieve parity barrier.
2. **Twin-Prime Wheel-Exception Rule:** Because every twin prime pair $(n, n+2)$ with $n \geq 3$ already has n odd, the parity modulus $p = 2$ excludes no twin prime pair; $(3, 5)$ and $(5, 7)$ fail the odd-prime wheel ($3 \leq p \leq \beta$) only when $p \in \{3, 5\}$ divides one of the primes themselves, leaving $n \equiv 5 \pmod 6$ for all twin pairs beyond $(3, 5)$.
3. **The Diagonal Midpoint Sum $2N_c = m^2 + 1$ vs. the Subdiagonal $2a^2 + 1$:** In an odd chamber m, a mirror-prime pair $\{N_c - k, N_c + k\}$ around $N_c = (m^2 + 1)/2$ (§7.1) is a Goldbach midpoint representation of $2N_c = m^2 + 1 = (N_c - k) + (N_c + k)$ restricted to $1 \leq k \leq (m-1)/2 = O(\sqrt{N_c})$. The quadratic residue conditions on the **diagonal** and the **subdiagonal** carry distinct Legendre characters:
   - **The diagonal midpoint sum $2N_c = m^2 + 1$ and $n^2 + 1$:** Odd prime divisors $p \mid (n^2 + 1)$ satisfy $\left(\frac{-1}{p}\right) = +1 \iff p \equiv 1 \pmod 4$ ($\nu_p = 2$ for $p \equiv 1 \pmod 4$, $\nu_p = 0$ for $p \equiv 3 \pmod 4$).
   - **The subdiagonal $N_{\mathrm{sub}}(a) = 2a^2 + 1$ at $(a + 1, a)$ in even chamber $m = 2a$:** Odd prime divisors $p \mid (2a^2 + 1)$ satisfy $(2a)^2 \equiv -2 \pmod p$, so $\left(\frac{-2}{p}\right) = +1 \iff p \equiv 1 \text{ or } 3 \pmod 8$ ($\nu_p = 2$ for $p \equiv 1, 3 \pmod 8$, $\nu_p = 0$ for $p \equiv 5, 7 \pmod 8$, with $a = 1 \mapsto N_{\mathrm{sub}}(1) = 3$ prime, $a = 2 \mapsto 9 = 3^2$, $a = 3 \mapsto 19$ prime, and $a = 11 \mapsto 243 = 3^5$).

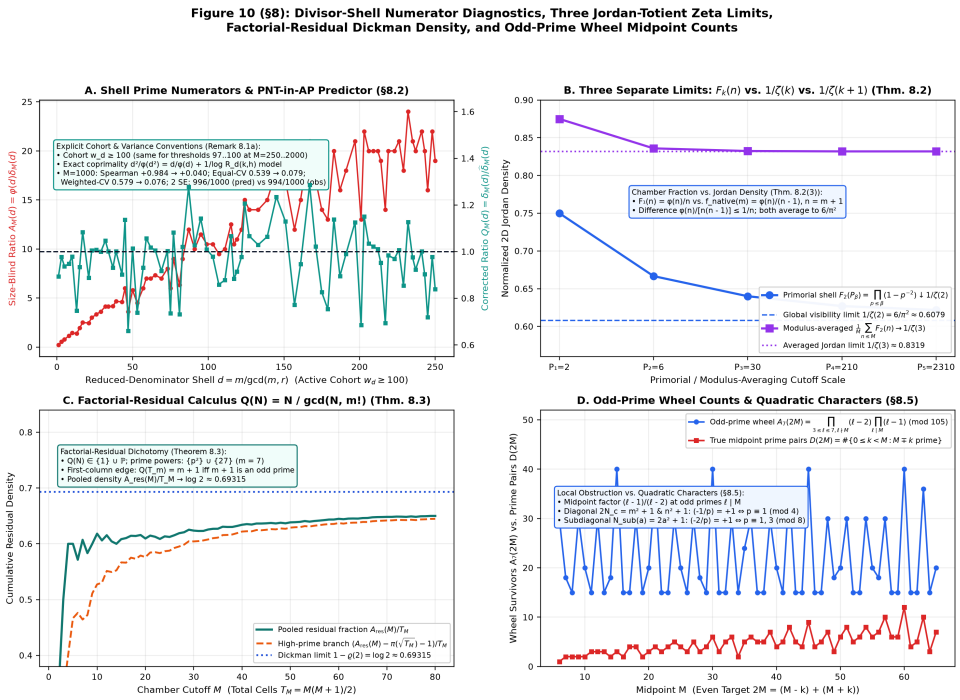


Figure 10 (Arithmetic structures on the Grid addresses across four panels): **A.** Active shell cohort $w_d \geq 100$ (§8.2, Remark 8.1a): dividing by the cellwise PNT-in-progressions predictor $\widehat{\delta}_M(d)$ flattens the size-blind climb $A_M(d) = \varphi(d)\delta_M(d)$ to $Q_M(d) \approx 1$. **B.** The separate limits of Theorem 8.2: primorial density $F_2(P_\beta) \downarrow 1/\zeta(2) = 6/\pi^2$ and modulus-averaged density $\frac{1}{M}\sum_{n\leq M} F_2(n) \to 1/\zeta(3) \approx 0.8319$. **C.** Cumulative factorial-residual fraction $A_{\mathrm{res}}(M)/T_M$ converging to the Dickman limit $1 - \varrho(2) = \log 2 \approx 0.69315$ (Theorem 8.3). **D.** Odd-prime wheel survivor counts $A_7(2M)$ with the midpoint factor $(\ell-1)/(\ell-2)$ vs. true midpoint prime pairs $D(2M)$ (§8.5).

8.6 Mathematical Synthesis and Remaining Open Problems

Taken together, §§1–8 establish a clean structural boundary across the Notebook Grid:

1. **Unconditionally Proved Coordinate, Carrier, Measure, and One-Point / Smooth Laws:** The quadrant address bijection and its parity wedge (§1), affine quadratic paths and period-4 offset parity (§2), three chamber reflections and the anti-diagonal pair correspondence (§3), floor-selected Pell branches and diagonal square descent (§4), odd-square rational semicircle carriers and chamber budgets (§5, Appendix A), address-sheet geometry, three-dimensional directional stack shadows, and the common $(2n+1)^2 = 8T_n + 1$ balanced-split / PGF / Gamma / stack synthesis (§6, Appendix B), divisor-shell uniqueness and the three Jordan-totient zeta limits (§§8.2–8.3), and the factorial-residual dichotomy $Q(N) \in \{1\} \cup \mathbb{P}$ with Dickman density $\log 2$ and entire coefficient lift $G_{\pm}(z)$ (§§8.4–8.4a) all hold unconditionally with self-contained proofs.
2. **Explicitly Open All-Index and Analytic Questions:** Five mathematical problems encountered along the boundary of these theorems remain open and are recorded without speculative promotion:
   - *(a) All-Index Odd-Chamber Mirror Primes (§7.1):* Proving that every odd chamber $m \geq 1403$ contains a prime pair $\{N_c - k, N_c + k\}$ $(1 \leq k \leq (m-1)/2)$ around $N_c = (m^2+1)/2$, beyond the verified finite range $1403 \leq m \leq 20001$.
   - *(b) All-Index Record-Chamber Exclusion on $E(\mathbb{Z})$ (§7.2):* Proving over all indices $j \geq 0$ that $m_0 \in \{1, 5, 29\}$ (E_0, E_1, E_2) are the only positive intersections between the 45° Pell record chambers and the $a = 2$ excluded-target record chambers on $E : C^2 = (A-2)(A^2-200)$.
   - *(c) Two-Point Prime Occupancy vs. Sieve Parity (§8.5):* Passing from exact finite odd-prime wheel survivor counts $A_\beta, A_\beta(2M)$ and quadratic characters $\left(\frac{-1}{p}\right), \left(\frac{-2}{p}\right)$ to infinite prime occupancy along n^2+1, $2a^2+1$, or short chamber intervals.
   - *(d) Optimal Multi-Prime Divisor-Window Constant (§8.2):* Determining the sharp multi-prime supremum constant refining $\sup_{0\leq\beta\leq 1}|\Delta_{m,D}(\beta)| \leq \sum_{d\in D} 2^{\omega(d)}$ in Theorem 8.1(1).
   - *(e) Local and Meromorphic Structure of the Residual Dirichlet Series $\mathcal{R}(s)$ (§8.4):* Determining whether $\mathcal{R}(s) = \sum_{m\geq 1} F_{\mathrm{res}}(m) m^{-s}$ admits meromorphic continuation left of $\mathrm{Re}\, s = 2$ beyond its leading asymptotic

$\frac{\log 2}{s-2}$, and characterizing the chamber-by-chamber variance and sign changes of $F_{\mathrm{res}}(m) - m\log 2$.

Appendix A. Complete Chamber-Budget Theory for Rational Carriers

This appendix proves the complete chamber-budget approximation theorems for centered and leg-sum rational carriers on the upper unit semicircle under an integer chamber bound $m \le M$ [9].

A.1 The 45° Centered Chamber-Budget Theorem and Stepwise Error

Fix an integer chamber budget $M \ge 1$, and restrict the admissible set to positive integer cells (r, c) with $m = r+c-1 \le M$ whose centered carrier point $\mathcal{C}(r, c)$ in (5.1) is rational. We minimize Euclidean chord distance to the 45° target $\mathbf{p}_* = (1/\sqrt{2}, 1/\sqrt{2})$. With $m_0, \ell_1, \ell_2, G = \ell_1 + \ell_2$, and $\delta_{\mathrm{leg}} = \ell_1 - \ell_2$ defined as in (5.7),

$$G^2 + \delta_{\mathrm{leg}}^2 = 2m_0^2, \qquad \|\mathbf{p}(U, W) - \mathbf{p}_*\|_2^2 = 2 - \frac{\sqrt{2}\,G}{m_0}. \quad \text{(A.1)}$$

Theorem A.1 (All-Budget 45° Optimum and Complete Minimizing Cell List). *Let (U_j, W_j) be the Pell carrier sequence (5.6) with first chambers $m_{0,j} = (U_j^2 + W_j^2)/2 \in \{1, 5, 29, 169, 985, \dots\}$. For any integer budget $M \ge 1$, let $j \ge 0$ be the unique index such that $m_{0,j} \le M < m_{0,j+1}$. Then:*

1. *The **unique minimizing circle point** among all rational centered carriers with $m \le M$ is $\mathbf{p}(U_j, W_j)$.*
2. *The **complete set of minimizing cells** in the grid with $m \le M$ consists of its odd-scale repeats:*

$$(r, c) = \left(\frac{\lambda U_j^2 + 1}{2}, \frac{\lambda W_j^2 + 1}{2}\right), \qquad \lambda \in \mathbb{Z}_{\ge 1} \text{ odd}, \qquad \lambda m_{0,j} \le M, \quad \text{(A.2)}$$

   and the number of such minimizing cells is $\left\lfloor (\lfloor M/m_{0,j} \rfloor + 1)/2 \right\rfloor$.
3. *Let $E_{45}(M) = \min_{m \le M} \|\mathbf{p}(U, W) - \mathbf{p}_*\|_2$. Along record chambers, $m_{0,j} E_{45}(m_{0,j}) \to 1/\sqrt{2}$, while over all integer budgets $M \ge 1$,*

$$\liminf_{M\to\infty} M\,E_{45}(M) = \frac{1}{\sqrt{2}}, \qquad \limsup_{M\to\infty} M\,E_{45}(M) = \frac{3 + 2\sqrt{2}}{\sqrt{2}}. \quad \text{(A.3)}$$

Proof. Since $\delta_{\mathrm{leg}} = (U^2 - W^2)/2 - UW$ is odd and $G^2 + \delta_{\mathrm{leg}}^2 = 2m_0^2$, any odd prime $p \mid \gcd(\delta_{\mathrm{leg}}, m_0)$ would divide G and hence divide $\ell_1 = (G + \delta_{\mathrm{leg}})/2$ and $\ell_2 = UW$, contradicting $\gcd(U, W) = 1$. Moreover, for any odd prime $p \mid \delta_{\mathrm{leg}}$, coprimality gives $p \nmid m_0$, and $G^2 + \delta_{\mathrm{leg}}^2 = 2m_0^2$ reduces to $G^2 \equiv 2m_0^2 \pmod p$. Thus 2 must be a quadratic residue modulo p, which excludes $p = 3$ and $p = 5$. Consequently every primitive carrier ray has either $|\delta_{\mathrm{leg}}| = 1$ or $|\delta_{\mathrm{leg}}| \ge 7$.

Every $|\delta_{\mathrm{leg}}| = 1$ pair belongs to (5.6): the base is $(1, 1)$, and if $U < W$ then $\delta_{\mathrm{leg}} < -UW \le -3$, while $U = W$ is primitive only at $(1, 1)$. For any nonbase solution, $U > W$ and $(U - W)^2 - 2W^2 = \pm 2$, which forces $2W < U \le 3W$ (for $W \ge 3$, $U \le 2W$ makes the left side $\le -W^2 < -2$, while at $W = 1$ the unique positive odd nonbase solution is $U = 3$; conversely $U > 3W$ makes the left side $> 2W^2 \ge 2$). Hence $(U', W') = (W, U - 2W)$ is positive, odd, and coprime, preserves $|\delta_{\mathrm{leg}}| = 1$, and strictly decreases $U + W$ until $(1, 1)$ is reached. The record chambers satisfy $m_{0,j+1} = 6m_{0,j} - m_{0,j-1}$ for $j \ge 1$, and the growth bound $m_{0,j+1} < 6m_{0,j}$ holds for all $j \ge 0$ (using $m_{0,1} = 5 < 6m_{0,0} = 6$ at $j = 0$). Any non-record primitive ray available at budget $M < m_{0,j+1}$ has $|\delta_{\mathrm{leg}}| \ge 7$ and $m_0 \le M < m_{0,j+1} < 6m_{0,j}$, so

$$\frac{|\delta_{\mathrm{leg}}|}{m_0} \ge \frac{7}{m_0} > \frac{7}{m_{0,j+1}} > \frac{7}{6m_{0,j}} > \frac{1}{m_{0,j}} = \frac{|\delta_{\mathrm{leg},j}|}{m_{0,j}}.$$

Since $G/m_0 = \sqrt{2 - (\delta_{\mathrm{leg}}/m_0)^2}$ for $G > 0$ (and $G \le 0$ cannot beat $j = 0$), $\mathbf{p}(U_j, W_j)$ strictly beats every non-record ray and every earlier record $i < j$. Finally, $\sqrt{2 - G_j/m_{0,j} \cdot \sqrt{2}} \sim \frac{1}{\sqrt{2}\, m_{0,j}}$ and $\lim_{j\to\infty} m_{0,j+1}/m_{0,j} = 3 + 2\sqrt{2}$ give (A.3). □

A.2 Excluded Opposite-Parity Rational Targets and the Finite-Prefix Exception

Let $A, C \in \mathbb{Z}_{\geq 1}$ be coprime integers of **opposite parity**, and set

$$D_0 = A^2 + C^2, \qquad \mathbf{p}_* = \left(\frac{A^2 - C^2}{D_0}, \frac{2AC}{D_0} \right). \quad \text{(A.4)}$$

Because A, C have opposite parity, $\mathbf{p}_*$ is never attained on the centered rational chart $\mathcal{C}(r, c)$. For any primitive centered carrier pair (U, W), define the nonzero odd determinant $\varepsilon = CU - AW$. Direct expansion gives the exact chord-distance identity

$$\|\mathbf{p}(U, W) - \mathbf{p}_*\|_2^2 = \frac{2(CU - AW)^2}{D_0 m_0} = \frac{2\varepsilon^2}{D_0 m_0}. \quad \text{(A.5)}$$

Let $\mathbf{b}_+ = (U_+, W_+)$ be the unique positive odd pair in $0 < U_+ < 2A, 0 < W_+ < 2C$ with $CU_+ - AW_+ = +1$, and set $\mathbf{b}_- = (2A - U_+, 2C - W_+)$, which satisfies $C(2A - U_+) - A(2C - W_+) = -1$. Then all positive odd pairs with $|\varepsilon| = 1$ form the two canonical Bézout progressions $\mathbf{b}_\pm + 2k(A, C)$ $(k \geq 0)$. Define the explicit tail cutoff

$$M_{\text{cut}} = \max \left\{ \frac{\|\mathbf{b}_+\|_2^2}{2}, \frac{\|\mathbf{b}_-\|_2^2}{2} \right\} \leq 2D_0 - 2(A + C) + 1. \quad \text{(A.6)}$$

Theorem A.2 (Bézout Tail Theorem and Necessary Finite-Prefix Exception). *For every integer budget $M \geq M_{\text{cut}}$, the unique minimizing point for $\mathbf{p}_*$ on the centered chart is the last available $|\varepsilon| = 1$ Bézout ray with $m_0 \leq M$, and $E_*(M) = \min_{m \leq M} \|\mathbf{p}(U, W) - \mathbf{p}_*\|_2$ satisfies*

$$\lim_{M \to \infty} M\, E_*(M)^2 = \frac{2}{D_0}. \quad \text{(A.7)}$$

On the finite initial prefix $1 \leq M < M_{\text{cut}}$, however, non-Bézout rays with $|\varepsilon| \geq 3$ can win: for $(A, C) = (3, 4)$ ($D_0 = 25$), the initial $|\varepsilon| = 1$ rays are $\mathbf{b}_+ = (1, 1)$ ($m_0 = 1$) and $\mathbf{b}_- = (5, 7)$ ($m_0 = 37 = M_{\text{cut}}$), and at budget $M = 17$ the unique winner is the non-Bézout pair $(U, W) = (3, 5)$ ($m_0 = 17, \varepsilon = -3$), which achieves $\varepsilon^2/m_0 = 9/17 < 1/1$ and squared distance $18/425 < 2/25$.

Proof. Write $\mathbf{p}(U, W) = \left(\frac{U^2 - W^2}{U^2 + W^2}, \frac{2UW}{U^2 + W^2}\right)$ and $\mathbf{p}_* = \left(\frac{A^2 - C^2}{D_0}, \frac{2AC}{D_0}\right)$ with $D_0 = A^2 + C^2$. Since both points lie on the unit circle,

$$\begin{aligned} \|\mathbf{p}(U, W) - \mathbf{p}_*\|_2^2 = 2\big(1 - \mathbf{p}(U, W) \cdot \mathbf{p}_*\big) &= \frac{2\big[(A^2 + C^2)(U^2 + W^2) - (A^2 - C^2)(U^2 - W^2) - 4ACUW\big]}{D_0(U^2 + W^2)} \\ &= \frac{4(CU - AW)^2}{D_0(U^2 + W^2)} = \frac{2\varepsilon^2}{D_0 m_0}, \end{aligned}$$

where $\varepsilon = CU - AW$ and $m_0 = (U^2 + W^2)/2$. Because U, W are both odd and A, C have opposite parity, CU and AW have opposite parity, so ε is always an odd integer ($|\varepsilon| \in \{1, 3, 5, \dots\}$).

1. **Unique Canonical Odd Bézout Pair Construction:** To construct the unique positive odd pair $\mathbf{b}_+ = (U_+, W_+)$ in the rectangle $0 < U_+ < 2A, 0 < W_+ < 2C$ with $CU_+ - AW_+ = +1$, start with any integer Bézout solution (a_0, b_0) to $Ca_0 - Ab_0 = +1$. Since A, C have opposite parity, one coordinate of (a_0, b_0) is already forced odd by $Ca_0 - Ab_0 = 1$; adding (A, C) if necessary makes the other coordinate odd while preserving the determinant. All odd integer solutions then differ by integer multiples of $2(A, C)$. Reducing the first coordinate modulo $2A$ by such shifts yields a unique odd representative $U_+ \in (0, 2A)$. The corresponding second coordinate $W_+ = (CU_+ - 1)/A$ is an odd integer; since $CU_+ - 1 \geq 0$, W_+ cannot be negative, and because W_+ is odd it cannot be zero, while $U_+ < 2A$ implies $W_+ < 2C$. This proves existence and uniqueness of $\mathbf{b}_+ = (U_+, W_+)$. The complementary pair $\mathbf{b}_- = (2A - U_+, 2C - W_+)$ is likewise positive and odd in $(0, 2A) \times (0, 2C)$ with determinant $C(2A - U_+) - A(2C - W_+) = -1$. All positive odd solutions with $|\varepsilon| = 1$ are therefore $\mathbf{b}_+ + 2k(A, C)$ and $\mathbf{b}_- + 2k(A, C)$ $(k \geq 0$, since $k < 0$ makes both coordinates negative), and each is automatically coprime because any common divisor divides $|\varepsilon| = 1$. Since $U_+ \leq 2A - 1$ and $W_+ \leq 2C - 1$, both initial chambers satisfy $m_{\pm,0} \leq \frac{(2A-1)^2 + (2C-1)^2}{2} = 2D_0 - 2(A + C) + 1$, giving (A.6).

2. **Complementary Projection Interleaving and Uniform Ratio Bound < 9:** Set $\mathbf{g} = (A, C)$ and let $\nu = (\mathbf{g} \cdot \mathbf{b}_+)/D_0 \in (0, 2)$; the complementary projection of $\mathbf{b}_-$ is $(\mathbf{g} \cdot \mathbf{b}_-)/D_0 = 2 - \nu$. Because $|\det(\mathbf{g}, \mathbf{b}_\pm)| = 1$, orthogonal decomposition along and perpendicular to $\mathbf{g}$ gives

$$\frac{\|\mathbf{b}_+ + 2k\mathbf{g}\|_2^2}{2} = \frac{D_0}{2}\big((\nu + 2k)^2 + D_0^{-2}\big), \qquad \frac{\|\mathbf{b}_- + 2k\mathbf{g}\|_2^2}{2} = \frac{D_0}{2}\big((2 - \nu + 2k)^2 + D_0^{-2}\big).$$

The value $\nu = 1$ is impossible: if $\nu = 1$, then $\mathbf{b}_+ - \mathbf{g}$ would be a nonzero integer vector orthogonal to the primitive vector $\mathbf{g}$, hence an integer multiple of $(C, -A)$, whose determinant with $\mathbf{g}$ is a multiple of $D_0 \geq 5$ rather than ± 1. Define $\beta = \min(\nu, 2 - \nu) \in (0, 1)$. Sorting the two complementary progressions by chamber size (without assuming the $+1$ ray is shorter), their positive projections interleave strictly as

$$\beta < 2 - \beta < 2 + \beta < 4 - \beta < 4 + \beta < \cdots$$

with corresponding Bézout-ray chambers $\hat{m}_0 < \hat{m}_1 < \hat{m}_2 < \cdots$, where $\hat{m}_1 = M_{\text{cut}} = \max(m_{+,0}, m_{-,0})$ has projection $2 - \beta > 1$. For every index $j \geq 1$, the current projection $\nu_j \geq 2 - \beta > 1$ and the next projection satisfies $\nu_{j+1} < \nu_j + 2$, so the successive chamber ratio is strictly bounded by 9:

$$\frac{\hat{m}_{j+1}}{\hat{m}_j} < \frac{(\nu_j + 2)^2 + D_0^{-2}}{\nu_j^2 + D_0^{-2}} < 9 \qquad (j \geq 1),$$

because $9(\nu^2 + D_0^{-2}) - \big((\nu + 2)^2 + D_0^{-2}\big) = 8\nu^2 - 4\nu - 4 + 8D_0^{-2} = 4(\nu - 1)(2\nu + 1) + 8D_0^{-2} > 0$ for all $\nu \geq 1$. Moreover, $\nu_{j+1}/\nu_j \to 1$ implies $\hat{m}_{j+1}/\hat{m}_j \to 1$.

1. **All-Budget Tail Optimality, Asymptotic Law, and Finite-Prefix Counterexample:** For any integer budget $M \geq M_{\text{cut}} = \hat{m}_1$, choose the last available Bézout ray $j \geq 1$ so that $\hat{m}_j \leq M < \hat{m}_{j+1}$. Any primitive odd pair outside the two Bézout progressions has odd determinant $|\varepsilon| \geq 3$; if it is available at budget M, its chamber satisfies $m_0 \leq M < \hat{m}_{j+1}$, so

$$\frac{\varepsilon^2}{m_0} \geq \frac{9}{m_0} \geq \frac{9}{M} > \frac{9}{\hat{m}_{j+1}} > \frac{1}{\hat{m}_j},$$

and it loses strictly to the j-th Bézout ray. Earlier Bézout rays ($i < j$) also lose strictly since $\hat{m}_i < \hat{m}_j$ and $\varepsilon^2 = 1$. Because $\hat{m}_{j+1}/\hat{m}_j \to 1$ forces $\hat{m}_j/M \to 1$, the minimum squared chord error $E_*(M)^2 = \frac{2}{D_0 \hat{m}_j}$ satisfies $M\, E_*(M)^2 = \frac{2}{D_0}\frac{M}{\hat{m}_j} \to \frac{2}{D_0}$, proving (A.7). Finally, at $(A, C) = (3, 4)$ ($D_0 = 25$), $\mathbf{b}_+ = (1, 1)$ ($\hat{m}_0 = 1$) and $\mathbf{b}_- = (5, 7)$ ($\hat{m}_1 = M_{\text{cut}} = 37$); enumerating the seven primitive ordered odd pairs with $m_0 \leq 17$—namely $(1,1), (1,3), (3,1), (1,5), (5,1), (3,5), (5,3)$—shows that at budget $M = 17$, $(U, W) = (3, 5)$ ($m_0 = 17, \varepsilon = -3$) achieves $\varepsilon^2/m_0 = 9/17 < 1 = 1/\hat{m}_0$ and squared distance $18/425 < 2/25$. □

Remark A.2a (Sharp Dichotomy for the Minimal Tail Onset $M_{\text{tail}}(A, C)$). Put $D_0 = A^2 + C^2$, $\nu = (AU + CW)/D_0$, $\varepsilon = CU - AW$, and $\hat{m} = m_0 = (U^2 + W^2)/2$. Orthogonal decomposition $D_0(U^2 + W^2) = (AU + CW)^2 + \varepsilon^2$ gives the exact normalized chamber formula $\hat{m} = \frac{D_0\nu^2 + \varepsilon^2/D_0}{2}$, so the two initial $|\varepsilon| = 1$ rays $\mathbf{r}_0 = (U_0, W_0)$ ($\nu = \beta = p/D_0$ with integer $p = AU_0 + CW_0 \in [A + C, D_0 - 1]$) and $\mathbf{r}_1 = (2A - U_0, 2C - W_0)$ ($\nu = 2 - \beta$) have chambers $\hat{m}_0 = \frac{D_0\beta^2 + D_0^{-1}}{2}$ and $M_{\text{cut}} = \hat{m}_1 = \frac{D_0(2-\beta)^2 + D_0^{-1}}{2}$. On $[\hat{m}_0, M_{\text{cut}} - 1]$, only $\mathbf{r}_0$ is available from $|\varepsilon| = 1$, while the minimum error among available $|\varepsilon| \geq 3$ rays is non-increasing in M. A primitive positive odd pair (U, W) with $|\varepsilon| \geq 3$ ties or beats $\mathbf{r}_0$ before M_{cut} iff $\hat{m} = \frac{D_0\nu^2 + \varepsilon^2/D_0}{2} \geq \varepsilon^2\hat{m}_0 = \frac{\varepsilon^2 D_0\beta^2 + \varepsilon^2/D_0}{2} \iff \nu^2 \geq \varepsilon^2\beta^2 \iff \nu \geq |\varepsilon|\beta$ and $\hat{m} < M_{\text{cut}} \implies \nu < 2 - \beta$. Since $\nu \equiv \pm|\varepsilon|\beta \pmod 2$ and $\nu = |\varepsilon|\beta$ is the non-primitive multiple $|\varepsilon|\mathbf{r}_0$, any primitive intruder has $\nu = 2 - |\varepsilon|\beta$ and $(U, W) = \mathbf{w}_{|\varepsilon|} = (2A - |\varepsilon|U_0, 2C - |\varepsilon|W_0)$, whose positivity and $2 - |\varepsilon|\beta \geq |\varepsilon|\beta \iff \beta \leq 1/|\varepsilon|$ imply the same conditions for $|\varepsilon| = 3$ (with $3\beta \neq 1$ since $\gcd(A, C) = 1 \implies 3 \nmid D_0$). Conversely, when $\mathbf{w}_3 = (2A - 3U_0, 2C - 3W_0) \in \mathbb{Z}^2_{>0}$ and $3p < D_0$, $\mathbf{w}_3$ is primitive (as $\gcd(2A - 3U_0, 2C - 3W_0)$ divides both $C(2A - 3U_0) - A(2C - 3W_0) = \pm 3$ and $\gcd(2A, 2C) = 2$ if 3 divided both coordinates) and its chamber $\hat{m}(\mathbf{w}_3) = \frac{D_0(2-3\beta)^2 + 9/D_0}{2}$ satisfies the strict bounds $\hat{m}(\mathbf{w}_3) - 9\hat{m}_0 = 2D_0(1 - 3\beta) = 2(D_0 - 3p) > 0$ and $M_{\text{cut}} - \hat{m}(\mathbf{w}_3) = \frac{4[p(D_0 - p) - 1]}{D_0} > 0$ (since $p \geq A + C \geq 3$ and $D_0 - p \geq 1$ are positive integers). Thus $\mathbf{w}_3$ enters at $\hat{m}(\mathbf{w}_3) \leq M_{\text{cut}} - 1$ and strictly beats $\mathbf{r}_0$ across $[\hat{m}(\mathbf{w}_3), M_{\text{cut}} - 1]$, proving the universal two-value dichotomy: $M_{\text{tail}}(A, C) = M_{\text{cut}}$ if $3U_0 < 2A,\ 3W_0 < 2C,\ 3(AU_0 + CW_0) < D_0$, and $M_{\text{tail}}(A, C) = \hat{m}_0$ otherwise.

A.3 Adjoining the Positive Leg-Sum Chart κ_{leg} and the Explicit Leg-Ratio Involution

For any cell $(r,c)\in\mathbb{Z}^2_{\geq 1}$, the positive leg ratio $a:=r/c\in\mathbb{Q}_{>0}$ determines the leg-sum phase through the map

$$\psi(a):=\frac{a}{1+a}=\frac{r}{r+c}=\frac{r}{m+1}=\kappa_{\mathrm{leg}}(r,c)\in(0,1).$$

Multiplicative inversion $a\mapsto 1/a=c/r$ (exchanging legs $(r,c)\mapsto(c,r)=R_{\mathrm{mid}}(r,c)$ in chamber $m=r+c-1$) conjugates to phase reflection across $1/2$:

$$\psi\left(\frac{1}{a}\right)=\frac{1/a}{1+1/a}=\frac{1}{1+a}=1-\psi(a),\qquad \mathbf{p}_{\mathrm{leg}}(c,r)=\left(-\frac{r-c}{r+c},\,\frac{2\sqrt{rc}}{r+c}\right),$$

which is the algebraic form of the complementary fraction pairing $r/n\leftrightarrow(n-r)/n=c/n$ $(n=r+c=m+1)$.
Using the leg-normalized phase $\kappa_{\mathrm{leg}}=r/(r+c)=r/(m+1)$ defines the alternative **leg-sum carrier map**

$$\mathbf{p}_{\mathrm{leg}}(r,c)=\left(\frac{r-c}{r+c},\,\frac{2\sqrt{rc}}{r+c}\right).\quad\text{(A.8)}$$

Its rational points correspond uniquely to $(r,c)=k(A^2,C^2)$ for $k\in\mathbb{Z}_{\geq 1}$ and coprime $A,C\in\mathbb{Z}_{\geq 1}$, with first chamber $m=A^2+C^2-1$ and repeats at $m=k(A^2+C^2)-1$. In particular, every opposite-parity target (A.4) is realized **exactly** on the leg-sum chart at cell (A^2,C^2) in chamber D_0-1 (for example, $(3/5,4/5)$ appears exactly at $(4,1)$ in chamber $m=4$).

Theorem A.3 (One-Chamber Advance Under the Combined Two-Chart Budget). *When rational points from both $\mathcal{C}(r,c)$ and $\mathbf{p}_{\mathrm{leg}}(r,c)$ with chamber $m\leq M$ are admitted to approximate $\mathbf{p}_*=(1/\sqrt{2},1/\sqrt{2})$, let $j\geq 0$ be chosen by $m_{0,j}\leq M+1<m_{0,j+1}$. For $j\geq 1$:*

- *At $M=m_{0,j}-1$ (e.g., $M=4,28,168$), the unique minimizing point is the coordinate swap of $\mathbf{p}(U_j,W_j)$, realized on the leg-sum chart at (A_j^2,C_j^2) where $A_j=(U_j+W_j)/2$ and $C_j=(U_j-W_j)/2$.*
- *For $m_{0,j}\leq M<m_{0,j+1}-1$, the minimizing points are precisely that leg-sum swapped point and the centered point $\mathbf{p}(U_j,W_j)$, which are distinct and equidistant from $\mathbf{p}_*$.*

Base Budgets and All Cell Realizations. For $M\in\{1,2,3\}$ $(j=0)$, the unique minimizing point is $\mathbf{p}_0=(0,1)$, realized in either chart by the diagonal cells (r,r) with $2r-1\leq M$ (the swapped boundary point $(1,0)$ is excluded because both charts require positive input cell parameters $r,c\geq 1$, which forbids a zero leg). For $j\geq 1$, the centered minimizing cells are the odd-scale repeats in (A.2), the leg-sum swapped point $\tau(\mathbf{p}_j)$ is realized by $(r,c)=k(A_j^2,C_j^2)$ with $k\in\mathbb{Z}_{\geq 1}$ and $km_{0,j}-1\leq M$, and the centered point $\mathbf{p}_j$ also has leg-sum realizations $(r,c)=k(U_j^2,W_j^2)$ whenever $2km_{0,j}-1\leq M$, giving $\left\lfloor(\lfloor M/m_{0,j}\rfloor+1)/2\right\rfloor+\lfloor(M+1)/m_{0,j}\rfloor+\lfloor(M+1)/(2m_{0,j})\rfloor$ chart-labeled minimizing cells in total.

Proof. First, if any candidate cell (r,c) on either chart has $r<c$, its carrier point (p_1,p_2) has $p_1<0$ and $p_2>0$; transposing the cell $(r,c)\mapsto(c,r)$ on the same chart and at the exact same chamber $m=r+c-1$ produces $(-p_1,p_2)$, which has strictly larger inner product $(-p_1+p_2)/\sqrt{2}>(p_1+p_2)/\sqrt{2}$ with the target $\mathbf{p}_*=(1/\sqrt{2},1/\sqrt{2})$. Thus every minimizing cell on either chart satisfies $r\geq c$ and $p_1\geq 0$.

On the positive leg-sum chart (A.8), $\mathbf{p}_{\mathrm{leg}}(r,c)=\left(\frac{r-c}{r+c},\frac{2\sqrt{rc}}{r+c}\right)$ is rational iff rc is a square, i.e., $(r,c)=k(A^2,C^2)$ for a unique primitive pair of coprime positive integers $A,C\geq 1$ and scale $k\in\mathbb{Z}_{\geq 1}$, with first leg-sum chamber $m=A^2+C^2-1$, repeats at $k(A^2+C^2)-1$, and circle point $\left(\frac{A^2-C^2}{A^2+C^2},\frac{2AC}{A^2+C^2}\right)$ (where for arbitrary coprime $A,C\geq 1$, setting $U=A+C$ and $W=|A-C|$ gives the signed identity $A^2-C^2=\mathrm{sgn}(A-C)\,UW$). Restricting to the non-negative half-quadrant $r\geq c\iff A\geq C\geq 1$ $(p_1\geq 0)$, there are two parity cases:

1. **Opposite Parity ($A+C$ odd with $A>C\geq 1$):** The reduced denominator is $m_0=A^2+C^2\equiv 1\pmod 4$, the first reduced numerator $A^2-C^2>0$ is odd, and the second numerator $2AC>0$ is even. Setting $U=A+C$ and $W=A-C>0$ (coprime positive odd integers with $(U^2+W^2)/2=A^2+C^2=m_0$), we have $A^2-C^2=UW$ and $2AC=(U^2-W^2)/2$. Thus this point is $\tau(\mathbf{p}(U,W))\in\tau(\mathcal{H})$ (where $\tau(p_1,p_2)=(p_2,p_1)$) and first appears on the leg-sum chart at chamber $m=m_0-1$.

2. **Both Odd ($A \geq C \geq 1$ with $A \equiv C \equiv 1 \pmod 2$):** Dividing numerators and denominator by 2, the reduced denominator is $m_0 = (A^2 + C^2)/2 \equiv 1 \pmod 4$, with reduced point $\left(\frac{(A^2-C^2)/2}{m_0}, \frac{AC}{m_0}\right) = \mathbf{p}(A, C)$ already in the centered parity class $\mathcal{H}$. On the centered chart it is already available at chamber m_0 (via cell $\big((A^2{+}1)/2, (C^2{+}1)/2\big)$), whereas its first realization on the leg-sum chart is $(r, c) = (A^2, C^2)$ at chamber $A^2 + C^2 - 1 = 2m_0 - 1 \geq m_0$, with equality $2m_0 - 1 = m_0$ if and only if $m_0 = 1$ at the diagonal base $(A, C) = (1, 1)$ (where both charts realize $\mathbf{p}_0 = (0, 1)$ at $(1, 1)$ in chamber 1) and strict inequality $2m_0 - 1 > m_0$ for all $m_0 \geq 5$ (for example, $(r, c) = (9, 1)$ with $(A, C) = (3, 1)$ gives $(4/5, 3/5)$ at leg-sum chamber $9 = 2(5) - 1 > 5$, whereas the centered chart already realizes $(4/5, 3/5)$ at $(5, 1)$, chamber 5).

By Cases 1 and 2, every admitted point with $p_1 \geq 0$ at combined budget $m \leq M$ is either a non-negative centered point $\mathbf{p}(U, W) \in \mathcal{H}$ $(U \geq W)$ with $m_0 \leq M$ or the coordinate swap $\tau(\mathbf{p}(U, W)) \in \tau(\mathcal{H})$ of a positive centered point $(U > W)$ with $m_0 - 1 \leq M \iff m_0 \leq M + 1$. Since τ preserves the linear score $p_1 + p_2$, the maximum score $p_1 + p_2$ at combined budget M is bounded above by the centered-only optimum score $S_j = G_j/m_{0,j}$ at hypothetical centered budget $M + 1$, where $j \geq 0$ is defined by $m_{0,j} \leq M + 1 < m_{0,j+1}$ (Theorem A.1).

For $j = 0$ $(M \in \{1, 2, 3\})$, $\mathbf{p}_0 = (0, 1)$ is admitted from chamber 1 on both charts at (r, r) $(2r - 1 \leq M)$, while its swap $(1, 0)$ lies outside the positive-parameter domain $r, c \geq 1$. For $j \geq 1$, the integers $A_j = (U_j + W_j)/2$ and $C_j = (U_j - W_j)/2$ are positive, coprime, and of opposite parity with $A_j^2 + C_j^2 = m_{0,j}$, so the leg-sum cell (A_j^2, C_j^2) has chamber $m_{0,j} - 1 \leq M$ and realizes $\tau(\mathbf{p}(U_j, W_j))$, attaining the upper bound S_j. The unswapped point $\mathbf{p}(U_j, W_j)$ is admitted iff $m_{0,j} \leq M$ (entering on the centered chart at $m_{0,j}$ and on the leg-sum chart only at $2m_{0,j} - 1$). Because a line $p_1 + p_2 = S_j$ intersects the unit circle in at most the two points $\mathbf{p}(U_j, W_j)$ and $\tau(\mathbf{p}(U_j, W_j))$—which are distinct for all $j \geq 1$ since $U_j > W_j > 0$ implies $\ell_{1,j} \neq \ell_{2,j}$—no other point can tie. □

Figure A.1 (Appendix A): All-Budget 45° Pell Staircase, Excluded Target (3, 4)
Budget-17 Exception, Two-Chart One-Chamber Advance, and Record Convergence

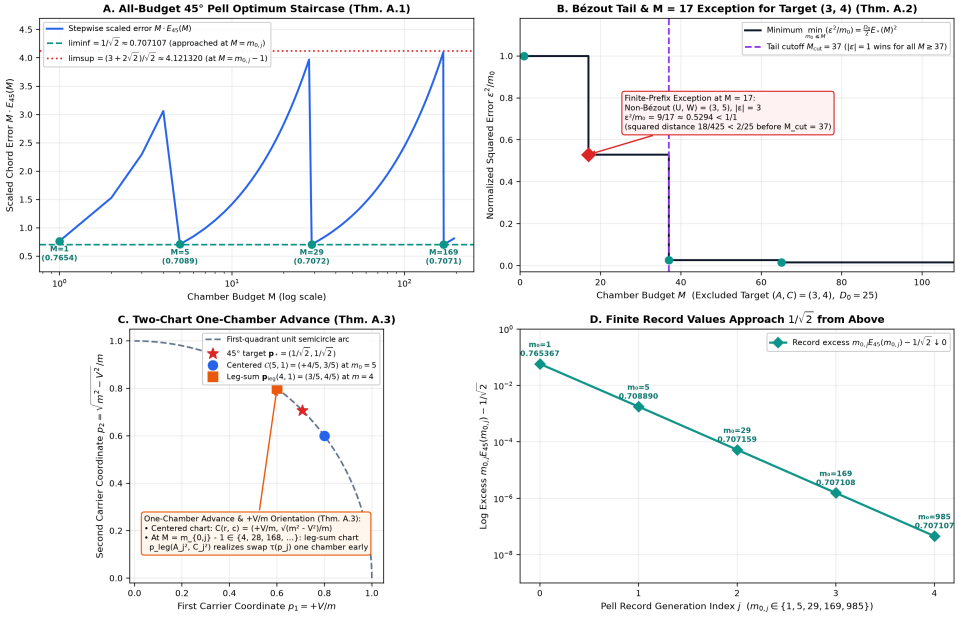


Figure A.1 (Rational-carrier chamber budgets and two-chart advance): **A.** Stepwise scaled chord error $M \cdot E_{45}(M)$ to the 45° target $\mathbf{p}_* = (1/\sqrt{2}, 1/\sqrt{2})$ on the centered chart (Theorem A.1), where finite record values $m_{0,j} E_{45}(m_{0,j})$ **approach** $\liminf M \cdot E_{45}(M) = 1/\sqrt{2} \approx 0.707107$ as $j \to \infty$ $(M = 1 \mapsto 0.7654,\ M = 5 \mapsto 0.7089,\ M = 29 \mapsto 0.7072,\ M = 169 \mapsto 0.7071)$ and pre-record peaks at $M = m_{0,j} - 1$ approach $\limsup M \cdot E_{45}(M) = (3 + 2\sqrt{2})/\sqrt{2} \approx 4.1213$. **B.** Normalized squared error $\varepsilon^2/m_0 = \frac{D_0}{2} E_*(M)^2$ for the excluded opposite-parity target $(A, C) = (3, 4)$ ($D_0 = 25$, Theorem A.2 & Remark A.2a): at budget $M = 17$, the non-Bézout ray $(U, W) = (3, 5)$ ($|\varepsilon| = 3, \varepsilon^2/m_0 = 9/17 < 1$) strictly beats $\mathbf{b}_+ = (1, 1)$ before the canonical $|\varepsilon| = 1$ Bézout tail takes over for all $M \geq M_{\text{cut}} = 37$. **C.** Adjoining the positive leg-sum chart $\mathbf{p}_{\text{leg}}(r, c)$ (Theorem A.3) realizes the coordinate swap $\tau(\mathbf{p}(U_j, W_j))$ one chamber earlier at $M = m_{0,j} - 1 \in \{4, 28, 168, \dots\}$.

Appendix B. The Odd-Square Stack Ω_n and Its Directional Shadows

This appendix establishes the all-direction orthographic union-shadow, convex-hull, hiding-cone, and isotropic-mean theorems for the three-dimensional unit-height odd-square stack Ω_n, extending the tetrahedral sum $\sum_{j=0}^{n}(2j+1)^2 = \binom{2n+3}{3}$ to continuous solid projections [9].

B.1 Explicit Solid Model and Exact Union-Shadow Area Law

For each integer $n \geq 0$, define the unit-height **odd-square stack** $\Omega_n \subset \mathbb{R}^3$ by

$$\Omega_n = \bigcup_{j=0}^{n} \left[-j-\frac{1}{2}, j+\frac{1}{2}\right]^2 \times [j, j+1], \quad \text{(B.1)}$$

and let $\pi_{\boldsymbol{v}} : \mathbb{R}^3 \to \boldsymbol{v}^\perp$ denote orthogonal projection along a nonzero viewing vector $\boldsymbol{v} = (A, C, D) \neq 0$, where D is explicitly declared as the vertical third-axis component. *(Orientation, Slab-Center Translation & Affine-Point vs. Linear-Camera Reflection Between Top-Widest Ω_n and Bottom-Widest $\Omega_n^{\mathrm{bot}}/S_n$:* In (B.1), slab $j \in \{0, \ldots, n\}$ has side $2j+1$ on height $[j, j+1]$, so Ω_n is **top-widest** with widest slab $j = n$ at $[n, n+1]$. Applying the **affine point reflection** $R_3^{\mathrm{aff}}(p_1, p_2, p_3) = (p_1, p_2, n+1-p_3)$ maps Ω_n isometrically onto the **bottom-widest** solid stack $\Omega_n^{\mathrm{bot}} = R_3^{\mathrm{aff}}(\Omega_n) = \bigcup_{\ell=0}^{n}[-n+\ell-\frac{1}{2}, n-\ell+\frac{1}{2}]^2 \times [\ell, \ell+1]$ ($\ell = n-j$). Each bottom slab $\ell \in \{0, \ldots, n\}$ is a union of unit cubes centered at half-integer heights $(p_1, p_2, \ell+\frac{1}{2})$ with $|p_1|, |p_2| \leq n-\ell$; **translating those slab centers downward by** $(0, 0, \frac{1}{2})$ via $(p_1, p_2, \ell+\frac{1}{2}) \mapsto (p_1, p_2, \ell)$ identifies them bijectively with the discrete integer point stack $S_n = \{(p_1, p_2, \ell) \in \mathbb{Z}^3 : 0 \leq \ell \leq n,\ |p_1|, |p_2| \leq n-\ell\}$ of §6.5 Proposition 6.5. On viewing directions $\boldsymbol{v} = (A, C, D)$, the induced **linear directional reflection** is the homogeneous differential $R_3^{\mathrm{lin}}(\boldsymbol{v}) = \mathrm{d}R_3^{\mathrm{aff}}(\boldsymbol{v}) = (A, C, -D)$ (distinct from the affine point map R_3^{aff}), which conjugates orthographic projection along $\boldsymbol{v}$ on Ω_n to projection along $R_3^{\mathrm{lin}}(\boldsymbol{v}) = (A, C, -D)$ on Ω_n^{bot} and preserves $\mathcal{A}_n(\boldsymbol{v})$ and $\mathcal{H}_n(\boldsymbol{v})$ identically since (B.2)–(B.8) depend only on $|A|, |C|, |D|$.)* Denote by $\mathcal{A}_n(\boldsymbol{v}) = \mathrm{Area}_2(\pi_{\boldsymbol{v}}(\Omega_n))$ the **actual union-shadow area** and by $\mathcal{H}_n(\boldsymbol{v}) = \mathrm{Area}_2(\pi_{\boldsymbol{v}}(\mathrm{conv}\,\Omega_n))$ the **projected convex-hull area**.

Theorem B.1 (All-Direction Actual Union-Shadow Area Law). *For every integer $n \geq 0$ and $\boldsymbol{v} = (A, C, D) \neq 0$:*

1. **Horizontal Views ($D = 0$):** *Because the open slab height bands $(j, j+1)$ are disjoint, their projected strips have disjoint interiors and sum to*

$$\mathcal{A}_n(A, C, 0) = (n+1)^2 \frac{|A| + |C|}{\sqrt{A^2 + C^2}}. \quad \text{(B.2)}$$

2. **Non-Horizontal Views ($D \neq 0$):** *Set $a = \min(|A|, |C|)/|D|$ and $b = \max(|A|, |C|)/|D|$. Then $\mathcal{A}_n(\boldsymbol{v}) = \frac{|D|}{\|\boldsymbol{v}\|_2}\widetilde{\mathcal{A}}_n(a, b)$, where $\widetilde{\mathcal{A}}_n(a, 0) = (2n+1)^2$ and for $b > 0$, with $\nu = b/\max(1, a)$ and $(\tau)_+ = \max(0, \tau)$,*

$$\widetilde{\mathcal{A}}_n(a, b) = (2n+1)^2 + (2n+1)(a+b) + n^2\big[(a-1)_+ + (b-1)_+\big] + \frac{a}{2b}\sum_{j=0}^{n-1}\Big[(\nu-1)_+^2 - (\nu-2j-2)_+^2\Big]. \quad \text{(B.3)}$$

Writing $k = \min(n, \lfloor \nu/2 \rfloor)$, the first term $(\nu-1)_+^2$ in (B.3) contributes across all n summands whenever $\nu > 1$ while $(\nu-2j-2)_+^2$ contributes only for $0 \leq j < k$, so the corner-notch correction reduces in $O(1)$ arithmetic operations to

$$\frac{a}{2b}\left[n(\nu-1)_+^2 - k(\nu-k-1)^2 - \frac{k(k^2-1)}{3}\right] = \frac{a}{2b}\left[n(\nu-1)_+^2 - k\nu^2 + 2\nu k(k+1) - \frac{2}{3}k(k+1)(2k+1)\right],$$

which holds identically across all regimes $\nu \leq 1$, $1 < \nu < 2$, and $\nu \geq 2$.

Negative Control Against Naive Positive-Part Extrapolation. At $n = 1$ and $\boldsymbol{v} = (1/3, 3/2, 1)$, formula (B.3) gives quotient union area $\widetilde{\mathcal{A}}_1(1/3, 3/2) = 541/36$ (Euclidean area $541/66$), whereas the projected convex hull has quotient area $31/2$ (Euclidean area $93/11$) and omitting the final corner-notch sum in (B.3) gives the false value 15.

Proof.

1. **Horizontal Views ($D = 0$):** When $D = 0$, orthogonal projection onto $(A, C, 0)^{\perp}$ preserves the vertical coordinate p_3. For each slab interior $j < p_3 < j+1$, the horizontal cross-section $[-R_j, R_j]^2$ ($R_j = j + \frac{1}{2}$) projects to a segment of length $(2j+1)(|A|+|C|)/\sqrt{A^2+C^2}$. Because distinct slabs occupy disjoint open p_3-intervals $(j, j+1)$ whose shared horizontal boundaries have planar measure zero, the projected union area is the sum of the individual strip areas:

$$\mathcal{A}_n(A, C, 0) = \frac{|A|+|C|}{\sqrt{A^2+C^2}} \sum_{j=0}^{n} (2j+1) = (n+1)^2 \, \frac{|A|+|C|}{\sqrt{A^2+C^2}},$$

establishing (B.2) directly for all $n \geq 0$ without taking a limit as $D \to 0$.

1. **Quotient Projection and All-n Markov Intersection Nesting ($D \neq 0$):** For $D \neq 0$, map each point $(p_1, p_2, p_3) \in \mathbb{R}^3$ to the horizontal plane $p_3 = 0$ along $\boldsymbol{v}$ via $(p_1, p_2, p_3) \mapsto (p_1 - (A/D)p_3,\, p_2 - (C/D)p_3)$. A planar region of quotient area $\widetilde{\mathcal{A}}$ in $p_3 = 0$ lifts to an orthogonal projection of Euclidean area $\frac{|D|}{\|\boldsymbol{v}\|_2}\,\widetilde{\mathcal{A}}$ in $\boldsymbol{v}^{\perp}$ because the unit normal to $p_3 = 0$ makes cosine $|D|/\|\boldsymbol{v}\|_2$ with $\boldsymbol{v}/\|\boldsymbol{v}\|_2$. By sign reflection and coordinate swap on the square base $[-R_j, R_j]^2$, we may take sorted nonnegative quotient parameters $0 \leq a \leq b$ with $a = \min(|A|, |C|)/|D|$ and $b = \max(|A|, |C|)/|D|$. The j-th slab $\Omega^{(j)} = [-R_j, R_j]^2 \times [j, j+1]$ then has quotient shadow $P_j = \{(p_1 - ap_3, p_2 - bp_3) : (p_1, p_2, p_3) \in \Omega^{(j)}\}$, which is the Minkowski sum of $[-R_j, R_j]^2$ and the segment $[-(j+1)(a, b),\, -j(a, b)]$, described explicitly by

$$-R_j - a(j+1) \leq p_1 \leq \frac{1}{2} + j(1-a), \qquad -R_j - b(j+1) \leq p_2 \leq \frac{1}{2} + j(1-b), \qquad |bp_1 - ap_2| \leq R_j(a+b).$$

(For $a, b > 0$ these inequalities cut out a convex hexagon; if $a = 0 < b$ they reduce to a rectangle, and if $a = b = 0$ they give the square $[-R_j, R_j]^2$.) For any higher slab $k > j$, the lower bounds $-R_k - a(k+1) < -R_j - a(j+1)$ and $-R_k - b(k+1) < -R_j - b(j+1)$ strictly relax, and the diagonal strip $|bp_1 - ap_2| \leq R_k(a+b)$ strictly widens (or is identically $0 \leq 0$ when $a = b = 0$). Thus the only constraints of P_k ($k > j$) that can cut P_j are the upper coordinate bounds

$$p_1 \leq \bar{p}_1(k) = \frac{1}{2} + k(1-a), \qquad p_2 \leq \bar{p}_2(k) = \frac{1}{2} + k(1-b).$$

If $a \leq 1$, then $\bar{p}_1(k)$ is nondecreasing in k, so $p_1 \leq \bar{p}_1(k)$ is already implied on P_j by $p_1 \leq \bar{p}_1(j)$; if $a > 1$, then $\bar{p}_1(k)$ strictly decreases with k. The identical dichotomy holds for b and $\bar{p}_2(k)$. Consequently, every active constraint from P_k ($k > j$) tightens monotonically with k, which proves the **Markov intersection-nesting property**

$$P_j \cap P_n \subseteq P_j \cap P_{n-1} \subseteq \cdots \subseteq P_j \cap P_{j+1}.$$

Therefore, the set of shadow points whose highest covering slab is j simplifies to $\Delta_j = P_j \setminus \bigcup_{k>j} P_k = P_j \setminus P_{j+1}$ for $0 \leq j < n$, with $\Delta_n = P_n$. Since $\Delta_0, \ldots, \Delta_n$ partition $\bigcup_{j=0}^{n} P_j$ without any convexity assumption on the union,

$$\widetilde{\mathcal{A}}_n(a, b) = \mathrm{Area}_2\left(\bigcup_{j=0}^{n} P_j\right) = \mathrm{Area}_2(P_n) + \sum_{j=0}^{n-1} \mathrm{Area}_2(P_j \setminus P_{j+1}).$$

1. **Local Difference Area Across All (a, b) Branches and $O(1)$ Sum Reduction:** Fix j and translate P_j by $(R_j + a(j+1),\, R_j + b(j+1))$ into local nonnegative coordinates $(p_1', p_2') \in [0, 2j+1+a] \times [0, 2j+1+b]$. In (p_1', p_2'), P_j is the bounding rectangle $[0, 2j+1+a] \times [0, 2j+1+b]$ minus the two disjoint open corner triangles $p_2' > 2j+1+(b/a)p_1'$ and $p_1' > 2j+1+(a/b)p_2'$ (for $a > 0$; each has area $ab/2$), giving $\mathrm{Area}_2(P_j) = (2j+1+a)(2j+1+b) - ab = (2j+1)^2 + (2j+1)(a+b)$ (and $\mathrm{Area}_2(P_n) = (2n+1)^2 + (2n+1)(a+b)$). For $P_j \setminus P_{j+1}$:

- If $b \le 1$ (inside the hiding cone), both $\bar{p}_1(k)$ and $\bar{p}_2(k)$ are nondecreasing, so $P_j \subseteq P_{j+1}$ and $\mathrm{Area}_2(P_j \setminus P_{j+1}) = 0$.
- If $a = 0 < b$ and $b > 1$ (axis tilt outside the cone), the rectangle $P_j = [0, 2j+1] \times [0, 2j+1+b]$ is cut at $p_2' \le 2j+2$, leaving a protruding strip of width $2j+1$ and height $b-1$, so $\mathrm{Area}_2(P_j \setminus P_{j+1}) = (2j+1)(b-1)$.
- If $0 < a \le b$ and $b > 1$, put $\hat{a} = \min(1, a)$ (covering both $0 < a \le 1 < b$, where $\hat{a} = a$, and $1 < a \le b$, where $\hat{a} = 1$). In the translated (p_1', p_2') coordinates, the upper bounds $p_1 \le \bar{p}_1(j+1)$ and $p_2 \le \bar{p}_2(j+1)$ become $p_1' \le 2j+1+\hat{a}$ and $p_2' \le 2j+2$. Thus $P_j \cap P_{j+1}$ is the clipped rectangle $[0, 2j+1+\hat{a}] \times [0, 2j+2]$ minus the portions of the two corner triangles lying inside it:
  - The northwest triangle $p_2' > 2j+1+(b/a)p_1'$ meets $[0, 2j+1+\hat{a}] \times [0, 2j+2]$ in a right triangle of legs $a/b \le \hat{a}$ and 1, with area $\frac{a}{2b}$.
  - The southeast triangle $p_1' > 2j+1+(a/b)p_2'$ has horizontal width $(2j+1+\hat{a}) - (2j+1+(a/b)p_2') = \hat{a} - (a/b)p_2'$ inside $p_1' \le 2j+1+\hat{a}$ for $0 \le p_2' \le \min(b\hat{a}/a,\, 2j+2)$; integrating $\int_0^{\min(b\hat{a}/a, 2j+2)} (\hat{a} - (a/b)p_2')\, dp_2'$ gives area

$$\frac{b\hat{a}^2}{2a} - \frac{a}{2b}\left(\frac{b\hat{a}}{a} - 2j - 2\right)_+^2.$$

Subtracting $\mathrm{Area}_2(P_j \cap P_{j+1}) = (2j+1+\hat{a})(2j+2) - \frac{a}{2b} - \frac{b\hat{a}^2}{2a} + \frac{a}{2b}\left(\frac{b\hat{a}}{a} - 2j - 2\right)_+^2$ from $\mathrm{Area}_2(P_j) = (2j+1)^2 + (2j+1)(a+b)$ and using $a + b - 1 - \hat{a} = (a-1)_+ + (b-1)_+$ together with the algebraic identity

$$\frac{a}{2b} + \frac{b\hat{a}^2}{2a} - \hat{a} = \frac{a}{2b}\left(\frac{b\hat{a}}{a} - 1\right)^2 = \frac{a}{2b}(\nu - 1)_+^2 \qquad \left(\nu = \frac{b}{\max(1, a)} = \frac{b\hat{a}}{a}\right)$$

gives $\mathrm{Area}_2(P_j \setminus P_{j+1}) = (2j+1)\big[(a-1)_+ + (b-1)_+\big] + \frac{a}{2b}\big[(\nu-1)_+^2 - (\nu - 2j - 2)_+^2\big]$. Summing $\sum_{j=0}^{n-1}(2j+1) = n^2$ proves (B.3), and indexing $i = j+1 \in \{1, \dots, k\}$ with $k = \min(n, \lfloor \nu/2 \rfloor)$ evaluates $\sum_{i=1}^{k}(\nu - 2i)^2 = k\nu^2 - 2\nu k(k+1) + \frac{2}{3}k(k+1)(2k+1)$ in $O(1)$ operations. □

B.2 The Square Hiding Cone, Convex Hull Gap, and Global Extrema

Theorem B.2 (Square Hiding Cone, Hull Area, and Extrema). *Let $\delta_+ = (|A| - |D|)_+ + (|C| - |D|)_+$. Then for every $\boldsymbol{v} = (A, C, D) \neq 0$:*

1. **Projected Convex Hull Area:**

$$\mathcal{H}_n(\boldsymbol{v}) = \frac{|D|(2n+1)^2 + (2n+1)(|A| + |C|) + n(n+1)\delta_+}{\|\boldsymbol{v}\|_2}. \quad \text{(B.4)}$$

2. **Exact Hiding Cone and Convexity Equivalence ($n \ge 1$):** *The following four conditions are equivalent:*
   - *All lower slabs hide inside the widest top slab's shadow: $\pi_{\boldsymbol{v}}(\Omega_n) = \pi_{\boldsymbol{v}}\big([-n - \frac{1}{2}, n + \frac{1}{2}]^2 \times [n, n+1]\big)$.*
   - *The actual shadow $\pi_{\boldsymbol{v}}(\Omega_n)$ is a convex polygon.*
   - *The hull gap vanishes: $\mathcal{H}_n(\boldsymbol{v}) - \mathcal{A}_n(\boldsymbol{v}) = 0$.*
   - *The viewing direction lies inside the **square cone***

$$\max(|A|, |C|) \le |D|. \quad \text{(B.5)}$$

   In polar angle ω from the vertical axis at azimuth ψ, the hiding boundary is $\omega_{\max}(\psi) = \arctan\big(1/\max(|\cos\psi|, |\sin\psi|)\big)$, which equals $45°$ in the coordinate vertical planes and reaches $\arctan\sqrt{2} \approx 54.7356°$ along the isometric cube diagonals $(\pm 1, \pm 1, \pm 1)$.

3. **Global Minimum, Isometric View, Global Maximum, and Sharp Hull Gaps:**

$$\min_{\boldsymbol{v} \neq 0} \mathcal{A}_n(\boldsymbol{v}) = (n+1)^2 \quad \text{at } \boldsymbol{v} = (1, 0, 0) \text{ or } (0, 1, 0), \qquad \mathcal{A}_n(1, 1, 1) = \frac{(2n+1)(2n+3)}{\sqrt{3}}, \quad \text{(B.6)}$$

$$\max_{\boldsymbol{v}\neq 0} \mathcal{A}_n(\boldsymbol{v}) = (2n+1)\sqrt{(2n+1)^2+2} \quad \text{at } (|A| : |C| : |D|) = (1 : 1 : 2n+1), \tag{B.7}$$

$$\max_{\boldsymbol{v}\neq 0} \big(\mathcal{H}_n(\boldsymbol{v}) - \mathcal{A}_n(\boldsymbol{v})\big) = \sqrt{2}\, n \quad \text{at } (1,1,0), \qquad \max_{\boldsymbol{v}\neq 0} \frac{\mathcal{H}_n(\boldsymbol{v}) - \mathcal{A}_n(\boldsymbol{v})}{\mathcal{A}_n(\boldsymbol{v})} = \frac{n}{(n+1)^2}. \tag{B.8}$$

Proof.

1. **Three-Dimensional Convex Hull and Facet Projection Formula (B.4):** Write $\mathcal{P}_n = \{(p_1,p_2,p_3) : 0 \le p_3 \le n,\ |p_1|,|p_2| \le p_3\}$. Each slab $\Omega^{(j)}$ is the Minkowski sum of the base unit cube $\Omega_0 = [-\frac{1}{2},\frac{1}{2}]^2 \times [0,1]$ and the horizontal square $[-j,j]^2 \times \{j\}$. Since convexification commutes with Minkowski addition and the convex hull of $\bigcup_{j=0}^{n}([-j,j]^2 \times \{j\})$ is the inverted square pyramid $\mathcal{P}_n$, we have

$$\operatorname{conv}\Omega_n = \Omega_0 + \mathcal{P}_n = \left\{(p_1,p_2,p_3) \in \mathbb{R}^3 : 0 \le p_3 \le n+1,\ |p_1|,|p_2| \le \min\left(p_3 + \frac{1}{2},\, n+\frac{1}{2}\right)\right\}.$$

For $n > 0$, $\operatorname{conv}\Omega_n$ is a square frustum of height n topped by a square prism of height 1: its boundary consists of a bottom square of area 1 (normal $(0,0,-1)$), a top square of area $(2n+1)^2$ (normal $(0,0,1)$), four vertical rectangles of area $2n+1$ (normals $(\pm1,0,0),(0,\pm1,0)$), and four slanted trapezoids of area $\sqrt{2}\,n(n+1)$ (normals $(\pm1,0,-1)/\sqrt{2}$ and $(0,\pm1,-1)/\sqrt{2}$). For any convex polyhedron, almost every line parallel to $\boldsymbol{v}$ piercing the shadow meets the boundary twice, so $\mathcal{H}_n(\boldsymbol{v}) = \frac{1}{2\|\boldsymbol{v}\|_2}\sum_F \operatorname{Area}(F)\,|\boldsymbol{n}_F\cdot\boldsymbol{v}|$. Summing the ten facets and using $\frac{1}{2}(|p-|D||+|p+|D||) = \max(|p|,|D|) = |D| + (|p|-|D|)_+$ together with $\frac{1+(2n+1)^2}{2} + 2n(n+1) = (2n+1)^2$ yields (B.4).

1. **Strict Gap Inequality Outside the Cone and Convexity Equivalence ($n \ge 1$):** For $D \neq 0$, in normalized sorted coordinates $0 \le a \le b$, put $D_+ = (a-1)_+ + (b-1)_+$ and $\mathcal{C}_n = \sum_{j=0}^{n-1} C_j(a,b)$ where $C_j(a,b) = \frac{a}{2b}\big[(\nu-1)_+^2 - (\nu-2j-2)_+^2\big]$. Comparing (B.4) and (B.3) gives

$$\mathcal{H}_n(\boldsymbol{v}) - \mathcal{A}_n(\boldsymbol{v}) = \frac{|D|}{\|\boldsymbol{v}\|_2}\big(nD_+ - \mathcal{C}_n\big).$$

Inside the cone ($b \le 1$), $D_+ = \mathcal{C}_n = 0$. Outside the cone ($b > 1$, so $D_+ > 0$), each summand $C_j(a,b)$ satisfies the strict bound $0 \le C_j(a,b) < D_+/2$:

- If $a = 0$, then $C_j = 0 < (b-1)/2 = D_+/2$.
- If $0 < a \le 1 < b$, then $\nu = b$ and $C_j \le \frac{a(b-1)^2}{2b} < \frac{b-1}{2} = \frac{D_+}{2}$ since $a(b-1) \le b-1 < b$.
- If $1 < a \le b$, then $\nu = b/a$ and $C_j \le \frac{a(b/a-1)^2}{2b} = \frac{(b-a)^2}{2ab} < \frac{a+b-2}{2} = \frac{D_+}{2}$ because $ab(a+b-2) - (b-a)^2 = a^2(b-1) + b^2(a-1) > 0$.

Summing over $0 \le j < n$ ($n \ge 1$) proves that for every non-horizontal view outside the cone,

$$\frac{n\delta_+}{2\|\boldsymbol{v}\|_2} < \mathcal{H}_n(\boldsymbol{v}) - \mathcal{A}_n(\boldsymbol{v}) \le \frac{n\delta_+}{\|\boldsymbol{v}\|_2},$$

while for horizontal views ($D = 0, n \ge 1$), $\mathcal{H}_n(A,C,0) - \mathcal{A}_n(A,C,0) = \frac{n(|A|+|C|)}{\sqrt{A^2+C^2}} > 0$. Because orthogonal projection commutes with convex hull ($\pi_{\boldsymbol{v}}(\operatorname{conv}\Omega_n) = \operatorname{conv}\pi_{\boldsymbol{v}}(\Omega_n)$), $\pi_{\boldsymbol{v}}(\Omega_n)$ is convex iff $\mathcal{H}_n(\boldsymbol{v}) - \mathcal{A}_n(\boldsymbol{v}) = 0$, which for $n \ge 1$ holds iff $\max(|A|,|C|) \le |D|$, where $\pi_{\boldsymbol{v}}(\Omega_n) = \pi_{\boldsymbol{v}}(\Omega_{n,\mathrm{top}})$. (At $n = 0$, Ω_0 is a single cube and every gap vanishes.)

1. **Global Minimum, Global Maximum Across All Four Linear Forms, and Sharp Gaps (B.6)–(B.8):** Let $M = (n+1)^2 = 2n+1+n^2$ and write the naive lower-bound numerator as $\mathcal{B} = |D|(2n+1)^2 + (2n+1)(|A|+|C|) + n^2\delta_+$. By (B.3) and (B.2), $\|\boldsymbol{v}\|_2\,\mathcal{A}_n(\boldsymbol{v}) \ge \mathcal{B}$ in every direction. Since $|p| - (|p|-|D|)_+ = \min(|p|,|D|)$,

$$\mathcal{B} - M\big(|A|+|C|+|D|\big) = (3n^2+2n)|D| - n^2\big[\min(|A|,|D|)+\min(|C|,|D|)\big] \geq n(n+2)|D| \geq 0,$$

whence $\mathcal{A}_n(\boldsymbol{v}) \geq \frac{\mathcal{B}}{\|\boldsymbol{v}\|_2} \geq M\,\frac{|A|+|C|+|D|}{\sqrt{A^2+C^2+D^2}} \geq M = (n+1)^2$, with equality for $n \geq 1$ iff $D = 0$ and $AC = 0$ (the horizontal coordinate axes).

For the global maximum, $\mathcal{A}_n(\boldsymbol{v}) \leq \mathcal{H}_n(\boldsymbol{v})$ everywhere. On the nonnegative octant $(A, C, D) \geq 0$ with $\|\boldsymbol{v}\|_2 = 1$, $\mathcal{H}_n(\boldsymbol{v})$ is the maximum of four linear forms $\boldsymbol{w}_i \cdot (A, C, D)$ according to which positive parts in $(A-D)_+ + (C-D)_+$ are active:

$$\boldsymbol{w}_0 = (2n+1, 2n+1, (2n+1)^2), \quad \boldsymbol{w}_1 = (2n+1+n(n+1), 2n+1, (2n+1)^2 - n(n+1)), \quad \boldsymbol{w}_1' = (2n+1, 2n+1+n(n+1), (2n+1)^2 - n(n+1)), \quad \boldsymbol{w}_2 = (2n+1+n(n+1), 2n+1+n(n+1), (2n+1)^2 - 2n(n+1)).$$

Since $\|\boldsymbol{w}_0\|_2^2 = (2n+1)^4 + 2(2n+1)^2$, direct expansion gives

$$\|\boldsymbol{w}_1\|_2^2 - \|\boldsymbol{w}_0\|_2^2 = \|\boldsymbol{w}_1'\|_2^2 - \|\boldsymbol{w}_0\|_2^2 = -2n^2(n+1)(3n+1) < 0, \qquad \|\boldsymbol{w}_2\|_2^2 - \|\boldsymbol{w}_0\|_2^2 = -2n^2(n+1)(5n+1) < 0 \qquad (n \geq 1).$$

By Cauchy–Schwarz, every linear form is at most $\|\boldsymbol{w}_0\|_2 = (2n+1)\sqrt{(2n+1)^2+2}$, so $\mathcal{A}_n(\boldsymbol{v}) \leq \mathcal{H}_n(\boldsymbol{v}) \leq (2n+1)\sqrt{(2n+1)^2+2}$ over the entire sphere S^2, not only inside the cone. Equality holds precisely when $(|A| : |C| : |D|) = (2n+1 : 2n+1 : (2n+1)^2) = (1 : 1 : 2n+1)$, which lies inside the hiding cone ($a = b = 1/(2n+1) \leq 1$), where $\mathcal{A}_n = \mathcal{H}_n = (2n+1)\sqrt{(2n+1)^2+2}$. Finally, $\mathcal{H}_n - \mathcal{A}_n \leq \frac{n\delta_+}{\|\boldsymbol{v}\|_2} \leq \frac{n(|A|+|C|)}{\sqrt{A^2+C^2+D^2}} \leq \sqrt{2}\,n$ (attained at $(1,1,0)$), and for $|A|+|C| > 0$, using $\|\boldsymbol{v}\|_2\,\mathcal{A}_n \geq \mathcal{B} \geq M(|A|+|C|)$ and $\delta_+ \leq |A|+|C|$ gives

$$\frac{\mathcal{H}_n(\boldsymbol{v}) - \mathcal{A}_n(\boldsymbol{v})}{\mathcal{A}_n(\boldsymbol{v})} \leq \frac{n\delta_+}{M(|A|+|C|)} \leq \frac{n}{M} = \frac{n}{(n+1)^2},$$

with equality at every horizontal view ($D = 0$). □

B.3 Isotropic Mean Shadow, Silver-Ratio Leading Term, and $O(n^{-5})$ Tail Brackets

Averaging $\mathcal{A}_n(\boldsymbol{v})$ over the unit sphere S^2 with respect to the uniform probability measure yields the isotropic mean shadow $\overline{\mathcal{A}}_n$. Because Ω_n is non-convex for $n \geq 1$, its total exposed surface area is $\mathrm{Area}_2(\partial\Omega_n) = 2(2n+1)^2 + 4\sum_{j=0}^{n}(2j+1) = 12n^2+16n+6$, and Cauchy's surface average $\mathrm{Area}_2(\partial\Omega_n)/4 = 3n^2+4n+\frac{3}{2}$ counts ray-piercing multiplicity, exceeding $\overline{\mathcal{A}}_n$ by $(2-\sqrt{2})n^2 - \chi n + \frac{2}{\pi}\sum_{i=1}^{n} I(2i) > 0$. By contrast, the convex-hull mean is $\overline{\mathcal{H}}_n = \frac{(2n+1)^2+2(2n+1)}{2} + n(n+1)(\sqrt{2}-1) = (1+\sqrt{2})n^2 + (3+\sqrt{2})n + \frac{3}{2}$ (using $\mathbb{E}|A| = \frac{1}{2}$ and $\mathbb{E}\max(|A|,|D|) = \frac{1}{\sqrt{2}}$ on S^2), which shares the quadratic leading term $(1+\sqrt{2})n^2$ of $\overline{\mathcal{A}}_n$ and differs only at linear order $(\sqrt{2}-1-\chi)n + \frac{2}{\pi}\sum_{i=1}^{n} I(2i)$.

Theorem B.3 (Exact Isotropic Mean Shadow, Closed Constant C_*, and Tail Asymptotics). *For every integer $n \geq 0$, the isotropic mean actual shadow area of Ω_n is*

$$\overline{\mathcal{A}}_n = (1+\sqrt{2})n^2 + (4+\chi)n + \frac{3}{2} - \frac{2}{\pi}\sum_{i=1}^{n} I(2i) = (1+\sqrt{2})n^2 + (4+\chi)n + C_* + \varepsilon_n, \quad \text{(B.9)}$$

where $I(\beta) = \int_\beta^\infty \frac{(p-\beta)^2}{p(p^2+1)(p^2+2)}\,dp$ ($\beta \geq 1$), $\varepsilon_n = \frac{2}{\pi}\sum_{i>n} I(2i)$, and the exact constants are

$$\chi = \frac{\ln 3}{2\pi} - 1 + \frac{2\sqrt{2}}{\pi}\arctan\sqrt{2}, \qquad C_* = \frac{4}{3} + \frac{\ln 2}{2\pi} + \frac{\zeta(3) + \mathrm{Li}_3(e^{-\sqrt{2}\pi}) - 2\,\mathrm{Li}_3(e^{-\pi})}{\pi^3}. \quad \text{(B.10)}$$

To 50 rounded decimal places:

- $4+\chi = 4.03493671467655295067734553073116140549324173926145$,
- $C_* = 1.47999653090760042442100878465142982068794763080876$,
- $\overline{\mathcal{A}}_1 = 7.93754352744295952118684565150792784372616830715013$ (vs. facet average $\mathrm{Area}_2(\partial\Omega_1)/4 = 8.5$).

Moreover, for every integer $n \geq 1$, writing $P_3(n) = \frac{1}{24\pi n} - \frac{1}{48\pi n^2} + \frac{7}{1440\pi n^3}$ and $P_4(n) = P_3(n) + \frac{1}{320\pi n^4}$, the tail ε_n satisfies the global two-sided bounds

$$P_4(n) - \frac{1}{288\pi n^5} < \varepsilon_n < P_4(n) - \frac{19}{16128\pi n^5} \qquad (n \geq 1). \quad \text{(B.11)}$$

*The shifted sequence $(n+\tau)\varepsilon_n$ strictly increases to $\frac{1}{24\pi}$ for all $n \geq 1$ for every real shift $\tau \leq \frac{1}{2}$ (with $\tau = \frac{1}{2}$ the largest shift having this property: $24\pi(n+\frac{1}{2})\varepsilon_n = 1 - \frac{2}{15n^2} + O(n^{-3})$). By contrast, the third-order remainder extractor $G_n = n^3\big(\varepsilon_n - \frac{1}{24\pi n} + \frac{1}{48\pi n^2}\big)$ is **not monotone**, satisfying $G_1 < G_2 > G_3$.*

Proof.

1. **Equal Quotient-Chart Integrals and Exact Finite Mean Assembly:** On the sorted domain $0 \leq a \leq b$, define $W_\beta(a,b) = \frac{a}{2b}(\nu-\beta)_+^2$ for $\beta \geq 1$ (with $\nu = b/\max(1,a)$ and $W_\beta = 0$ at $b = 0$), so that $\sum_{j=0}^{n-1} C_j(a,b) = nW_1(a,b) - \sum_{i=1}^{n} W_{2i}(a,b)$. Combining the spherical surface Jacobian $(1+a^2+b^2)^{-3/2}$ with the orthogonal area factor $(1+a^2+b^2)^{-1/2}$ and the 16-fold sign/swap symmetry on S^2 gives the averaging operator $\frac{4}{\pi}\int_0^\infty \int_0^b \frac{(\cdot)}{(1+a^2+b^2)^2}\, da\, db$. Splitting at $a = 1$ by Tonelli's theorem:
   - **Chart 1 ($0 \leq a \leq 1$):** Here $\nu = b \geq \beta \geq 1$, leaving the full inner range $0 \leq a \leq 1$:

$$\int_\beta^\infty \frac{(b-\beta)^2}{2b}\left[\int_0^1 \frac{a}{(1+b^2+a^2)^2}\, da\right] db = \int_\beta^\infty \frac{(b-\beta)^2}{4b(b^2+1)(b^2+2)}\, db = \frac{1}{4}I(\beta).$$

   - **Chart 2 ($a \geq 1$):** Substitute $b = a\nu$ ($\nu \geq \beta$, $db = a\, d\nu$, $a/(2b) = 1/(2\nu)$):

$$\int_\beta^\infty \frac{(\nu-\beta)^2}{2\nu}\left[\int_1^\infty \frac{a}{\big(1+(1+\nu^2)a^2\big)^2}\, da\right] d\nu = \int_\beta^\infty \frac{(\nu-\beta)^2}{4\nu(\nu^2+1)(\nu^2+2)}\, d\nu = \frac{1}{4}I(\beta).$$

Adding the two equal chart contributions and multiplying by $\frac{4}{\pi}$ proves $\mathbb{E}_{S^2}\big[\frac{|D|}{\|\boldsymbol{v}\|_2} W_\beta(a,b)\big] = \frac{2}{\pi}I(\beta)$. Partial fractions $\frac{(p-\beta)^2}{p(p^2+1)(p^2+2)} = \frac{\beta^2}{2p} + \frac{(1-\beta^2)p-2\beta}{p^2+1} + \frac{(\beta^2/2-1)p+2\beta}{p^2+2}$ integrate directly to

$$I(\beta) = \frac{\beta^2-1}{2}\ln(1+\beta^{-2}) + \frac{2-\beta^2}{4}\ln(1+2\beta^{-2}) - 2\beta\arctan(\beta^{-1}) + \sqrt{2}\,\beta\arctan\left(\frac{\sqrt{2}}{\beta}\right),$$

giving $I(1) = \frac{\ln 3}{4} - \frac{\pi}{2} + \sqrt{2}\arctan\sqrt{2}$ and $\chi = \frac{2}{\pi}I(1)$. Since $\mathbb{E}_{S^2}[\delta_+/\|\boldsymbol{v}\|_2] = 2\big(\mathbb{E}\max(|A|,|D|) - \mathbb{E}|D|\big) = \sqrt{2}-1$, subtracting the mean gap $\mathbb{E}[\mathcal{H}_n - \mathcal{A}_n] = n(\sqrt{2}-1) - n\frac{2}{\pi}I(1) + \frac{2}{\pi}\sum_{i=1}^n I(2i)$ from $\overline{\mathcal{H}}_n = (1+\sqrt{2})n^2 + (3+\sqrt{2})n + \frac{3}{2}$ establishes (B.9).

1. **Closed Form for C_* via the Weighted Log-Sinh Integral:** For $\beta \geq 2$, expanding $\frac{1}{(1+p^{-2})(1+2p^{-2})} = \sum_{k=0}^\infty (-1)^k(2^{k+1}-1)p^{-2k}$ and integrating termwise via $\int_\beta^\infty \frac{(p-\beta)^2}{p^{2j+3}}\, dp = \frac{2\beta^{-2j}}{(2j)(2j+1)(2j+2)}$ gives the absolutely convergent series

$$I(\beta) = \sum_{j=1}^\infty \frac{(-1)^{j-1}2(2^j-1)\beta^{-2j}}{(2j)(2j+1)(2j+2)} \qquad (\beta \geq 2).$$

Setting $\beta = 2i$ and summing over $i \geq 1$ gives $R_\infty = \frac{2}{\pi}\sum_{i=1}^\infty I(2i) = \frac{4}{\pi}\sum_{j=1}^\infty \frac{(-1)^{j-1}(2^j-1)\zeta(2j)}{(2j)(2j+1)(2j+2)4^j} = \frac{4}{\pi}\big[F(1/\sqrt{2}) - F(1/2)\big]$, where $F(z) = \sum_{j=1}^\infty \frac{(-1)^{j-1}\zeta(2j)z^{2j}}{(2j)(2j+1)(2j+2)} = \frac{1}{2}\int_0^1 (1-\psi)\ln\big(\frac{\sinh(\pi z\psi)}{\pi z\psi}\big)\, d\psi$ by the Euler product for $\sinh(\pi z\psi)/(\pi z\psi)$. Writing $\ln\big(\frac{\sinh(k\psi)}{k\psi}\big) = k\psi - \ln(2k) - \ln\psi + \ln(1-e^{-2k\psi})$ and integrating against $(1-\psi)$ yields

$$L(k)=\int_0^1(1-\psi)\ln\!\left(\frac{\sinh(k\psi)}{k\psi}\right)d\psi=\frac{k}{6}-\frac{1}{2}\ln(2k)+\frac{3}{4}-\frac{\zeta(2)}{2k}+\frac{\zeta(3)-\mathrm{Li}_3(e^{-2k})}{4k^2}.$$

Evaluating $\frac{2}{\pi}\big[L(\pi/\sqrt{2})-L(\pi/2)\big]$ with $k_1=\pi/\sqrt{2}$, $k_2=\pi/2$, and $\zeta(2)=\pi^2/6$ combines the π-linear and $1/\pi$ terms to $\frac{k_1-k_2}{6}-\frac{\zeta(2)}{2}(k_1^{-1}-k_2^{-1})=\frac{\pi(\sqrt{2}-1)}{12}-\frac{\pi(\sqrt{2}-2)}{12}=\frac{\pi}{12}$, which multiplies by $\frac{2}{\pi}$ to contribute $\frac{1}{6}$ to R_∞ (while $-\frac{1}{2}\ln(2k_1)+\frac{1}{2}\ln(2k_2)=-\frac{\ln 2}{4}$ contributes $-\frac{\ln 2}{2\pi}$), yielding $R_\infty=\frac{1}{6}-\frac{\ln 2}{2\pi}+\frac{2\,\mathrm{Li}_3(e^{-\pi})-\mathrm{Li}_3(e^{-\sqrt{2}\pi})-\zeta(3)}{\pi^3}$ and $C_*=\frac{3}{2}-R_\infty$ in (B.10).

1. **Signed Power-Tail Bounds for (B.11):** Since the alternating terms of $I(2i)$ decrease in magnitude for $i\ge 1$, $\frac{1}{48i^2}-\frac{1}{320i^4}<I(2i)<\frac{1}{48i^2}-\frac{1}{320i^4}+\frac{1}{1536i^6}$, so with the Hurwitz zeta function [20, §25.11] $\zeta(k,n+1)=\sum_{i>n}i^{-k}$,

$$\frac{1}{24\pi}\zeta(2,n+1)-\frac{1}{160\pi}\zeta(4,n+1)<\varepsilon_n<\frac{1}{24\pi}\zeta(2,n+1)-\frac{1}{160\pi}\zeta(4,n+1)+\frac{1}{768\pi}\zeta(6,n+1).$$

In the Laplace representation $\zeta(k,n+1)=\frac{1}{(k-1)!}\int_0^\infty\frac{\psi^{k-1}e^{-n\psi}}{e^\psi-1}\,d\psi$, the partial-fraction series $\frac{1}{e^\psi-1}=\frac{1}{\psi}-\frac{1}{2}+2\psi\sum_{j=1}^\infty\frac{1}{\psi^2+4\pi^2j^2}$ has alternating geometric truncations for all $\psi>0$:

$$\frac{1}{\psi}-\frac{1}{2}+\frac{\psi}{12}-\frac{\psi^3}{720}<\frac{1}{e^\psi-1}<\frac{1}{\psi}-\frac{1}{2}+\frac{\psi}{12}-\frac{\psi^3}{720}+\frac{\psi^5}{30240}.$$

Integrating against $\psi^{k-1}e^{-n\psi}/(k-1)!$ yields $\frac{1}{n}-\frac{1}{2n^2}+\frac{1}{6n^3}-\frac{1}{30n^5}<\zeta(2,n+1)<\frac{1}{n}-\frac{1}{2n^2}+\frac{1}{6n^3}-\frac{1}{30n^5}+\frac{1}{42n^7}$, $\frac{1}{3n^3}-\frac{1}{2n^4}+\frac{1}{3n^5}-\frac{1}{6n^7}<\zeta(4,n+1)<\frac{1}{3n^3}-\frac{1}{2n^4}+\frac{1}{3n^5}$, and $\zeta(6,n+1)<\int_n^\infty\omega^{-6}\,d\omega=\frac{1}{5n^5}$. Substituting these signed brackets gives $\varepsilon_n>P_4(n)-\frac{1}{288\pi n^5}$ and $\varepsilon_n<P_4(n)-\frac{37}{11520\pi n^5}+\frac{41}{20160\pi n^7}\le P_4(n)-\frac{19}{16128\pi n^5}$ for all $n\ge 1$ (since $\frac{37}{11520}-\frac{41}{20160}=\frac{19}{16128}$), proving (B.11).

1. **Exact Signed-Tail Proof of Shifted Monotonicity:** Put $Q_i=i^2I(2i)$. Substituting $p=\beta\psi$ in $I(\beta)$ gives

$$\beta^2I(\beta)=\int_1^\infty\frac{(\psi-1)^2}{\psi(\psi^2+\beta^{-2})(\psi^2+2\beta^{-2})}\,d\psi,$$

whose integrand is positive, strictly increases with $\beta>0$, and is dominated by $(\psi-1)^2/\psi^5$ (of integral $1/12$). By dominated convergence, $Q_i=\frac{1}{4}(2i)^2I(2i)$ strictly increases with $i\ge 1$ toward $\lim_{i\to\infty}Q_i=\frac{1}{48}$. For $M=n+1$ and any shift $\tau\le\frac{1}{2}$, taking the forward difference gives

$$\frac{\pi}{2}\big[(n+1+\tau)\varepsilon_{n+1}-(n+\tau)\varepsilon_n\big]=\sum_{i>M}\frac{Q_i}{i^2}-\frac{(M+\tau-1)Q_M}{M^2}.$$

Because $Q_i>Q_M$ for every $i>M$ and the trapezoidal comparison on $[i-1,i]$ ($i\ge M+1$) gives the strict lower bound $\frac{1}{M}=\int_M^\infty\omega^{-2}\,d\omega<\frac{1}{2M^2}+\sum_{i>M}i^{-2}\implies\sum_{i>M}i^{-2}>\frac{1}{M}-\frac{1}{2M^2}$ (whereas the midpoint rule on $[i-1/2,i+1/2]$ gives the upper bound $\sum_{i>M}i^{-2}<\frac{1}{M+1/2}$), we obtain

$$\frac{\pi}{2}\big[(n+1+\tau)\varepsilon_{n+1}-(n+\tau)\varepsilon_n\big]>Q_M\left(\frac{1}{M}-\frac{1}{2M^2}-\frac{M+\tau-1}{M^2}\right)=\frac{Q_M(\frac{1}{2}-\tau)}{M^2}\ge 0\qquad\left(\tau\le\frac{1}{2}\right).$$

Since $(n+\tau)\varepsilon_n\to\frac{1}{24\pi}$, strict increase implies $(n+\tau)\varepsilon_n<\frac{1}{24\pi}$ for all $n\ge 1$ whenever $\tau\le\frac{1}{2}$ (yielding the sharp enclosure $0<\varepsilon_n<\frac{1}{24\pi(n+1/2)}$ at $\tau=\frac{1}{2}$). Conversely, for any $\tau>\frac{1}{2}$, the expansion $(n+\tau)\varepsilon_n=\frac{1}{24\pi}+\frac{\tau-1/2}{24\pi n}+O(n^{-2})$ lies strictly above its limit $\frac{1}{24\pi}$ for all large n, so it cannot be globally increasing. (Note that differentiating the asymptotic truncation $(\omega+\tau)P_4(\omega)$ cannot substitute for this exact discrete proof: at $\tau=\frac{1}{2}$, $\Phi(\omega)=24\pi(\omega+\frac{1}{2})P_4(\omega)=1-\frac{2}{15\omega^2}+\frac{2}{15\omega^3}+\frac{3}{80\omega^4}$ actually has $\Phi'(1)=-\frac{17}{60}<0$ and $\Phi(1)=\frac{83}{80}>\frac{757}{768}=\Phi(2)$, whereas the exact sequence $(n+\frac{1}{2})\varepsilon_n$ strictly increases

for all $n \geq 1$.) Finally, high-precision evaluation of $I(2), I(4), I(6)$ and C_* from (B.10) gives $G_1 \approx 0.00176526 < G_2 \approx 0.00180513 > G_3 \approx 0.00176694$. □

Remark B.3a (Slab-Center Sets, the Constant C_*, and Working Precision). In §B.1, let $\mathcal{Z}_n^{\mathrm{top}} = \{(p_1, p_2, n + \frac{1}{2} - \ell) : 0 \leq \ell \leq n,\ |p_1|, |p_2| \leq n - \ell\}$ denote the cube-center set of the top-widest solid stack Ω_n. The vertical affine reflection $R_3^{\mathrm{aff}}(p_1, p_2, p_3) = (p_1, p_2, n + 1 - p_3)$ maps $\mathcal{Z}_n^{\mathrm{top}}$ onto the bottom-widest slab-center set $\mathcal{Z}_n^{\mathrm{bot}} = \{(p_1, p_2, \ell + \frac{1}{2})\}$, and the translate $\mathcal{Z}_n^{\mathrm{bot}} - (0, 0, \frac{1}{2})$ is exactly the lattice point stack S_n of Proposition 6.5. Throughout Theorem B.3 and Figure B.1(D), the isotropic mean constant C_* and the tail sum $R_\infty = \frac{3}{2} - C_*$ are defined by the closed trilogarithm formula (B.10):

$$C_* = \frac{4}{3} + \frac{\ln 2}{2\pi} + \frac{\zeta(3) + \mathrm{Li}_3(e^{-\sqrt{2}\pi}) - 2\,\mathrm{Li}_3(e^{-\pi})}{\pi^3} \approx 1.47999653090760042442100878465142982068794763080876$$

(the numerical plots in Figure B.1(D) evaluate $\varepsilon_n = R_\infty - \frac{2}{\pi}\sum_{i=1}^{n} I(2i)$ at 90-digit working precision across $1 \leq n \leq 15$, while monotonicity for all n when $\tau \leq 1/2$ rests on the proof of Theorem B.3(4)).

Figure B.1 (Appendix B): Solid Odd-Square Stack Ω_n Quotient Shadow, Square Hiding Cone, Global Extrema, and Sharp Shifted-Tail Monotonicity

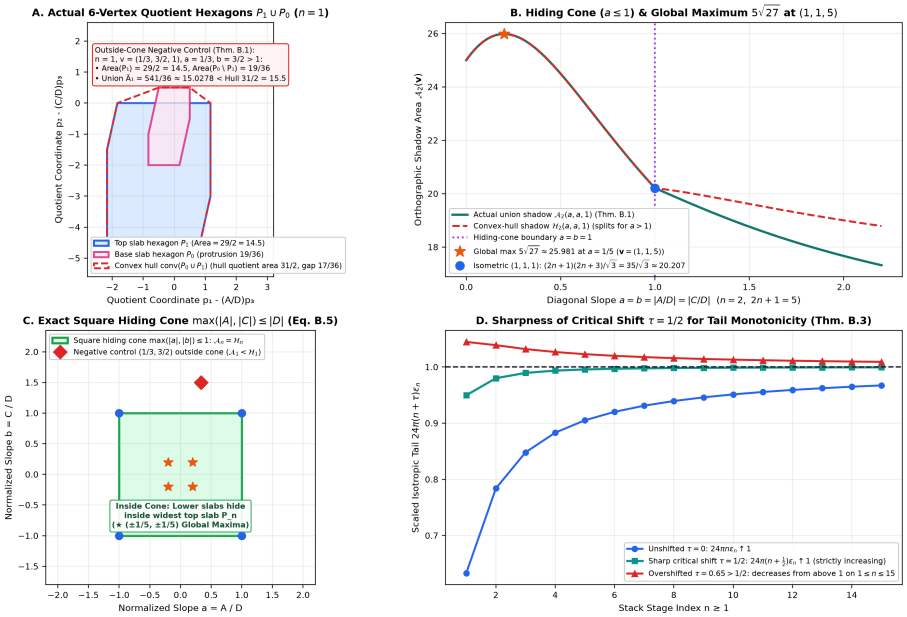


Figure B.1 (Three-dimensional odd-square stack Ω_n shadows, square hiding cone, and shifted tail monotonicity): **A.** Quotient shadow $P_0 \cup P_1$ in the plane $p_3 = 0$ for the negative-control witness $n = 1$, $\boldsymbol{v} = (1/3, 3/2, 1)$ (Theorem B.1), showing the top-slab hexagon P_1, base protrusion $P_0 \setminus P_1$, and corner-notch gap separating $\widetilde{\mathcal{A}}_1(1/3, 3/2) = 541/36$ from the projected convex hull 31/2 and naive extrapolation 15. **B.** Orthographic shadow area along the diagonal $a = b = |A/D| = |C/D|$ at $n = 2$ ($2n + 1 = 5$, Theorem B.2), showing $\mathcal{H}_2 = \mathcal{A}_2$ on $a \leq 1$, isometric value $35/\sqrt{3}$ at $a = 1$, and global maximum $5\sqrt{27}$ at $a = 1/5$. **C.** Slope-plane map $(a, b) = (A/D, C/D)$ of the square hiding cone $\max(|a|, |b|) \leq 1$ (Eq. B.5). **D.** Shifted tail product $24\pi(n + \tau)\varepsilon_n$ from Eq. (B.10), increasing strictly to 1 for $\tau = 0$ and at the sharp critical shift $\tau = 1/2$, while decreasing from above 1 across $1 \leq n \leq 15$ at $\tau = 0.65 > 1/2$.

Appendix C. Summary of Coordinates, Notation, and Static Geometric Constructions

C.1 Local Symbol and Coordinate Summary

All notation used in §§1–8 and Appendices A–B is defined locally at first appearance and collected below; the letters follow the notation register [7]:

Mathematical Object	Symbol & Defining Formula	Domain & Role	Section & Equation
Triangular polynomial & integers	$T(z) = z(z+1)/2$, $T_n = T(n)$	$z \in \mathbb{C}$, $n \in \mathbb{Z}$	§1.1 (1.1), §6.2 (6.4)–(6.5)
Cell address, chamber & offset	$N(r,c) = T_{m-1} + r$, $m = r + c - 1$, $V = r - c$	$(r,c) \in \mathbb{Z}^2_{\geq 1}$; $2N = m^2 + V + 1$	§1.1 (1.1)–(1.6)
Centered odd legs & anti-diagonal pair	$\widetilde{r} = 2r - 1 = m + V$, $\widetilde{c} = 2c - 1 = m - V$; $(k, p-k)$	$\widetilde{r} + \widetilde{c} = 2m$; $k \leftrightarrow p - k$ induces R_{mid}	§1.1 (1.2), §3.2 (3.6)
Affine path increments	$L = r_0 + c_0 - 2$, $D = \Delta_r + \Delta_c$	Degree-≤ 2 polynomial along $(r_0, c_0) + k(\Delta_r, \Delta_c)$	§2.1 (2.1)
Chamber phases & root displacement	$\kappa_{\mathrm{row}} = \frac{r}{m}$, $\kappa_{\mathrm{mid}} = \frac{\widetilde{r}}{2m}$, $\kappa_{\mathrm{root}} = \varepsilon + \frac{1}{2}$, $\kappa_{\mathrm{leg}} = \frac{r}{m+1}$	$\varepsilon = \sqrt{2N} - m \in (-\frac{1}{2}, \frac{1}{2})$	§3.1 (3.1), App. A.3 (A.8)
Three chamber reflections	$R_{\mathrm{row}}(N) = m^2 - N$, $R_{\mathrm{mid}}(N) = m^2 + 1 - N$, $R_{\mathrm{root}}(N) = \frac{(2m - \sqrt{2N})^2}{2}$	Induced by $\kappa \mapsto 1 - \kappa$ at fixed m	§3.1 Thm. 3.1, (3.2)
Scaled-square floor-branch parameters	$N_k = A(Qk)^2$, $P = \mathrm{round}(Q\sqrt{2A})$, $\delta = P^2 - 2AQ^2$, $\ell_k = \lfloor \frac{1}{2} + k\varepsilon \rfloor$	$m_k = Pk + \ell_k$; $\ell_k = 0 \iff -P \leq \delta k < P$	§4.1 (4.1)–(4.3)
Centered rational carrier parameters	$\mathcal{C}(r,c) = \left(\frac{V}{m}, \frac{\sqrt{\widetilde{r}\widetilde{c}}}{m}\right)$, $(\widetilde{r}, \widetilde{c}) = \lambda(U^2, W^2)$, $m_0 = \frac{U^2 + W^2}{2}$	$U, W, \lambda \geq 1$ odd, $\gcd(U,W) = 1$, $m_0 \equiv 1 \pmod 4$	§5.1 (5.1)–(5.5), App. A
Address sheet	$\mathbf{p}_N = \left(-\frac{r}{m+1}, \frac{1}{m+1}\right)$, $\widetilde{\mathbf{p}}_N = \left(\frac{r-m+1}{m+1}, \frac{1}{m+1}\right)$	Chamber-m row at height $p_2 = \frac{1}{m+1}$ in $Q = [-1, 0] \times [0, 1]$	§§6.1–6.3 (6.1)–(6.7)
Discrete stack S_n & solid stack Ω_n	$S_n \subset \mathbb{Z}^3$ ($\lvert S_n \rvert = \binom{2n+3}{3}$); $\Omega_n \subset \mathbb{R}^3$, viewing vector $\boldsymbol{v} = (A, C, D)$	Fiber depth $w_n(a,b)$; orthographic shadow $\mathcal{A}_n(\boldsymbol{v})$	§6.5 (6.10)–(6.11), App. B
Shells, Jordan totient & residual	$R_d(k,h) = d^2k - d + h$, $J_k(d) = d^k \prod_{p \mid d}(1 - p^{-k})$, $Q(N) = N/\gcd(N, m!)$	$d = m/\gcd(m,r)$, $h = r/\gcd(m,r)$; $Q(N) \in \{1\} \cup \mathbb{P}$	§§8.2–8.4 Thms. 8.1–8.3
Rising product & reduced quotient	$\Pi_n(y) = \prod_{j=1}^{n}(1 + jy) = \sum_k e_k(n)\, y^k$, $T_n/n! = a_n/b_n$, $g_n = \gcd(e_1(n), \ldots, e_{n-1}(n))$	$g_n = a_n \in \{1, n+1\}$ for $n \geq 2$	§8.4 Thm. 8.3(5)
Entire triangular coefficient lift	$E_{\mathrm{Ei}}(z) = \sum_{n \geq 1} \frac{z^n}{n\, n!}$, $\Theta_z = z\frac{d}{dz}$	$G_+(z) = \frac{z(z+2)}{2}e^z$, $G_-(z) = \frac{z^2}{2}e^z$ on $\mathbb{C}$	§8.4a (8.1)–(8.4)

C.2 Rail Definitions and Static Geometric Summary

1. **Rails (§2.2):** The five reference rays are the **first-row edge** $(1,k)$ (orange; $N = T_{k-1} + 1$, $\widetilde{r} = 1$), the **first-column edge** $(k,1)$ (yellow; $N = T_k$, $\widetilde{r} = 2m - 1$), the **diagonal** (k,k) (purple; $V = 0$, $N = (m^2+1)/2$), the **superdiagonal** $(k, k+1)$ (teal; $V = -1$, $N = 2k^2$), and the **subdiagonal** $(k+1, k)$ (pink; $V = +1$, $N = 2k^2 + 1$). The colors are figure keys only.
2. **Ideal Gapless Solid Ω_n (`gap = 0`) vs. Schematic Display-Gap Render (`gap > 0`):** Theorems B.1–B.3 apply strictly to the gapless union of unit-height slabs Ω_n (`gap = 0`, where each quotient shadow $P_j = [-R_j, R_j]^2 + [-(j+1)(a,b), -j(a,b)]$ is a convex hexagon of area $(2j+1)^2 + (2j+1)(a+b)$, smaller by ab than its axis-aligned bounding box). Shrinking displayed cells to side $(1 - \mathrm{gap}) \times$ pitch (`gap = 0.14` in Figure 11(D)) is solely a visual aid for exposing interior layers and alters the projected silhouette.

Structural Domain	Geometric Map & Invariant	Distinguishing Witness & Scope
Quadrant, Wedge & Rails (§§1–2)	$(r,c) \mapsto N = T_{m-1} + r \mapsto (m, V)$ straightens quadratic curves $N(m)$ into affine lines in $(m, \widetilde{r})$ and preserves period-4 parity T_{V+1} mod 2.	$N = 25 \leftrightarrow (4,4)$, $m = 7$, $V = 0$; parity cycle $(1,1,0,0)$ on $V = 0, 1, 2, 3$.
Reflections & Floor Drift (§§3–4)	Fixed-m phase flip $\kappa \mapsto 1 - \kappa$ separates $R_{\mathrm{row}}, R_{\mathrm{mid}}, R_{\mathrm{root}}$; $\ell_k = \lfloor \frac{1}{2} + k\varepsilon \rfloor$ selects polynomial branches of $N_k = A(Qk)^2$.	$N = 5$ ($m = 3$): $4 < 23 - 6\sqrt{10} < 5$; 181/128 jumps at $k = 26$ ($m = 4707$) before 4^{12} ($k = 32$).
Semicircle Budgets (§5 & App. A)	Centered $\mathcal{C}(r,c) = (+V/m, \sqrt{m^2 - V^2}/m)$ vs. leg-sum $\mathbf{p}_{\mathrm{leg}}(r,c)$ under budget $m \leq M$.	Least nontrivial $m_0 = 5$ at $(5,1) \mapsto (4/5, 3/5)$; target $(3,4)$ exception $(3,5)$ at $M = 17 < M_{\mathrm{cut}} = 37$.

Structural Domain	Geometric Map & Invariant	Distinguishing Witness & Scope
Address Sheet & Balanced Split (§6)	Row map $\mathbf{p}_N = (-r/(m+1), 1/(m+1))$ into hull $\mathcal{K}$ ($R_{\text{in}} = (\sqrt{2}-1)/2$); 8-sector $\mathbb{Z}^2 \rtimes \mathrm{O}(2,\mathbb{Z})$ congruence and the finite reciprocal identity $\mathcal{S}_L \Pi_{\triangle,L}(-1/8) = 1$.	$(2,1) \mapsto N = 3, 14, 34$ on $p_1 = -2/3$; $m = 19 \mapsto \varphi(20) = 8$; $L = 1$: $\mathcal{S}_1 = 8/9,\ \Pi_{\triangle,1} = 9/8$.
3D Point Stack S_n vs. Solid Ω_n (§6.5 & App. B)	Discrete S_n along $(1,1,1)/\sqrt{3}$ has fiber depth $w_n(a,b)$ and atomic PMFs $\to 2\omega, 6\mathfrak{f}(\omega)$; solid Ω_n (`gap = 0`) has hiding cone $\max(\lvert A\rvert, \lvert C\rvert) \le \lvert D\rvert$.	$n = 2$ stack size $\lvert S_2\rvert = 35$; $n = 1,\ \boldsymbol{v} = (1/3, 3/2, 1)$ gives $\widetilde{\mathcal{A}}_1 = 541/36 < 31/2$ and $\mathcal{A}_1 = 541/66$.

Figure 11 (Appendix C): Static Geometric Summary — Straightened Parity Wedge, Address-Sheet Primitive Columns & Hull Incircle, Oblique Fiber Depth, and Solid vs. Display-Gap Domain

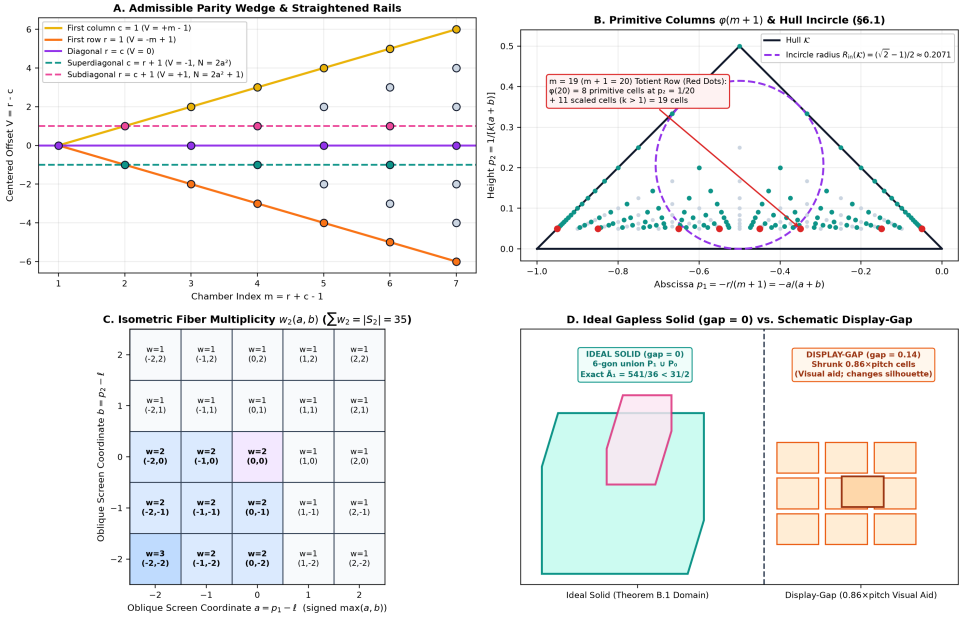


Figure 11 (Static geometric summary across four panels): **A.** Admissible parity wedge (m, V) straightening the five rails into affine rays. **B.** Address-sheet primitive columns in Q ($\varphi(20) = 8$ primitive cells in red at $m = 19$) and hull incircle radius $R_{\text{in}}(\mathcal{K}) = (\sqrt{2}-1)/2$. **C.** Oblique fiber multiplicity $w_2(a,b) = 1 + \lfloor (2 - \max(a,b))/2 \rfloor$ summing to $\lvert S_2\rvert = 35$. **D.** Comparison between the gapless solid domain (`gap = 0`) of Appendix B and a schematic display-gap render (`gap = 0.14`).

References

1. T. Nagell, *The Diophantine equation* $x^2 + 7 = 2^n$, Arkiv för Matematik **4** (1961), 185–187. https://doi.org/10.1007/BF02592006
2. M.-G. Leu and G.-W. Li, *The Diophantine equation* $2x^2 + 1 = 3^n$, Proceedings of the American Mathematical Society **131** (2003), 3643–3645. https://doi.org/10.1090/S0002-9939-03-07212-5
3. J. H. E. Cohn, *Perfect Pell powers*, Glasgow Mathematical Journal **38** (1996), 19–20. https://doi.org/10.1017/S0017089500031207
4. J. Huckstead, *Triangular-n Postmaster: From the Triangular Primitive to the Completed Source Frontier*, Volume I, Version 6.3, Cerebral Graphix / Zenodo, October 2026. https://doi.org/10.5281/zenodo.23510962
5. J. Huckstead, *Reading the Fold: A Global Newton Series for the Riemann Xi Function*, Version 1.3, Cerebral Graphix / Zenodo, October 2026. https://doi.org/10.5281/zenodo.23511096
6. H. B. Curry and I. J. Schoenberg, *On Pólya frequency functions IV: the fundamental spline functions and their limits*, Journal d'Analyse Mathématique **17** (1966), 71–107. https://doi.org/10.1007/BF02788653
7. J. Huckstead, *Triangular Index Notation Register and Modular Coefficient-State Notes* (Version 1.1) and *Cross-Project Symbol Concordance* (Version 0.1), Cerebral Graphix working manuscripts, October 2026.
8. J. Huckstead, *Cayley–Casimir Bridge to Exact Semidiscrete Flux Scattering*, Version 0.8, Cerebral Graphix / Zenodo, October 2026. https://doi.org/10.5281/zenodo.23307973

9. J. Huckstead, *The Notebook Grid: Exact Addresses, Three Reflections, Pell Branches, and Rational Carriers*, Version 1.5 (earlier working-paper deposit), Zenodo, October 2026. https://doi.org/10.5281/zenodo.23459201 (Historical concept record: https://doi.org/10.5281/zenodo.23459200)
10. J. Huckstead, *The Phase-Complement Collar: An Exact Odd-Cell Bridge from Finite-Observer Phase Accounting to the Triangular / Casimir Coordinate* (Versions 0.1–0.2), Cerebral Graphix working manuscripts, August 2026.
11. J. Huckstead, *Divisor-Band Bijections and Totient Shells in the Triangular-Fractional Grid*, Version 5, Cerebral Graphix / Zenodo, July 2026. https://doi.org/10.5281/zenodo.21440877
12. J. Huckstead, *The Chamber Lift Series: Farey Chambers, Jordan Denominator-Shell Collapse, Zeta-Exponent Three Ledgers, and the Triangular Factorial-Residual Calculus* (Versions 4–9), Cerebral Graphix working manuscripts, June–August 2026.
13. K. Dickman, *On the frequency of numbers containing prime factors of a certain relative magnitude*, Arkiv för Matematik, Astronomi och Fysik **22A** (1930), 1–14; N. G. de Bruijn, *On the number of positive integers $\leq x$ and free of prime factors $> y$*, Indagationes Mathematicae **13** (1951), 50–60.
14. J. Huckstead, *Prime Numerators and Shell Stratification in the Triangular-Fractional Grid* (Version 0.1), Cerebral Graphix working manuscript, July 2026.
15. J. Huckstead, *Diagonal-Center Sum–Difference Geometry and Arithmetic* (Version 1.1) and *Exponential-Integral Triangular Coefficient Investigation* (Version 0.1), Cerebral Graphix working manuscripts, 2026.
16. J. Huckstead, *Mersenne-Triangular Stations, Simplex-Factorial Closure, and Triangular Canonical Product / Brouncker Continuant Notes*, Cerebral Graphix working manuscripts, August 2026.
17. J. Huckstead, *Bounded Address-Sheet Totient Partitions, Staircase Fixed Points, and Chamber-Offset Entropy Notes*, Cerebral Graphix working manuscripts, October 2026.
18. J. Huckstead, *Three-Dimensional Cone/Cube Ratios, Orthochronous Double-Pell Boosts, Tetrahedral-Hexagonal Projections, and Projective Cayley / Möbius Notes*, Cerebral Graphix working manuscripts, March–August 2026.
19. J. Huckstead, *Exact-Rational Euler-Transform Enclosure for the Telescoping Logarithmic Series S_+*, Cerebral Graphix working manuscript, October 2026.
20. F. W. J. Olver, A. B. Olde Daalhuis, D. W. Lozier, B. I. Schneider, R. F. Boisvert, C. W. Clark, B. R. Miller, B. V. Saunders, H. S. Cohl, and M. A. McClain (eds.), *NIST Digital Library of Mathematical Functions*, §6.2 (exponential integrals Ei, Ein) and §25.11 (Hurwitz zeta function). https://dlmf.nist.gov/

Acknowledgments and Computational Reproducibility

Author & Collaboration Note. Authored by Jeffery Huckstead (Cerebral Graphix, cerebralgraphix.com, ORCID 0009-0007-0234-2177). AI-assisted mathematical drafting, symbolic reorganization, proof checking, and computational verification tools were used under the author's direction during the preparation of Version 4.1; responsibility for all mathematical definitions, scope boundaries, and conclusions rests with the author.

Optional Computational & Interactive Supplements. Every theorem and proof in this paper is self-contained in print. For readers wishing to replay finite-range algebraic, rational, decimal, and sieve checks, the supplementary archive provides the standalone Python 3 standard-library script `check_notebook_grid_v4_1.py` alongside an optional offline single-file interactive HTML reader (`Notebook_Grid_v4_1_Interactive_Reader.html`).